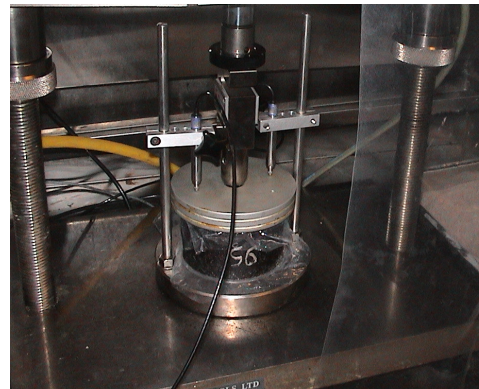
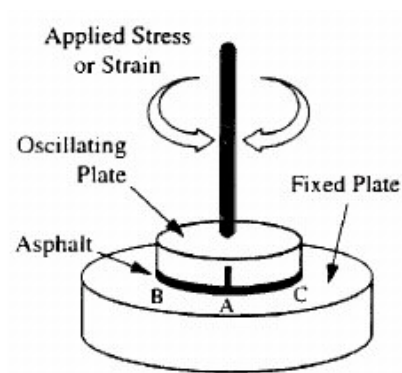
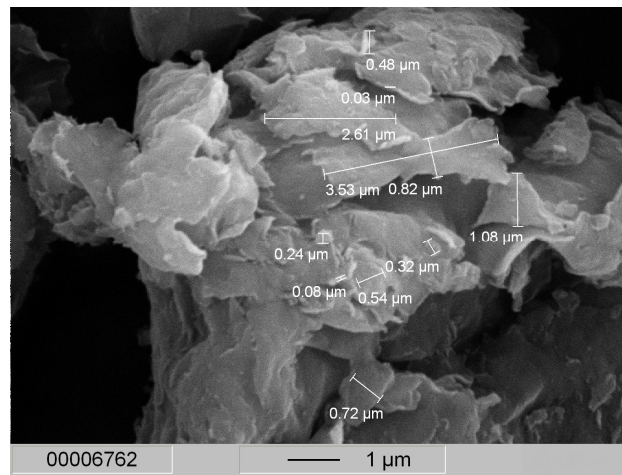


DELFT UNIVERSITY OF TECHNOLOGY



Effects of Nanoclay Modification on Rheology of Bitumen and on Performance of Asphalt Mixtures

Daniel Beyene Ghile

**M.Sc. Thesis
June 2006**

Effects of Nanoclay Modification on Rheology of Bitumen and on Performance of Asphalt Mixtures

By

Daniel Beyene Ghile

Submitted in partial fulfillment of the requirements for the
degree of

**MASTERS OF SCIENCE IN
ROAD AND RAILWAY ENGINEERING**

From

**DELFT UNIVERSITY OF TECHNOLOGY, DELFT,
THE NETHERLANDS**

Examining committee :

Prof.dr..A.A.A. Molenaar

ir. M.F.C. Van de Ven

Drs. Jeroen Th.M. Besamusca

Ing. Wim Verwaal

Ir. L.j.M. Houben (coordinator)

Msc Thesis TUDelft

June 2006

Acknowledgement:

I would like to express my deep and sincere appreciation to my supervisors A.A.A Molenaar and Martin van de Ven for their guidance, advice, technical and moral support during my research work.

Jeroen Besamusca has helped me a lot in the rheology part of my research work and his work is highly appreciated.

My appreciation also goes to Marco Poot for his guidance and help in the lab and for being a real friend during my working period in the laboratory. I would also like to acknowledge the warm approach and help given to me by Jan Willem Bientjes, Jan Moraal, Robin van Dijk, Raoul Hieralal, Mrs. J. Barnhoorn, Mrs. S.v.d Bos, Wim Verwaal. Without their help this research work could not have been realized.

I want to express my gratitude for the guidance given to me in technical and administrative works by L.J.M. Houben.

My thanks also goes to Eyasu Tesfamairam, Patrick Muraya, T.O.Medani, Million Fekade for their technical help, their friendship and for making my stay in TU delft comfortable.

I want to express my appreciation to Samson Habte for being a real friend during my stay in Delft and my appreciation also goes to all my families, my friends Tamirat Woldu, Abrahm M. Haile, Kibreab and all other friends who in one way or another made this research work possible.

Furthermore, I want to express my sincere gratitude to contracting company “Gebr. Van der Lee”, who was willing to sponsor my stay in Delft during my MSc research work. Without this help this research work could not have been possible.

My sincere thanks also goes to ing. Rob van der Tang. He was the initiator of the project and made the financial arrangements. Finally the support of the “ Nano Team” (TNO, Q8, DGW&T, Ministry of Defense, Gebr.v.d. Lee, Schiphol) is highly appreciated.

Abstract

Physical properties and temperature susceptibility characteristics of the asphalt binder influence pavement performance at low and high field operating temperatures. It was proven that addition of additives like polymers can influence the temperature susceptibility of asphalt cements and as a result an improvement in characteristics and performance of asphalt mixtures can be obtained in a wide temperature ranges. In addition a number of physical properties of polymers are successfully enhanced when a polymer is modified with small amount of nanoclay on condition that the clay is dispersed at nanoscopic level. Based on the same principle as used with polymer modifications, TNO suggests some nanoclay modification of the bitumen. Two types of nanoclay modifications were suggested: nanofill and cloisite. The expectation with the nanoclay modification is influencing properties like stiffness, fatigue resistance, strength, resistance to ageing and thermal stability.

Based on these issues, the main objective of the study work was to conduct a comparative test program on binders and asphalt mixtures containing standard and nanoclay modified asphalts and assess the effects of asphalt properties on pavement performances. To meet this objective the main targets of the study work are to find out if the nanoclays alter the critical properties of asphalt binder and influence the ageing and rheology of the binder and in addition to study if the nanoclay modifications influence the performance of asphalt mixtures.

Different tasks were performed in the study work to meet the objective. The first task performed was studying the nanoclay modifiers at nanoscopic level and the tests performed in this area are microscopic analysis and x-ray analysis of the nanoclay modifiers. The second task is studying the influence of nanoclay modifiers on binder characteristics and the tests performed related to this are rheological studies of fresh (un aged) and aged bitumen types by dynamic shear rheometer (DSR); by empirical tests like penetration and softening points. The third task performed is studying the effect of the nanoclay modified binder on asphalt mixtures and the tests performed in this area are indirect tensile strength test, fatigue resistance test, dynamic creep test and resilient modulus test.

Findings of the tests performed on binders and dense asphalt mixes proved that the cloisite nanoclay modifications helped to increase the stiffness, to improve the rutting resistance of the standard 40/60 binder. This is especially true if the 6% cloisite modification is used. In addition, the 6% cloisite modification helped to increase the indirect tensile strength and fracture energy values of dense asphalt mixtures. The nanofill (6%) modification helps to improve the ageing resistance of the 70/100 binder in the short term and long terms.

However, the nanoclay modifications were observed to negatively influence the fatigue resistance performance of asphalt binders/mixes especially at low temperature values. An overall conclusion from these findings is the nanoclay modifications helped to improve some characteristics of asphalt binders and asphalt mixtures but at this level they are not at a stage to justify application at large scale.

Hence, further studies on the chemistry of the nanoclay and bitumen and further development of the nanoclay technology is recommended to utilize the full potential of the nanoclay modifications.

TABLE OF CONTENTS:

ACKNOWLEDGEMENTS	i
ABSTRACT	ii
1 INTRODUCTION	1
1.1 Motive of the Study Work.....	1
1.2 Objective of the Study	1
1.3 Significance of the Study	2
1.4 Scope of the Study.....	2
1.5 Organization of the thesis	3
2 Literature Review	5
2.1 Introduction	5
2.2 Back Ground on Nano technology and Nanoclay modification	5
2.3 Rheological properties of bitumen binders	10
2.3.1 Empirical tests	10
2.3.2 Fundamental Rheological tests by Dynamic Shear Rheometers(DSR).....	11
2.4 Performance related tests on Asphalt Mixtures	16
2.4.1 Indirect Tensile Strength Test.....	16
2.4.2 Indirect Tensile Resilient Modulus Test.....	17
2.4.3 Indirect Tensile Fatigue Tests.....	19
2.4.4 Cyclic Uniaxial compression Test.....	20
3 Testing Preparations and Programs	24
3.1 Testing program on nanoclay modifiers.....	24
3.2 Testing program on rheological tests of modified and unmodified binders.....	24
3.2.1 Empirical rheological testing program	25
3.2.2 DSR testing program	26
3.3 Specimen preparation and testing program of asphalt mixtures.....	27
3.3.1 Specimen preparation	27
3.3.2 Physical Properties of the specimens.....	28
3.3.3 Pre-treatment of specimens before test.....	32
3.3.4 Testing program on dense asphalt mixtures	32
4 Tests and Characterization of Nanoclay Modifiers	41
4.1 Microscopic analysis of the nanoclay modifiers.....	41
4.2 X-ray analysis of the nanoclay modifiers.....	44
4.2.1 Qualitative wavelength dispersive spot analyses.....	44
4.2.2 X-ray diffraction (XRD) analysis	45
4.3 Plastic Limit of nanoclay modifiers	49
5 Rheological Tests on Modified and Unmodified asphalt binders	50
5.1 Empirical rheological tests.....	50
5.1.1 Penetration and softening point	50
5.1.2 Retained penetration and increment in softening point	51
5.2 DSR test results	54
5.2.1 Typical analysis of DSR test results	54
5.2.2 Analysis and comparison of stiffness and phase angle values: standard 70/100 binder versus nanofill 6% modified 70/100 binder	58

5.2.3	Analysis and comparison of stiffness and phase angle values: standard 40/60 binder versus cloisite 3% modified 40/60 binder	65
5.2.4	Analysis and comparison of stiffness and phase angle values: standard 40/60 binder versus cloisite 6% modified 40/60 binder	71
5.3	Permanent deformation and fatigue analysis from DSR results.....	76
5.3.1	Rutting Parameter	76
5.3.2	Fatigue resistance parameter.....	79
6	Performance Tests on Modified and Unmodified Dense Asphalt	
Mixtures.....		84
6.1	Indirect Tensile Strength Test.....	84
6.1.1	Purpose of performing the test.....	84
6.1.2	Typical Indirect tensile strength test result.....	84
6.1.3	Test result analysis.....	86
6.1.4	Test results Comparison	87
6.1.5	Fracture Energy analysis and comparison	88
6.2	Resilient Modulus	90
6.2.1	Purpose of performing the test.....	90
6.2.2	Typical resilient modulus test result	90
6.2.3	Test result analysis.....	91
6.2.4	Test result Comparison	93
6.2.5	Master curve construction and comparison	95
6.3	Dynamic creep tests	98
6.3.1	Purpose of performing the test.....	98
6.3.2	Typical dynamic creep test result	98
6.3.3	Results of the dynamic creep tests.....	100
6.3.4	Test result analysis and comparison	103
6.4	Fatigue Resistance test	106
6.4.1	Purpose of performing the test.....	106
6.4.2	Typical fatigue resistance test result.....	106
6.4.3	Test result analysis.....	107
6.4.4	Fatigue life comparison	111
7	Conclusions and Recommendations.....	120
7.1	Conclusions on nanoclay characterization	120
7.2	Conclusions on Rheology of asphalt binders.....	120
7.3	Conclusions on performances tests of asphalt mixtures	121
7.4	General Conclusions.....	122
7.5	Recommendations.....	123

LIST OF TABLES:

Table 1: Empirical rheological testing program	25
Table 2: DSR testing program	26
Table 3: DSR input parameters and test configuration.....	27
Table 4: Composition of dense mixture	27
Table 5: Input parameters in specimen preparation.....	28
Table 6: Theoretical maximum Density of mixture components	29
Table 7: Theoretical maximum Density of Cloisite modified bitumen.....	30
Table 8: Theoretical maximum Density of standard and 6% cloisite modified mixtures	30
Table 9: Average Actual Density values of modified and unmodified specimens.....	31
Table 10: Average void content of modified and unmodified specimens	32
Table 11: Pre-treatment of specimens before test.....	32
Table 12: Number of specimens tested for the different tests	33
Table 13: Testing input and control parameters for indirect tensile strength.....	34
Table 14: Testing input and control parameters for Resilient modulus test using ITT	35
Table 15: Loading pulse in resilient modulus test using ITT	35
Table 16: Loading pulse amplitude in resilient modulus test using ITT	36
Table 17: Testing input and control parameters for dynamic creep test.....	37
Table 18: Peak stress values in dynamic creep test	38
Table 19: Testing input and control parameters for fatigue resistance test	39
Table 20: Peak stress values in fatigue resistance test.....	40
Table 21: Plastic limit analysis for nanofill.....	49
Table 22: Plastic limit analysis for cloisite.....	49
Table 23: penetration and softening point tests on fresh and aged materials	50
Table 24: Frequency matching table	58
Table 25: Stiffness values of standard and nanofill modified 70/100 binders (fresh and short term aged)@20°C	59
Table 26: Phase angle values of standard and nanofill modified 70/100 binders (fresh and short term aged) @ 20°C	60
Table 27: stiffness values of standard and nanofill modified 70/100 binders (fresh and long term aged by RCAT) @20°C	62
Table 28: Phase angle values of standard and nanofill modified 70/100 binders at selected frequency (fresh and long term aged).....	63
Table 29: comparison of stiffness and phase angle of PAV and RCAT long term aged nanofill modified 70/100	65
Table 30: Stiffness values of standard and cloisite 3% modified 40/60 binders (fresh and short term aged) @20°C	65
Table 31: Phase angle values of standard and cloisite 3% modified 40/60 binders at selected frequencies (fresh and short term aged).....	66
Table 32: stiffness and phase angle analysis after short term ageing for modified and unmodified binders	68
Table 33: stiffness values of standard and cloisite 3% modified 40/60 binders (fresh and long term aged by RCAT) @20°C	69
Table 34: Phase angle values of standard and cloisite 3% modified 40/60 binders (fresh and long term aged) @20°C	70
Table 35: Stiffness values of standard and 6% cloisite modified 40/60 binders (fresh and short term aged)@20°C	71
Table 36: Phase angle of standard and modified binders (aged and un-aged) @20°C	72

Table 37: stiffness values @20°C of standard and cloisite 6% modified 40/60 binders (fresh and long term aged by RCAT).....	74
Table 38: Phase angle values @20°C of standard and cloisite 6% modified 40/60 binders (long term aged).....	75
Table 39: comparison of $G^*/\sin\delta$ of modified and unmodified 40/60 binders.....	77
Table 40: comparison of $G^*/\sin\delta$ of modified and unmodified 70/100 binders.....	78
Table 41: Temperature values at minimum limits of $G^*/\sin\delta$	79
Table 42: comparison of $G^* \times \sin\delta$ of modified and unmodified 40/60 binders.....	80
Table 43: comparison of $G^* \times \sin\delta$ of modified and unmodified 70/100 binders.....	82
Table 44: Temperature values at minimum limits of $G^*/\sin\delta$	83
Table 45: Indirect tensile strength test results and analysis (standard dense mix).....	86
Table 46: Indirect tensile strength test results and analysis (cloisite 6% modified dense mix)	86
Table 47: ITS comparison between modified and unmodified dense mixes.....	87
Table 48: Fracture energy values of standard and modified dense mix	89
Table 49: Resilient modulus of standard and 6% cloisite modified dense mixes	92
Table 50: Resilient modulus comparison of standard and 6% cloisite modified dense mixes.....	93
Table 51: values of the master curves of stiffness for standard and modified dense mixes....	96
Table 52: values of constants of sigmoidal, WLF and Arrhenius models.....	97
Table 53: summation of difference between model stiffness and actual stiffness	97
Table 54: Rutting resistance indicators for standard dense mix	103
Table 55: Rutting resistance indicators for 6% cloisite modified dense mix	104
Table 56: relationship between N_f and σ for standard dense mixture at 5°C.....	108
Table 57: k and R-square values at 5°C test temperature.....	108
Table 58: relationship between N_f and σ for standard dense mixture at 20°C	110
Table 59: k and R-square values at 5°C test temperature.....	111
Table 60: Fatigue life comparison at 5°C	112
Table 61: Fatigue life comparison at 20°C	113
Table 62: Computation of the constant factors in fatigue relationship.....	117
Table 63: Fatigue relationship based on Medani's Equations	118
Table 64: Fatigue life comparison for selected strain values	118
Table 65: Summary of rheological comparison results	121
Table 66: Summary of comparison results of performance tests on dense mixtures	122

LIST OF FIGURES:

Figure1. Generalized tasks of the main thesis part	4
Figure2: Schematic representation of montmorillonite structure	6
Figure3: Pictorial representation of montmorillonite structure	6
Figure 4: Nanoclay Surface treatment	8
Figure 5: Formation of intercalated and exfoliated nanocomposites from layered silicates and polymers	9
Figure 6: Visco-elastic Materials under Constant Stress Loading	12
Figure 7 :Dynamic Shear Rheometer	12
Figure 8: Relationship between G^* , G' , G'' and δ	14
Figure 9: phase angle determination.....	14
Figure 10: indirect tensile strength test.....	16
Figure 11: Indirect tension test, set-up (left) and stresses along the vertical and horizontal cross section.....	17
Figure 12: stress versus number of load repetitions	19
Figure 13: unconfined cyclic compression test	21
Figure 14: Typical relationship between cumulative permanent axial strain and number of cycles	22
Figure15: half sine loading pulse in resilient modulus test using ITT	34
Figure16: half sine loading pulse in dynamic creep test.....	37
Figure17: Haversine loading pulse in fatigue resistance test.....	40
Figure18: Microscopic image of nanofill	42
Figure19: Microscopic image of cloisite	43
Figure 20: X_ray analysis with crystal spectrometer (Nanofill)	45
Figure 21: X_ray analysis with crystal spectrometer (Cloisite)	46
Figure 22: X_ray diffraction analysis (Nanofill)	47
Figure 23: X_ray diffraction analysis (cloisite).....	48
Figure 24: Retained penetration and increment in softening point for standard and modified 70/100 binder.....	52
Figure25: Retained penetration and increment in softening point for standard and modified 40/60 binder.....	53
Figure26: Frequency sweep of DSR test results (standard fresh 40/60 binder)	55
Figure27: Mater curve for standard fresh 40/60 binder.....	56
Figure28: Black diagram for standard fresh 40/60 binder.....	57
Figure29: Master curve of stiffness for modified and unmodified 70/100 binder (fresh and short term aged)	59
Figure30: Master curve of phase angle for modified and unmodified 70/100 binder (fresh and short term aged)	60
Figure31: master curve of stiffness of modified and unmodified 70/100 binders (fresh and RCAT long term aged)	62
Figure32: master curve of phase angle for modified and unmodified 70/100 binder (fresh and long term aged).....	63
Figure33: master curve of stiffness and phase angle for long term aged modified and unmodified 70/100 binders (using RCAT and PAV)	64
Figure34: master curve of stiffness of modified and unmodified 40/60 binders(fresh and short term aged)	66

Figure35: master curve of phase angle of modified and unmodified 40/60 binder (fresh and short term aged)	67
Figure36: master curve of stiffness of cloisite 3% modified 40/60 binder and unmodified 40/60 binders (fresh and RCAT long term aged)	69
Figure37: master curve of phase angle of modified and unmodified 40/60 binder (fresh and long term aged)	70
Figure38: master curve of stiffness of standard and 6% cloisite modified binder (fresh and short term aged)	71
Figure39: master curve of phase angle of standard and modified binders (aged and un-aged)	72
Figure40: master curve of stiffness of cloisite 6% modified 40/60 binder and unmodified 40/60 binders (fresh and RCAT long term aged)	74
Figure41: master curve of phase angle of 6% cloisite modified 40/60 binder and unmodified 40/60 binders (fresh and RCAT long term aged)	75
Figure42: Comparison of $G^*/\sin\delta$ of modified and unmodified 40-60 binders	77
Figure43: Comparison of $G^*/\sin\delta$ of modified and unmodified 70-100 binders	79
Figure44: Comparison of $G^* \times \sin\delta$ of modified and unmodified 40-60 binders	81
Figure45: Comparison of $G^* \times \sin\delta$ of modified and unmodified 70-100 binders	82
Figure 46: typical test result output of indirect tensile strength (ITS) test	85
Figure 47: Failure mechanism in ITS	87
Figure 48: Comparison of ITS results of modified and unmodified dense mixes.....	87
Figure 49: Fracture Energy from ITS	88
Figure 50: Fracture energy values of standard and modified dense mix	89
Figure 51: typical resilient modulus output results.....	91
Figure 52: Comparison of resilient modulus values of standard and 6% cloisite modified dense mixes.....	94
Figure 53: Master curves of standard and 6% cloisite modified dense mixes	97
Figure 54: typical permanent deformation test result	99
Figure 55: Dynamic creep test results at 40°C	101
Figure 56: Dynamic creep test results at 50°C	102
Figure 57: Dynamic creep test results at 60°C	103
Figure 58: Rate of permanent deformation (K)	104
Figure 59: Typical fatigue resistance test result	107
Figure 60: S-N curve at 5°C for standard and 6% cloisite modified dense mixes	109
Figure 61: Relationship between logarithmic values of N_f and σ at 5°C.....	109
Figure 62: S-N curve at 5°C for standard and 6% cloisite modified dense mixes	110
Figure 63: Relationship between logarithmic values of N_f and σ at 20°C.....	111
Figure 64: Fatigue life comparison at 5°C.....	112
Figure 65: Fatigue life comparison at 20°C.....	113
Figure 66: slope of modified and unmodified 40-60 binders	116
Figure 67: slope of modified and unmodified dense mixtures	117
Figure 68: fatigue life comparison for selected strain values	118

1 INTRODUCTION

1.1 Motive of the Study Work

Physical properties and temperature susceptibility characteristics of the bitumen influence pavement stiffness, both at high and low field-operating temperatures, and thereby can dramatically affect final performance of the mixture. To improve the performance of bitumen and asphalt concrete mixtures, addition of modifiers like polymers has gained popularity in recent years. This is because modification provides the versatile properties needed to build better performing roads.

Polymeric nano composites are one of the most exciting and promising classes of materials discovered recently. A number of physical properties are successfully enhanced when a polymer is modified with small amount of nanoclay on condition that the clay is dispersed at nanoscopic level.

Based on similar principles as used in polymer modifications with nanoclays, TNO has suggested some nanoclay modifications that can be well mixed with bitumen. To see the effect of the nanoclay modification, if any, on the characteristics and overall performance of the binder, a preliminary test was performed by Q8 Petroleum Research and Technology on both modified and unmodified binders. Those preliminary test results showed improvement of the characteristics of the bitumen due to the nanoclay modification. These initial promising results of the nanoclay modification on the binder gave the start line for the study work.

Hence the main points which gave an initiative for the study work are:

1. the keen interest to influence the temperature susceptibility of bitumen by adding additives so as to improve its characteristics and performance in wide temperature ranges;
2. performance enhancements observed in polymers and other thermoplastic materials due to nanoclay modifications;
3. the improvements observed by Q8 Petroleum Research and Technology due to the nanoclay modification by performing preliminary empirical tests on the modified and unmodified binders.

1.2 Objective of the Study

The main objective of the study work was to conduct a comparative test program on binders and asphalt mixtures containing standard and nanoclay modified bitumens and assess the effects of bitumen properties on pavement performance. To meet this main objective the following targets were taken into consideration

1. study the nanoclay modifiers at nanoscale level;
2. find out how the nanoclay modification alter the critical properties of bitumen;
3. investigate and evaluate the role of different nanoclay modifiers in changing the rheological properties of bitumens;
4. study the effect of the nanoclay modifiers on ageing effect of the binder;
5. find out how the nanoclay modifications can affect the performance of asphalt mixtures;
6. consider different asphalt mixtures and investigate the effect of the nanoclay modification in each mixture type.

1.3 Significance of the Study

The study work investigates the characteristics of the nanoclay modifiers, the effect of the nanoclay modifiers in bitumens and asphalt mixtures and the difference between the two types of nanoclay modifiers. Hence, the main topics of the study work are:

- to determine if the nanoclay modifiers bring the desired improvement on bitumens and asphalt mixtures;
- to determine the positive as well as the negative impacts of the nanoclay modifications on the performance of asphalt mixtures;
- to determine which nanoclay modifier is good for which type of asphalt mixture;
- to determine the proportion of nanoclay modifiers to be mixed with the binder so as to bring the desired changes, if any, on characteristics and performance of bitumens and mixtures;
- to determine if further development of the nanoclay modifiers is required before doing tests on large scale projects.

1.4 Scope of the Study

The study work investigates different areas including the nanoclay modifiers characterization, studying rheological properties of the modified binders in comparison to standard binders, studying the functional properties of modified asphalt mixtures in relation to standard mixtures. The study comprises two types of nanoclay modifiers (cloisite, nanofill) on two types of binders (40/60, 70/100). The proportions of the nanoclay modifiers considered in the study work are 3% and 6% in relation to the weight of the binder. Taking into account the different test types performed, the different types and proportions of modifiers and the different mixture types, the overall study work done is broad and versatile.

Due to the versatility of the study work and due to limitations in time, the number of specimens considered for each test is limited in number and as a result only a limited statistical analysis could be done. In addition, a limited number of test types are considered for the study work.

1.5 Organization of the thesis

In this study work two phases of experimental tests are performed and reported. The first phase of the study work comprises analysis of rheological properties of the modified binder in relation to standard binder. The tests performed include empirical rheological analysis (penetration, softening point) and fundamental rheological properties measured with the dynamic shear rheometer (DSR). The binders considered for the test are 40/60 and 70/100 and the proportion of the modifications are 3% cloisite, 6% cloisite and 6% nanofill. In addition x-ray and microscopic analyses of the nanoclay modifiers are performed in this phase.

The second phase comprises comparative tests and analyses between 6% cloisite modified mixtures and standard dense mixtures. The tests performed in this phase are indirect tensile strength tests at five temperature values, dynamic stiffness tests at 5 temperature values, fatigue resistance tests at 2 temperature values and permanent deformation at three different temperatures and three different loading values.

The generalized tasks performed in this study work are summarized in figure 1.

In this study work, following this introductory part, a literature review about nanoclay modifications on thermoplastic materials, about rheological properties of binders and on the theoretical bases of the tests performed on the mixtures is discussed in chapter 2. Chapter 3 describes the input parameters and the preparations done for the different tests performed. In addition the detailed testing program is described in this chapter. Chapter 4 describes the tests performed on nanoclay modifiers and their characterization. Chapter 5 deals with the rheological test results and the corresponding analyses and discussion. In chapter 6, the tests performed on the asphalt mixtures, their result analyses and the corresponding discussions are presented. Finally chapter 7 gives the conclusions and recommendations.

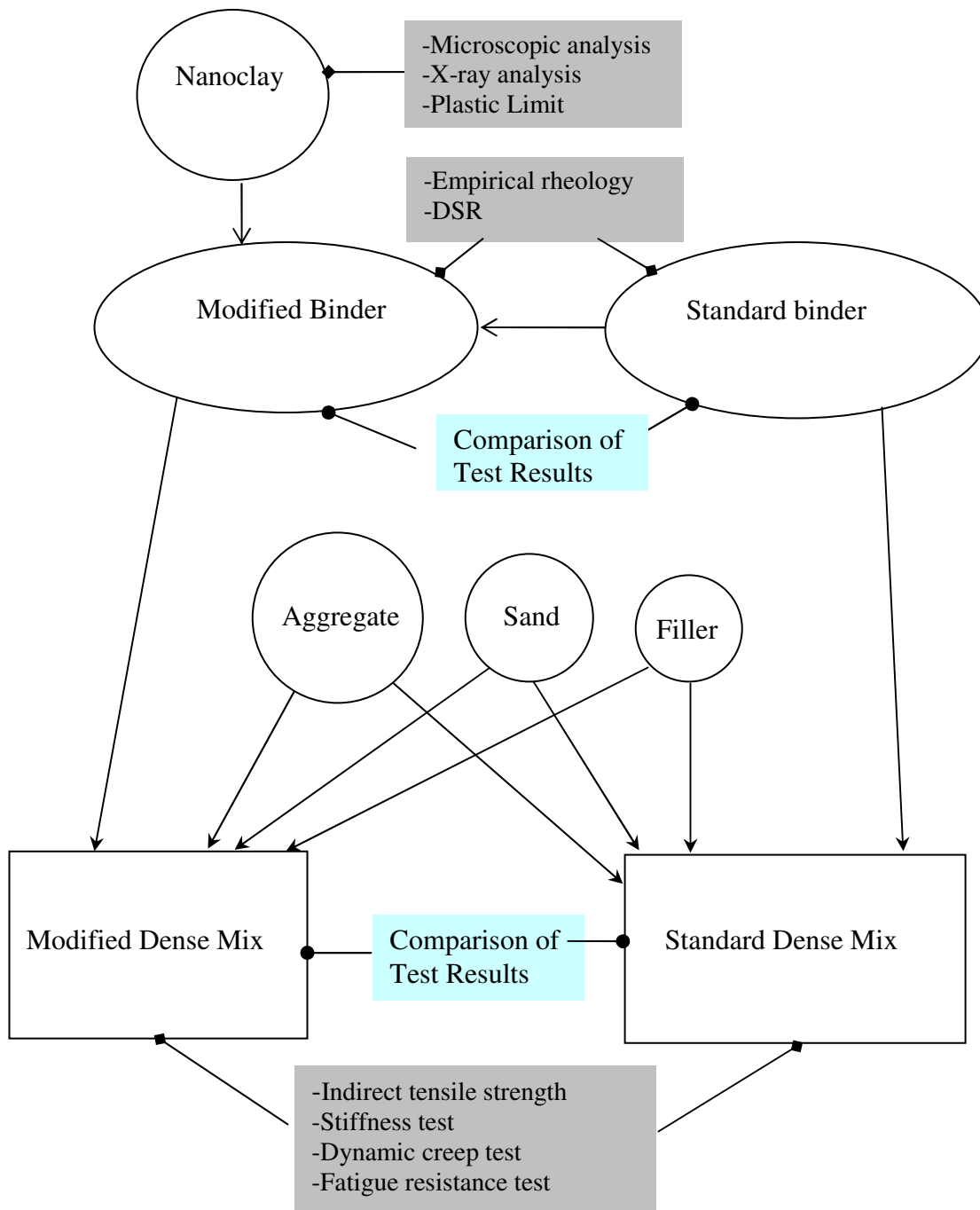


Figure 1. Generalized tasks of the main thesis part

2 Literature Review

2.1 Introduction

In this chapter first some theoretical knowledge about nanoclay, their interaction and modification effect on thermoplastic materials, their merits and limitations is presented. Theoretical knowledge about rheological properties of binders and their relationship with the performance related characteristics is described next. Finally, the theoretical knowledge about the different experimental tests performed on the asphalt mixtures is given.

2.2 Back Ground on Nano technology and Nanoclay modification

Nanotechnology is:

1. the understanding and control of matter at the atomic, molecular or macromolecular levels, in the length scale of approximately 1 nanometer to 100 nanometer range;
2. creating and using structures, devices and systems that have novel properties and functions because of their small and/or intermediate size;
3. implying that new materials and applications are being developed to specifically exploit the properties found in this size range.

Little published information concerning nanoclay modified bitumen is available. However, relatively a large number of studies were done on nanoclay modified polymers. Hence, while this study focuses on nanoclay modified bitumen, a reference and literature review of nanoclay modified polymers is of significance since both modifications can be based on similar principles.

Important among nanoscale structural materials are nanocomposites in which the constituents are mixed at nanoscale length. The term nanocomposite is in the broadest sense referring to every type of material with fillers in the nanometer size range at least in one dimension. Polymeric nanocomposites are one of the most exciting and promising classes of materials discovered recently. A number of physical properties are successfully enhanced when a polymer is modified with small amount of nanoclay on the condition that the clay is dispersed at nanoscopic level. Material variables which can be controlled and which can have a profound influence on the nature and properties of the final nanocomposite include the type of clay, the choice of clay pre-treatment, the selection of polymer component and the way in which the polymer is incorporated into the nanocomposite.

Common clays are naturally occurring minerals and are thus subject to natural variability in their constitution. The purity of the clay can affect final nanocomposite properties. Many

clays are aluminosilicates, which have a sheet-like (layered) structure, and consist of silica SiO₄ tetrahedron bonded to alumina AlO₆ octahedron in a variety of ways. A 2:1 ratio of the tetrahedron to the octahedron results in smectite clays, the most common of which is montmorillonite. In these types of clays, the apical oxygen atoms of the tetrahedral sheet are all shared with the octahedral sheet. Other metals such as magnesium, iron or zinc may replace the aluminum in the crystal structure. In addition, a portion of silicon in the tetrahedral can be replaced by aluminum. The thickness of the layers (platelets) is of the order of 1 nm and aspect ratios are high, typically 100-1500.

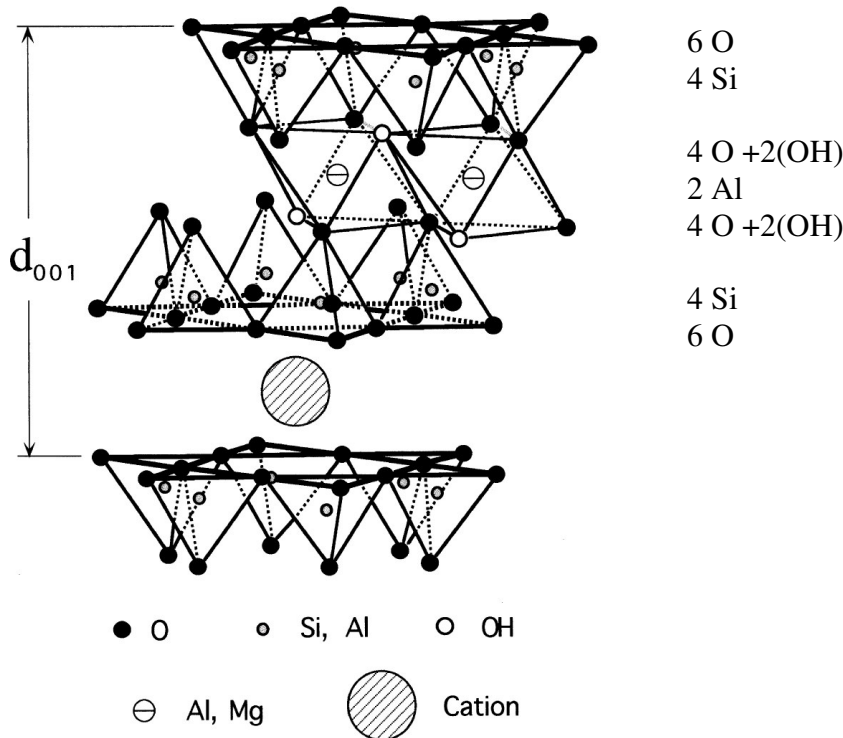


Figure2: Schematic representation of montmorillonite structure

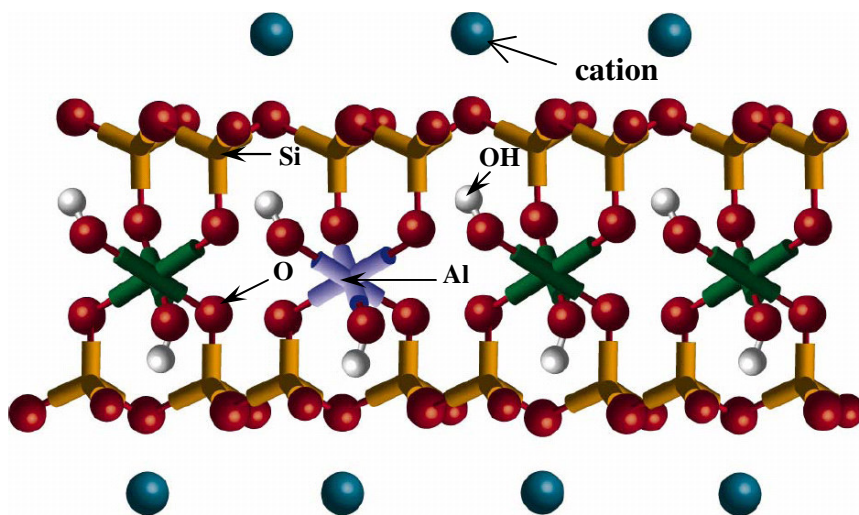


Figure3: Pictorial representation of montmorillonite structure

All positions at the top and base of the lattice layers of the montmorillonite are completely occupied by oxygen atoms. These layers are held together by a relatively weak intermolecular force. As a result, water molecules easily penetrate the interlayer region and can cause the expansion of the lattice. Depending on the precise chemical composition of the clay, the sheets bear a charge on the surface and edges, this charge being balanced by counter-ions (cations), which reside in part in the inter-layer spacing of the clay. The hydrated cations between the layers increase the distance between adjacent layers. Accordingly montmorillonite are expandable clay minerals. The whole surface of layers including internal and external surface can be hydrated and the exchange reaction of cations can occur there. The degree of expansion of montmorillonite is determined by their ion (e.g. cation) exchange capacities, which can vary widely. A characteristic number of these types of clay is the cation exchange capacity (CEC), which is a number for the amount of cations between the surfaces. The CEC of montmorillonite can range from 80 to 120 meq/100g (milli-equivalents per 100 grams) where as kaolinite can have CEC values ranging between 3-5.

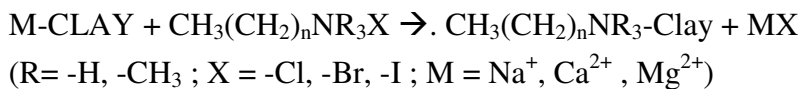
The expansion pressure of montmorillonite in which sodium ions constitute the majority of the adsorbed cations (called Na-montmorillonite) is very high, leading to the exfoliation and dispersion of the crystal in the manner of fine particles or even single layers. When Ca^{2+} , Mg^{2+} and ammonium are the dominant exchangeable cations, the dispersion is relatively low and the size of the particle is relatively large.

Separating of the clay discs from each other will result in a nanoclay with an enormous large active surface area (it can be as high as 700 to 800 m² per gram). This helps to have an intensive interaction between the nanoclay and its environment (bitumen in our case). The process to realize the separation (surface treatment) is dependent on the type of material to be mixed, which can be explained as follows.

Clay discs are negatively charged, but stay together in a clay particle because of the positive ions between the clay discs. In this way the clay particle as a whole is neutral. In addition, unmodified montmorillonite clays are generally highly hydrophilic species and therefore naturally incompatible with a wide range of polymer types. A necessary prerequisite for successful formation of polymer-clay nanocomposites is therefore alteration of the clay polarity to make the clay 'organophilic'. To achieve fine dispersion, mechanical forces alone are not enough; there should be a thermodynamic driving force as well to separate the layers into the primary silicate sheets. This thermodynamic driving force is introduced by inserting a certain coating of surfactants (an agent such as detergent which reduces surface tension) on each individual layer. These surfactant molecules increase the layer distance, improve the

compatibility with the polymer and can give an increase in entropy because they can mix with the polymer. To enable each layer to be coated with the surfactant, the layers should be accessible for the surfactant molecules from the solution, and for this reason the clay layers need to swell or exfoliate in the solvent (usually water). Smectite clay, such as montmorillonite, is negatively charged and swells in water, and can therefore be coated with a cationic surfactant in an aqueous suspension. The surfactant provides a hydrophobic nature to the silicate surface, which causes the layers to precipitate as organophilic clay, also known as organoclay.

An organophilic clay can be produced from a normally hydrophilic clay by ion exchange with an organic cation. The organic reagents are quaternary ammonium salt with alkyl chains such as 12-aminododecanoic acid (ADA), octadecanoic alkyl trimethyl quaternary ammonium salt. The reaction process is described as :



Addition of a positively loaded surface active material, a kind of ADA, will in this case form an ADA layer around each clay disc. The clay disc in this case changes from a hydrophilic disc into a hydrophobic disc. These modified clay discs will separate automatically in water and can be used as nano-particles. Figure 4 shows the process of surface treatment of the nanoclay material.

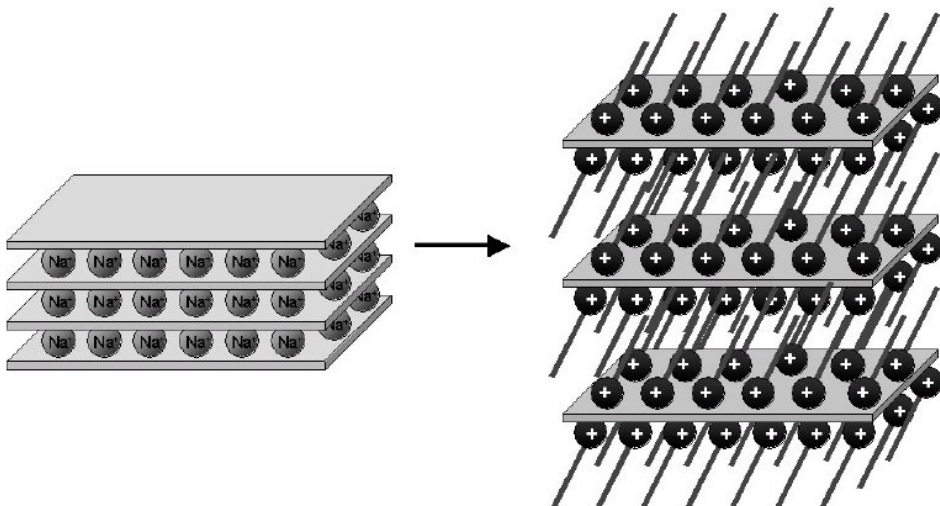


Figure 4: Nanoclay Surface treatment

The synthetic route of choice for making a nanocomposite depends on whether the final material is required in the form of an intercalated or exfoliated hybrid (Figure5). In the case of an intercalate, the organic component is inserted between the layers of the clay such that the interlayer spacing is expanded, but the layers still bear a well-defined spatial relationship to each other. In an exfoliated structure, the layers of the clay have been completely separated

and the individual layers are distributed throughout the organic matrix. The final interlayer distance depends on the size and type of the organic cation molecules, the curing agent and the clay's treatment.

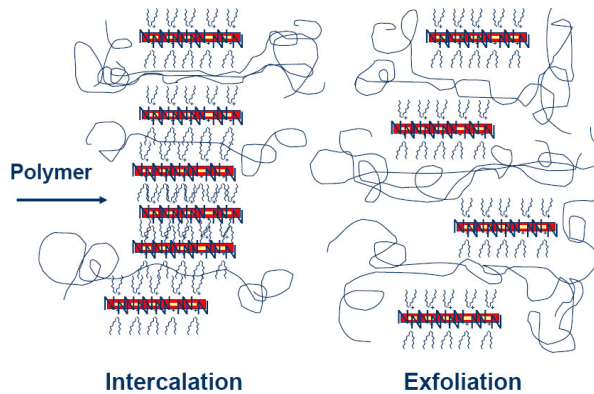


Figure 5: Formation of intercalated and exfoliated nanocomposites from layered silicates and polymers

Unfavorable interactions of clay edges with polymers can be overcome by use of silane (any of a group of silicon hydrides having the general formula SiH_3) coupling agents to modify the edges. These can be used in conjunction with the treated organo-clay. An alternative approach to compatibilising clays with polymers has been introduced by TNO, based on use of block or graft copolymers where one component of the copolymer is compatible with the clay and the other with the polymer matrix.

The correct selection of modified clay is essential to ensure effective penetration of the polymer into the interlayer spacing of the clay and result in the desired exfoliated or intercalated product. Indeed, further development of compatibiliser chemistry is undoubtedly the key to expansion of this nanocomposite technology beyond the systems where success has been achieved to date.

When dispersed in a thermoplastic material (a material that is plastic or deformable, melts to a liquid when heated, and freezes to a brittle, glassy state when cooled sufficiently) nanoclays can give the following performance enhancements:

- increased stiffness and tensile strength, tensile modulus, flexural strength and modulus;
- thermal stability;
- flame retardancy;
- barrier properties to moisture, solvents, gases, water vapour etc

These improvements are more pronounced if the clay platelets are completely exfoliated. Using the same principle, TNO has developed some nanoclay modifications that can be well mixed with bitumen. Similarly bentonite and montmorillonite discs are selected to be used

for this purpose. The developed nanoclay which is also called organoclay can be processed to fit the binder. If the modifier is fully compatible with the binder, it is possible to get a homogeneous distribution of the clay at nano scale within the binder by intensive mixing.

The mixing of a few percentage of nanoclay in bitumen can lead to improvement of properties like strength, durability, thermal stability, resistance against organic solvents. In addition, it can lead to low permeability of oxygen, carbon dioxide, nitrogen and water vapor. However, if the clay platelets are not well dispersed or if the thermoplastic material doesn't fit well between the intercalated or exfoliated platelets then the expected improvements may not be realized.

There is a difference in the structure of bitumen and polymers. It can be said that bitumen is a very complex polymer. The structure of polymers is mostly well defined and it can be altered and tailored to meet the demand where as the structure of bitumen is more complex and not stable. The structure of asphaltenes on a bitumen depends on the chemical composition of the binder and on temperature. In gel type of bitumen, the asphaltenes are highly associated to each other, form net type of network and contain high proportion of asphaltenes. In sol type of bitumen they are not associated to each other, have poor network and lower asphaltene proportions. This complex nature of the bitumen could probably be a drawback to the success of the interaction of bitumen and the clay or it could probably demand a different approach of clay and bitumen interaction or it could probably limit the successes obtained in polymer nanoclay modifications.

2.3 Rheological properties of bitumen binders

2.3.1 Empirical tests

Penetration test:

This test provides a measure of the consistency or hardness of the bitumen. The penetration test is the most common control test for penetration grade bitumen. In this test, a needle of specified dimensions is allowed to penetrate a sample of bitumen, under a known load(100g), at a fixed temperature (25°C), for a known time(5s). The penetration is defined as the distance traveled by the needle into the bitumen and it is measured in tenths of a millimeter (decimillimeter). The lower the value of the penetration the harder the bitumen is and conversely, the higher the value of penetration the softer the bitumen is.

Ring and ball test:

The ring and ball test is a test to determine the temperature at which a specific viscosity of the bitumen is reached at some point during its transition from solid to liquid. In this test, a ball (weight 3.5g) is placed on a sample of bitumen contained in a brass ring that is then

suspended in water bath. The bath temperature is raised at 5°C per minute, the bitumen softens and eventually deforms slowly with the ball moving through the ring. At the moment the bitumen and the steel ball touch a base plate 25mm below the ring, the temperature is recorded. This temperature is designated as the softening point of the bitumen and represents an equi-viscous temperature.

Retained penetration:

When bitumen gets aged it increases its hardness and the retained penetration value helps in checking the increase in hardness in relation to the previous value obtained on unaged material. It is computed as:

$$\text{Retained penetration}(\%) = \frac{\text{aged penetration}}{\text{unaged penetration}} \times 100$$

A lower retained penetration value means that the material is more susceptible to ageing.

Increment in softening point:

Similar to retained penetration value the increment in softening point can be a help in checking susceptibility of the material to ageing. It is computed as :

$$\text{Increment in softening point (}^\circ\text{C)} = \text{aged softening point(}^\circ\text{C)} - \text{unaged softening point(}^\circ\text{C)}$$

A smaller increment in softening point means the material is less susceptible to ageing.

2.3.2 Fundamental Rheological tests by Dynamic Shear Rheometers(DSR)

Visco-elastic behavior of Asphalt binders:

Stress-strain behavior defines the response of materials to load. Materials with time-independent stress-strain behavior can be effectively characterized by their elastic modulus. On the contrary, time-dependent materials that exhibit constant non-zero strain after the stress is removed behave in a viscous fashion. Asphalt binders exhibit aspects of both elastic and viscous behaviors; hence they are called visco-elastic materials. Figure 6 shows a visco-elastic response for a constant load applied at t_0 and removed at t_1 . Visco-elastic materials experience an immediate strain followed by a gradual time-dependent strain increase up to time t_1 . When the load is removed the material experiences a partial immediate strain recovery, followed by a time-dependent strain recovery.

Binders are mostly tested under dynamic conditions by applying sinusoidal shear forces and one of those test types that is used to characterize the visco-elastic behavior of asphalt binders is the DSR (dynamic shear rheometer).

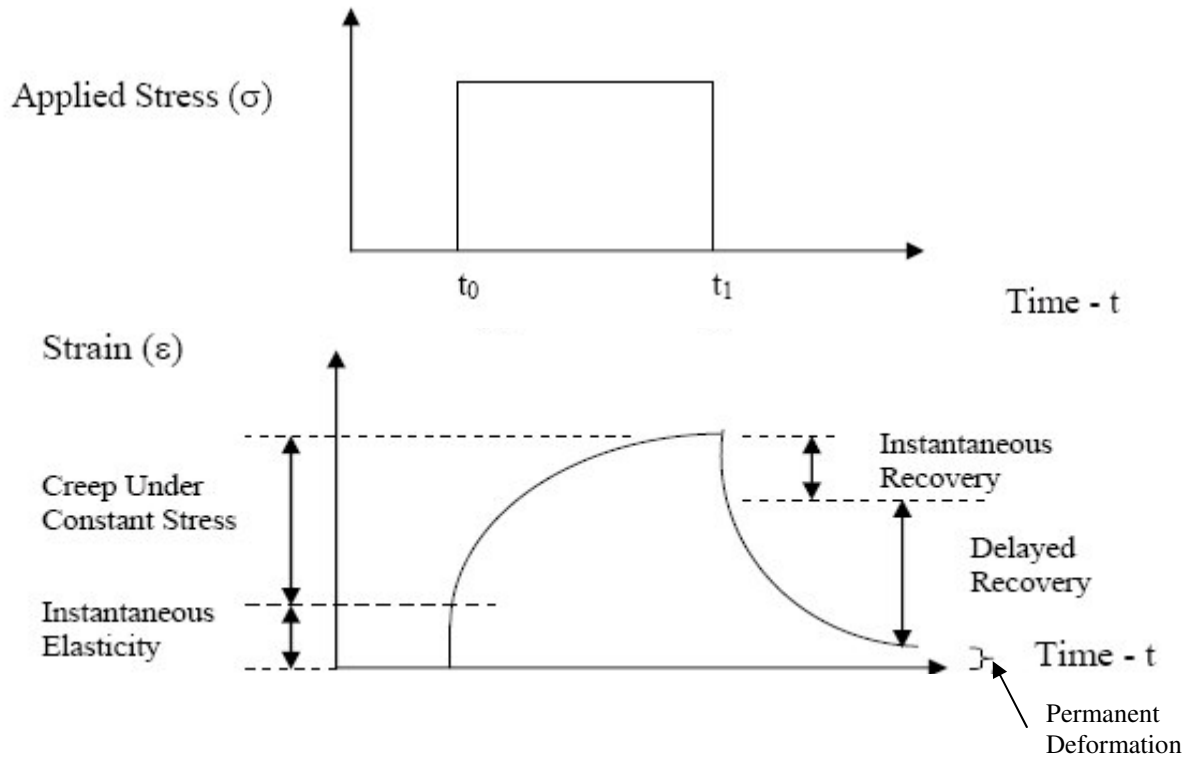


Figure 6: Visco-elastic Materials under Constant Stress Loading

Dynamic Shear Rheometers (DSR):

This type of test applies an oscillatory shear force to a bitumen sample sandwiched between two parallel plates. The typical arrangement of DSR is of a fixed lower plate and an oscillating upper plate through which the shear force is applied to the specimen as shown in figure 7. The centre line of the upper plate described by point A in figure 7, moves to point B then passes through its original position to point C and then returns to point A, representing one cycle. This movement is then repeated continuously throughout the duration of the test. The most common DSR test is strain controlled.

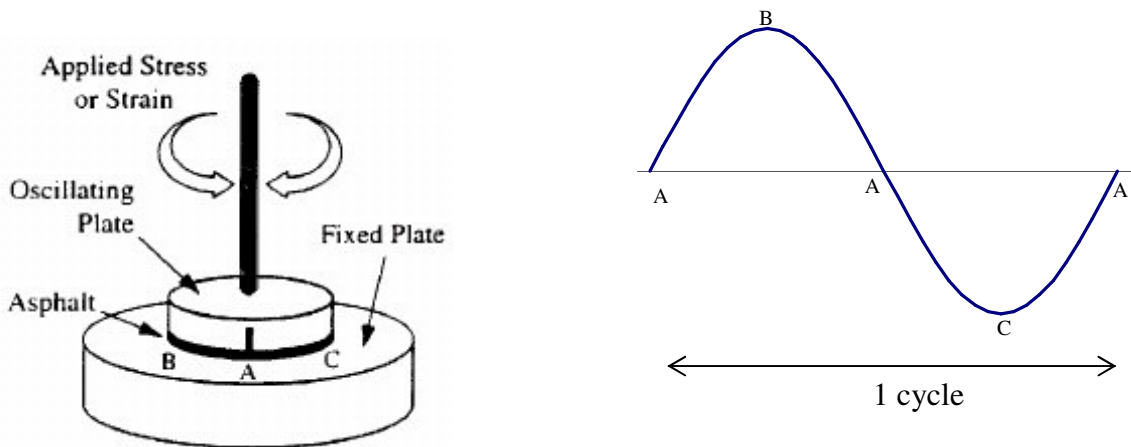


Figure 7 : Dynamic Shear Rheometer

The DSR can be used to characterize both viscous and elastic behavior of bitumen by measuring the complex shear modulus G^* , and the phase angle δ , from a single test run at a given temperature, loading frequency, and strain magnitude as defined by the binder film thickness and the rotation amplitude.

*Dynamic complex shear modulus, G^**

The dynamic complex shear modulus G^* is a measure of the total resistance of the binder to deformation when repeatedly sheared. For visco-elastic materials like bitumen, the complex shear modulus is composed of a loss modulus (viscous component, G'') and a storage modulus (elastic component, G'), the relative magnitude of which dictates how the material responds to applied loads. Materials with higher storage moduli have greater ability to recover from deformation, and materials with higher loss moduli have greater ability to resist deformation at any prescribed frequency. The relationship between the two components is shown graphically in figure 8 and described mathematically below.

$$|G^*| = \frac{\tau_{\max}(f)}{\varphi_{\max}(f)} \quad \text{(Eq.1)}$$

$$\tau_{\max} = \frac{Tr}{J} \quad \text{and} \quad \varphi_{\max} = \frac{\theta r}{h}$$

$$J = \frac{1}{2} \pi R^4 \text{ (circle)}. \quad \text{Hence, } \tau_{\max} = \frac{2T}{\pi r^3}$$

$$\delta(f) = \omega \delta^* \frac{180}{\pi}, \quad G^*(f) = G'(f) + i G''(f), \quad |G^*(f)| = \sqrt{G'(f)^2 + G''(f)^2}$$

$$\omega = 2\pi f \quad G'(f) = G^*(f) \cos \delta(f), \quad G''(f) = G^*(f) \sin \delta(f),$$

$$\delta(f) = \tan^{-1} \left(\frac{G''(f)}{G'(f)} \right)$$

δ = time lag between τ_{\max} and φ_{\max} (sec)

ω = angular frequency

$G^*(f)$ = complex shear modulus at frequency f ,

$G'(f)$ = dynamic storage modulus at frequency f ,

$G''(f)$ = dynamic loss modulus at frequency f ,

$\delta(f)$ = phase angle in degree at frequency f ,

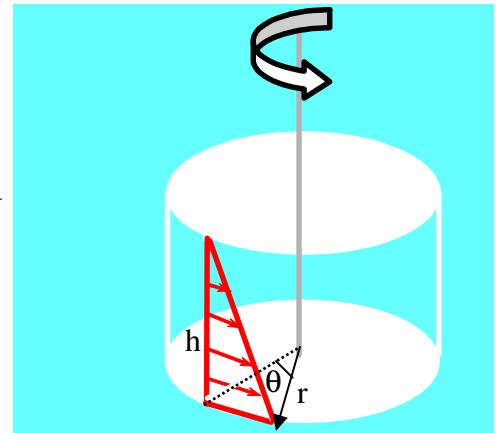
i = complex number (equal to $\sqrt{-1}$).

T = applied torque,

$\tau_{\max}(f)$ = maximum shear stress at frequency f ,

$\varphi_{\max}(f)$ = maximum shear strain at frequency f ,

r = radius of binder specimen (either 4mm, 12.5mm or 20mm)



θ = rotation angle and h = height of specimen (1mm or 2mm)

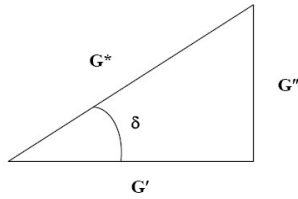


Figure 8: Relationship between G^* , G' , G'' and δ

Phase angle, δ :

The phase angle δ is a measure of the degree of elasticity of the bitumen under the test conditions. The phase angle represents the immediate elastic and the delayed viscous responses of the binder, obtained from the lag between the measured shear stresses and the induced strains. It is shown graphically in figure 9. A purely elastic material would not show any phase difference between the stress and strain whereas a pure viscous material shows a phase angle of 90° or one quarter of a cycle. With viscoelastic materials such as bitumen, the phase angle between stress and strain is between 0° and 90° , depending on the type and grade of bitumen, temperature and frequency. Small phase angles are found at low temperature and high frequency since the bitumen approximates elastic behavior at these conditions and higher values for the phase angle are exhibited at high temperature and lower frequency when the bitumen approximates viscous behavior.

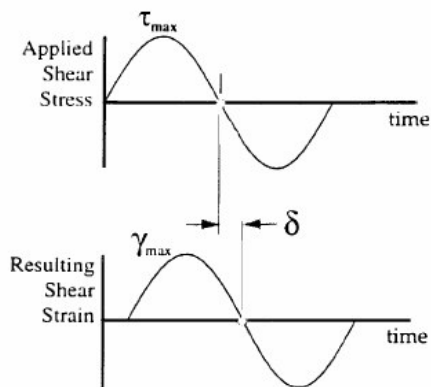


Figure 9: phase angle determination

In addition, DSR tests are usually conducted by inducing small strains (within the linear viscoelastic region) to enable the rheological data to be transposed between different frequencies and temperatures using the time–temperature principle of superposition

Master curve construction:

One is interested to get stiffness and phase angle values in a wide range of temperature and frequency values. It is however not practical to perform test over the entire temperature and frequency ranges. Stiffness/phase angle values covering the entire temperature and frequency

domain however can be obtained by making use of the equivalency principle between frequency and temperature. This equivalency is a result of the thermorheological simple behavior of bitumen, which allows us to construct a master curve relating stiffness to load frequency for a selected temperature. The data at various temperatures are shifted with respect to frequency until the curves merge into a single smooth function. The master curve of the modulus/phase angle, as a function of frequency, formed in this manner, describes the frequency (time) dependency of the material. The amount of shifting at each temperature required to form the master curve describes the temperature dependency of the material. The amount of shifting is performed using one of two common theoretical models. The first and most popular one is Williams-Landel-Ferry (WLF) equation given as :

$$\text{Log } a_t = \frac{-C_1(T-T_0)}{C_2 + (T-T_0)} \quad (\text{Eq.2})$$

Where:

C1 and C2 = constants,

T = measurement temperature (K),

T₀ = reference temperature (K),

a_t = the shift factor value

This equation is favored in the glass transition region.

The second theoretical equation is the Arrhenius equation and it is given as:

$$\text{Log } a_t = \frac{E}{2.303R} \left(\frac{1}{T} - \frac{1}{T_0} \right) \quad (\text{Eq.3})$$

Where

E is activation energy associated with relaxation,

R = gas constant ,

T = measurement temperature,

T₀ = reference temperature and

a_t = the shift factor value

This equation is typically used in the area outside the glass transition, but it can also be used in the glass transition region too.

Temperature dependency of bitumen can be described by the following three phases: a low-temperature region below the defining or glass transition temperature (around -30°C for asphalt binders), an intermediate region in which viscoelastic behavior predominates, and the Newtonian region in which the phase angle approximates 90 degrees. The temperature dependence in both the Newtonian region and the low-temperature region is described by Arrhenius equations. In the viscoelastic region, the Williams-Landers-Ferry (WLF) equation

appropriately describes the temperature dependence of asphalt binder. The shift factor model used in this study work is WLF.

2.4 Performance related tests on Asphalt Mixtures

A number of tests are performed in this study work to characterize and compare the mechanical properties of the standard and 6% cloisite modified asphalt mixtures. The tests selected to compare the two mixture types in this study are: indirect tensile strength test, diametral resilient modulus test, unconfined repeated load deformation and stress controlled fatigue test. A description of each of these tests is given below.

2.4.1 Indirect Tensile Strength Test

The indirect tensile strength test is one of the most popular tests used for asphalt mixture characterization. It is used to determine the indirect tensile/ splitting strength of asphalt mixture specimens. In this test, a cylindrical specimen is loaded diametrically in compression creating a somewhat uniform tension zone along the specimen's loaded diameter (fig 10). It is measured by loading the specimen at a constant strain rate until it fails by splitting along the diametral axis.



Figure 10: indirect tensile strength test

The horizontal tensile stress at the center of the test specimen is calculated using equation 4

$$\sigma_t = \frac{2F_{\text{peak}}}{\pi DT} \quad (\text{Eq.4})$$

Where

F_{peak} =compression load at failure,

D = diameter ,

T = thickness of the specimen.

2.4.2 Indirect Tensile Resilient Modulus Test

Flexible pavement design methods based on elastic theories require that the elastic properties of the pavement materials be known. Among the common methods of measurement of elastic properties of asphalt mixtures, the resilient modulus is more appropriate for use in multilayer elastic theories. In addition, the use of the resilient modulus provides a basis for comparison of changes in material stiffness at different temperatures for different mixture types. Hence, values of the resilient modulus can be used in two ways: to evaluate the relative quality of materials and as an input value for pavement design, evaluation, and analysis. The resilient modulus measured in the indirect tensile mode has been selected by most engineers as the way to measure the resilient modulus of asphalt mixtures.

The test equipment for determining the resilient modulus includes an indirect tensile test apparatus, a repetitive loading mechanism, a temperature controlled chamber for maintaining constant temperature during the test, and a measurement system (e.g., load cell and deformation sensors). The test is conducted on a cylinder shaped specimens placed on its side on a curved loading strip (the curvature of the loading strip is the same as that of the specimen). The cyclic load is applied along the vertical diameter of the specimen and the resulting deformations along the horizontal diameters are measured. For this case, a value of Poisson's ratio has to be assumed prior to the analysis of the data. The test setup and stress distribution along the horizontal and vertical direction along the diameter is shown in fig 11.

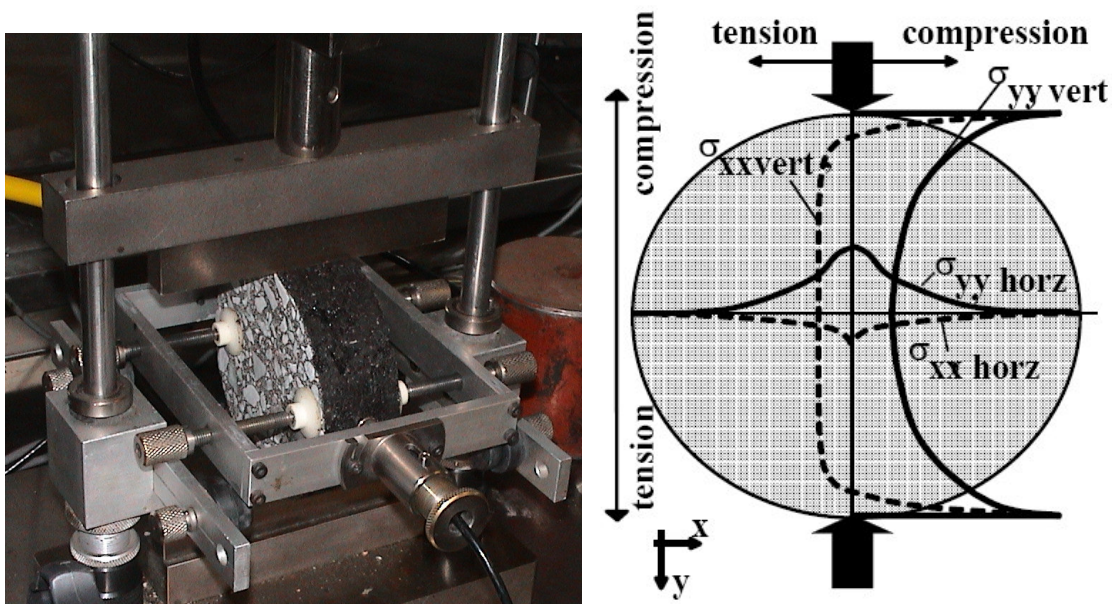


Figure 11: Indirect tension test, set-up (left) and stresses along the vertical and horizontal cross section

Using the principle of plane stress elastic theory for homogeneous and isotropic materials, the resilient modulus is calculated as:

$$E_r = \frac{F_{\text{peak}}}{\Delta H_t t} (0.27 + \nu) \quad (\text{Eq.5})$$

Where ,

E_r = resilient modulus,

F_{peak} = peak force ,

ν = poisson ratio ,

t = thickness

Equation 5 is developed based on the assumption that the material is homogenous, isotropic and linearly elastic. Asphalt mixtures are non - homogenous and it is doubtful that an asphalt mixture would be isotropic if the compaction effects (hence orientation) of the aggregates are considered. However, the assumption of an elastic response is reasonable if the tests are conducted in the linear viscoelastic range using a loading rate which produces low permanent deformations.

The most important factors that influence the resilient modulus are temperature, frequency of loading and air-voids. Lower temperatures, higher rates of loading and higher viscosity of bitumen result in higher resilient moduli. In addition, resilient modulus results are affected by rest period (which becomes negligible when the ratio of rest period over load duration exceeds 8) sample size (including diameter and thickness) and most importantly Poisson's ratio.

When using equation 5 to determine the resilient modulus, researchers normally assume a value of 0.35 for the Poisson's ratio of the mixture. Poisson's ratio is dependent on the binder properties, mixture composition, test frequency and the test temperature. However, the effect of the above factors has not been firmly established. Small changes in the assumed Poisson's ratio have little practical effect on the modulus. Ratios 0.3 to 0.4 are generally assumed when determining the resilient modulus although the values can vary 0.2 to 0.5. The reason why Poisson's ratio is not determined from the results is because the vertical resilient deformation is not measured. By means of using extra instrumentation this problem can be overcome but this was not done for the tests as performed.

The recommended load range for the resilient modulus test according to the ASTM D4123 standard, is 10 to 15 percent of the tensile strength

Master curve construction:

Similar to the case of the binder, master curve construction for the resilient modulus of the mixture is of importance to get stiffness value covering the entire domain of temperature and loading time(frequency).The shifting factor can be computed by WLF or Arrhenius equations and the fitting model can be a polynomial, sigmoidal or any other model. But better fitting

can be obtained by sigmoidal model (Medani, 2003). For details, the reader is referred to section 6.2.5

2.4.3 Indirect Tensile Fatigue Tests

Fatigue cracking is a major load-associated failure mode for asphalt pavements. This distress involves the progressive formation of cracks under repetitive loadings. As the number of loads increases, the crack propagates through the pavement layer, producing a crack in the pavement. In practice failure in fatigue is generally defined as the point when a given percent of the surface area becomes covered with fatigue cracking.

There are many different test methods for determining the fatigue properties of asphalt mixtures in the laboratory. Some of the tests are stress controlled and others are strain controlled. The fatigue life for the different types of tests can be different due to: difference in loading type, difference in geometry of specimens to be tested and difference in stress development within the specimens. Studies done on fatigue life have proven that the fatigue life determined for strain controlled tests is higher than those of the stress controlled tests. In addition, laboratory determined fatigue relationships generally predict failure much sooner than is observed in field performance studies. The reason is that fatigue life is a function of stress distribution and boundary conditions which is different for laboratory specimens than for asphalt pavements. However, the laboratory fatigue life allows us to make comparisons of the fatigue performance characteristics of various mixtures.

In the indirect tensile fatigue test (ITT fatigue), the fatigue life of a material is defined as the number of load cycles to specimen fracture. Each specimen is subjected to a different level of stress so that a range of values is obtained for N_f (number of cycles till failure). This range allows the development of the classical fatigue relationship between N_f and σ (stress) on a log –log model form as shown in figure 12 and mathematically expressed by equation 6.

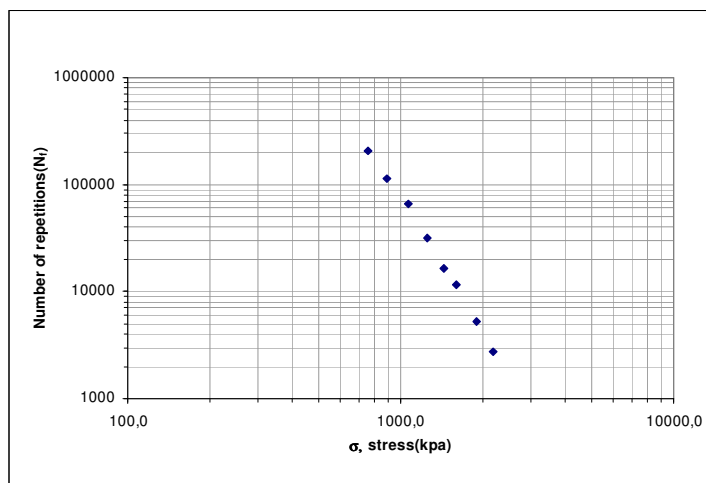


Figure 12: stress versus number of load repetitions

$$Nf = k_1 * \left(\frac{1}{\sigma} \right)^{k_2} \quad (\text{Eq.6})$$

Where: N_f = the number of load applications to fatigue life;

σ = applied radial stress

k_1, k_2 = material characteristics

For asphalt mixtures, as for most other materials, fatigue life steadily increases with decreasing stress or strain amplitude. If however the reduced tensile strains are purely elastic (which might occur at low temperatures and/or high frequencies) then no fatigue failure might occur. In general, stresses at or below the fatigue limit cause only elastic strains. It should be emphasized that in the indirect tensile fatigue test, plastic strain is ultimately responsible for fatigue damage and the consequent fatigue failure. As mentioned before a perfectly elastic material will never experience any fatigue damage regardless of the number of load applications.

The ITT fatigue test set-ups are very similar to that used for determining the resilient modulus by using the indirect tensile test. First, a sustained load is applied to prevent the separation between the loading piston and the specimen and then a cyclic load type can be applied with the selected frequency and load function type.

2.4.4 Cyclic Uniaxial compression Test

Permanent deformation in paving materials develops gradually with increasing numbers of load applications. Usually appears as longitudinal depressions in the wheel paths some times accompanied by small upheavals to the sides. In pavement structures, the total permanent deformation is summation of permanent deformation of all layers.

Asphalt concrete pavement permanent deformation (rutting) prediction has traditionally been based upon purely-empirical and phenomenological-empirical materials testing and road modeling techniques. However, the ever increasing number and weight of the traffic loads, the use of road materials with enhanced characteristics and the aging diversity of the road network are beyond the inference space of traditional empirical and phenomenological-empirical rut prediction models. This necessitates knowledge of the mechanical properties of the materials and the permanent deformation characteristics of asphalt mixtures.

To meet this requirement, different experimental tests can be proposed. A repetitive uniaxial compressive load on cylindrical specimens of asphalt concrete provides a reasonable simulation of asphalt pavements subjected to repetitive heavy axle loads. The set up used for this test is given in figure 13.

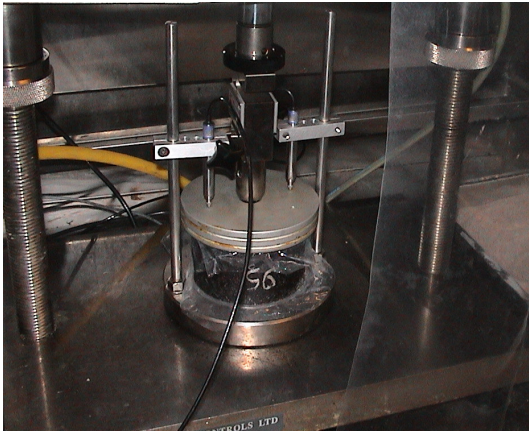


Figure 13: unconfined cyclic compression test

The following parameters need to be considered properly to get the desired failure type and minimize undesired effects.

Alignment of the specimen:

The alignment of the setup should be such that the loading plates are in a perfectly horizontal position and the load cell is in the center of the specimen during the test.

Friction:

Friction between the loading plates and the specimen can have a significant disturbing effect on the state of stress in a specimen, since it restrains the deformations. In a compression test, friction depends on the contact between specimen and loading plates. During the test, the specimen deforms in radial as well as in axial direction. At the contact surface between specimen and the loading plates, the radial deformation can be restrained due to friction. The resulting friction acts as a confinement for the top and bottom of the specimen, causing the well-known barrel-shape of specimens in compression. To avoid this type of failure and to get uniform compression deformation of the specimen, a friction reduction is required on the top and bottom part of the specimen.

Temperature gradient:

The temperature gradient between the bottom part and top part of the specimen should be minimized to zero so as to minimize its effect on the state of the stress on the specimen. This can be done by having uniform temperature distribution in the testing cabinet and by keeping the specimen and the loading plates within the test cabinet for long time so as all reach the target temperature.

The primary factors affecting permanent deformation are found to be temperature, number of load applications or time of loading, mixture properties, and the state of stress. Based on the values of these parameters one can have different shapes of the graph representing the development of cumulative permanent strain as a function of the number of load cycles.

A typical relationship between total cumulative permanent strain and the number of load cycles is given in fig. 14.

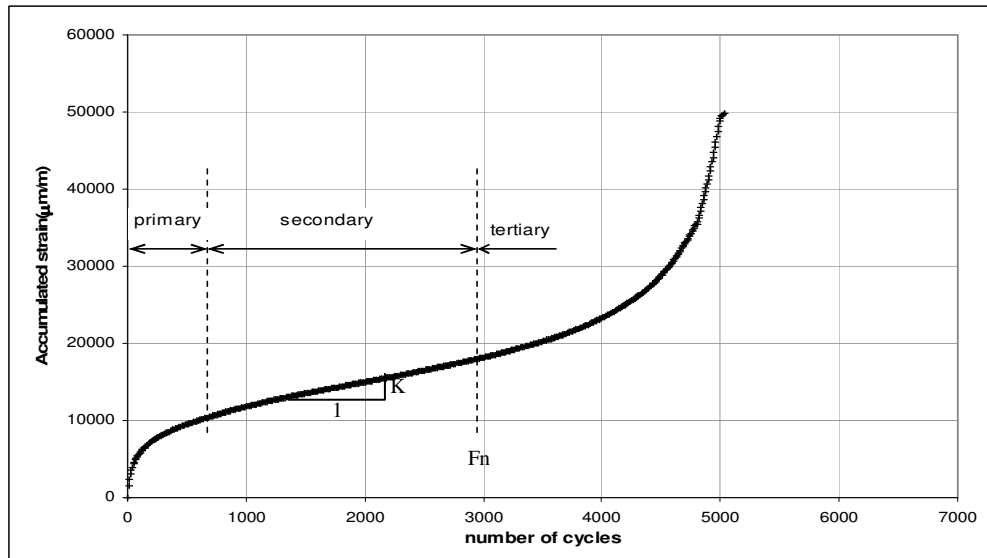


Figure 14: Typical relationship between cumulative permanent axial strain and number of cycles

This test result indicates that the accumulated permanent axial strain undergoes three distinct stages with increasing number of cycles. The three stages are: the primary, secondary and tertiary stage.

Primary stage:

Under the initial load application, a relatively large deformation develops during a short period of time and it is followed by a rapid decrease in the rate of deformation with an increased number of cycles. The highest rate of deformation can be due to irregular surface of the sample which leads to stress concentrations at relatively elevated points or it can be due to densification of the mix. The rapid decrease of the rate of deformation can be due to the change in the microstructure of the asphalt mixture associated with the aggregate reorientation which leads to a dense mixture with increased resistance to deformation.

Secondary stage:

During the secondary stage, the rate of accumulation of permanent deformation remains constant. Surface irregularities are no longer a factor because the load application during the primary stage flattened the surface. The permanent deformation during this stage is mainly caused by shear flow.

The rate of deformation during the secondary stage (**K**) is one of the main indicators of rutting susceptibility of asphalt mixtures.

Tertiary stage:

In the final stage, the rate of deformation accelerates until complete failure takes place. This stage is usually associated with the formation of cracks. The start of the tertiary stage is usually represented by the **flow number Fn**. This number is used as a rutting resistance indicator of asphalt mixtures.

3 Testing Preparations and Programs

In this chapter the testing programs on the nanoclay modifiers, the rheology of the modified and unmodified binders and the asphalt mixtures are described. In addition, the different preparations done for the different tests and specially for the preparations of the asphalt mixture specimens and their physical characteristics are described in this chapter.

3.1 Testing program on nanoclay modifiers

Different tests were performed on the nanoclay modifiers in order to get some knowledge about them at nanoscale level, to have some idea on their composition and to check their consistency. The tests performed comprise:

- i. **X- ray analysis:** the following two types of x-ray analyses were performed on the nanoclay modifiers in order to get information about their composition.
 - a. *Qualitative wavelength dispersive spot analyses:* this test was performed to get a qualitative analysis about the elemental composition of the nanoclay modifiers.
 - b. *X-ray diffraction:* this test was performed to get the chemical composition of the compounds of the nanoclay. This is done by determining the crystal shape of the nanoclay compounds through the test and correlating them with close match compounds from the library.
- ii. **Microscopic analysis:** this test was performed to get insight on the size, shape, arrangement and interaction of the particles of the nanoclay modifiers at nanoscale level.
- iii. **Plastic limit:** this test was performed to get some information on the consistency behavior of the nanoclay modifiers.

3.2 Testing program on rheological tests of modified and unmodified binders

The rheological testing program comprises of two sections: empirical rheological analysis and fundamental rheological analysis. The empirical rheological analysis is based on penetration and softening point tests, and the fundamental rheological analysis is based on Dynamic Shear Rheometer measurements. These two types of tests were performed on virgin (un-aged), short term aged and long term aged samples of the modified and unmodified bitumen.

Short ageing was carried out with the Rotating Cylindrical Ageing Tester (RCAT) and the long term ageing was performed with RCAT and pressure ageing vessel (PAV).

RCAT short term ageing :

The RCAT test was performed for 4 hours @ 163 °C in air atmosphere at 240l/h pressure.

RCAT Long term aging:

The test was performed for 140 hours @ 90 °C in oxygen atmosphere at 4l/h pressure.

PAV Long term aging:

These tests were performed for 20 hours @90°C and 2.1Mpa pressure in air atmosphere.

The difference in RCAT long term ageing and PAV ageing is the fact that in RCAT we have a rolling material; but in PAV the material is static. RCAT results might be influenced by difference in viscosities.

3.2.1 Empirical rheological testing program

Different types of modified and unmodified binders were considered for the empirical rheological tests. In addition, different ageing stages and ageing types are taken into account. Table 1 summarizes the testing program with the empirical tests performed.

Tests	Stages of ageing for measurements				
	Fresh material	After 1 hour high shear mixing	RCAT short term	RCAT long term	PAV long term
Rheoloical Tests	<i>40/60</i>	<i>40/60</i>	<i>40/60</i>	<i>40/60</i>	<i>70/100</i> <i>70/100</i> <i>70/100+6%N</i>
	<i>70/100</i>	<i>70/100</i>	<i>70/100</i>	<i>70/100</i>	
		<i>40/60+C*</i>	<i>40/60+C</i>	<i>40/60+C</i>	
		<i>70/100+6%N*</i>	<i>70/100+6%N</i>	<i>70/100+6%N</i>	
Softening point	<i>40/60</i>	<i>40/60</i>	<i>40/60</i>	<i>40/60</i>	<i>70/100</i> <i>70/100</i> <i>70/100+6%N</i>
	<i>70/100</i>	<i>70/100</i>	<i>70/100</i>	<i>70/100</i>	
		<i>40/60+C*</i>	<i>40/60+C</i>	<i>40/60+C</i>	
		<i>70/100+6%N*</i>	<i>70/100+6%N</i>	<i>70/100+6%N</i>	

C*= Cloisite and the amount of cloisite considered are 3% and 6% ; N* = nanofill

Table 1: Empirical rheological testing program

The empirical tests are performed according to the standard test procedures. In the penetration test an automatic timing device and digital reading is used, which is more reliable in accuracy and repeatability than manual timing and reading. In addition the softening point is measured with an apparatus, which ensures close temperature control and automatic recording of the test results. These tests were performed in the laboratory of Q8 Petroleum Research and Technology by Jeroen Besamusca and Jeroen Noordergraaf.

3.2.2 DSR testing program

DSR measurements were done over a wide temperature range of -15 C to 100 C. This was done in order to get a good knowledge of the rheological properties of the modified and unmodified binders over a wide temperature ranges. Different sizes of plate diameters and different thickness of binders are considered for the different test temperatures. This is necessary to get a good DSR measurements and results. The selection of the diameter sizes and thickness of the binders is based on the expected stiffness of the binders in the test temperature ranges, on preliminary testing and on past experience with the DSR device. Based on these grounds, it was decided to use the smaller diameter plates for the lower temperature range, the medium diameter plate for medium temperature ranges and the larger diameter for the higher temperature ranges. The sizes of the plates are 8mm, 25mm and 40 mm. The standard thickness of the binder for the different plate sizes are: 2mm for the 8mm diameter plate and 1 mm for the 25 and 40mm plates.

In addition, the DSR tests were performed in constant shear strain mode and the strain level was selected in relation to the values of the test temperature in order to prevent non-linear effects due to too high strain levels. The range of loading frequency selected for the test is in the range of 0.016 – 20hz and the ranges considered varies a bit based on the values of the test temperatures.

The different ageing steps and the different modified and unmodified binders considered for the DSR test are summarized in table2.

Tests	Stages of aging for measurements				
	Fresh material	After 1 hour high shear mixing	RCAT short term	RCAT long term	PAV long term
DSR test @ 3 temperature ranges	40/60 70/100	40/60 70/100 40/60+C* 70/100+6%N*	40/60 70/100 40/60+C 70/100+6%N	40/60 70/100 40/60+C 70/100+6%N	70/100 70/100 70/100+6%N

C*= Cloisite and the amount of cloisite considered are 3% and 6% ; N* = nanofill

Table 2: DSR testing program

In the DSR tests, some overlap of test temperatures were considered between the tests performed by the different sizes of plates. For instance, measurements at 5° C and 10°C were done with plate sizes of 8 mm and 25 mm and measurements at 50°C and 60°C were done with 25mm and 40mm plate sizes. The reason behind this is to see the effect of plate size on

the test results and in addition to check the efficiency of each plate on the selected test temperature range.

The input parameters and the test configuration with DSR measurement is given in table 3.

Temperature range (°C)	Low: -15°C – +10°C	Medium: +5°C – +60°C	High: +50°C - + 100°C
Frequency ranges (Hz)	0.016 - 20	0.016 - 20	0.5 - 20
DSR test Configuration	8 mm diameter plate 2 mm gap	25 mm diameter plate 1 mm gap	40 mm diameter plate 1 mm gap
Temperatures and frequencies	Decided on experience and during testing		
Type of loading	Constant strain (level dependent on temperature range)		

Table 3: DSR input parameters and test configuration

3.3 Specimen preparation and testing program of asphalt mixtures

This section discusses the making of dense mixture specimens, the characterization of the specimens and the preparation of the specimens for the different tests. In addition the testing program of the tests performed on the dense asphalt mixtures is presented here.

3.3.1 Specimen preparation

The specimens prepared for the different tests are marshall tablets with an average thickness of 60 – 65mm. In this section, the composition and the different inputs used in the preparation of the standard and 6% cloisite modified dense Marshall specimens is discussed below.

3.3.1.1 Composition of dense mixture:

The aggregate used in the preparation of specimens is Norwegian granite and the composition of the dense mixture is given in table 4

Component type	% [weight/(total weight of aggregates)]	% of components	weight of components
22.4 - 16	0,0%	0,0%	0,0
16 - 11.2	11,5%	10,8%	132,3
11.2 - 8	10,5%	9,9%	120,8
8 - 5.6	11,5%	10,8%	132,3
5.6 - 2 (8/4 and 6/2)	20,8%	19,6%	239,2
crushed sand	39,0%	36,8%	448,5
Wigro filler	6,7%	6,3%	77,1
*Binder	6,0%	5,7%	69,0
	106,0%	100,0%	1219,0

* binder = 40/60 for standard mixture and binder = 40/60+ 6% cloisite for modified dense mixture

Table 4: Composition of dense mixture

3.3.1.2 Control parameters in specimen preparation:

Due to its high viscosity, the 6% cloisite modified binder is not fluid enough at the normal mixing temperature used for the standard binder (170°C). Hence, a high mixing temperature is needed for the preparation of the modified mixtures. The mixing temperature and other input parameters considered in the preparation of the mixtures are given in table 5.

Mixture Type Conditions	Standard mixes	6% cloisite modified mixes
Temperature of binder	170°C	185°C
Temperature of aggregates	170°C	185°C
Compaction	2 x 75 marshal compaction	2 x 75 marshal compaction
Storage of specimens before tests	Minimum 7 days	Minimum 7 days

Table 5: Input parameters in specimen preparation

In table 5, compaction of dense mixture specimens is 2 x 75 blows and this is because the dense mixture studied in this work is for airfield pavements (Schiphol). People from Schiphol showed interest in the clay modified mixtures as an alternative for polymer modified mixtures.

3.3.2 Physical Properties of the specimens

In this part, a summary of the important physical properties of the specimens of the standard and modified dense mixture is presented.

3.3.2.1 Typical properties of 6% cloisite modified specimens:

Typical observations noticed during the preparation of the 6% cloisite modified specimens are:

- the modified binder has different smell ;
- 6 % cloisite modified binder heated @185°C is even more viscous than standard binder heated @ 170°C when it flows out of the heating pan;
- the mixtures of the modified binder are relatively less sticky to the mixing pan, to the molds, and to the aluminum foil as compared to the specimens of the standard mixes.

3.3.2.2 Density of specimens:

Two types of densities were computed in this section. The first one is the theoretical maximum density (TMD) computed based on the TMD of the components. This is the same for all specimens of the same mixture type. The second density is the actual density which is

specific for each specimen. Those two values are the main input parameters in the void content computation too.

Theoretical maximum density (TMD):

The theoretical maximum density (TMD) of the different aggregate components and bitumen was pre-determined. Based on the TMD values of the components, the TMD of the different mixture types is computed. The TMD value of the different mixture components is given in table 6.

Material	size	Theoretical maximum density (TMD)	Description
Aggregate	2-5.6 (4/8 and 2/6)	2781,0	Aggregate type 1
	5.6-8	2765,0	Aggregate type 2
	8-11.2	2762,0	Aggregate type 3
	11.2-16	2774,0	Aggregate type 4
sand	—	2677,0	
Wigro -filler	—	2750	
Bitumen 40/60	—	1035,0	Standard bitumen

Table 6: Theoretical maximum Density of mixture components

The theoretical maximum density of the mixtures is computed based on the TMD of the components and is computed as shown in Equation 7:

$$TMD_m = \frac{Pg_1 + Pg_2 + Pg_3 + Pg_4 + Ps + Pf + Pb}{\frac{Pg_1}{TMD_{g_1}} + \frac{Pg_2}{TMD_{g_2}} + \frac{Pg_3}{TMD_{g_3}} + \frac{Pg_4}{TMD_{g_4}} + \frac{Ps}{TMD_s} + \frac{Pf}{TMD_f} + \frac{Pb}{TMD_b}} \quad (\text{Eq 7})$$

Where :

- TMD_m = theoretical maximum density of the mixture;
- Pg₁, Pg₂, Pg₃, Pg₄, = proportion of aggregate types 1,2,3 and 4 in the mixture respectively (see table 6 for type of aggregates);
- Ps, Pf, and Pb = proportion of sand, filler and bitumen in the mixture;
- TMD_{g1}, TMD_{g2}, TMD_{g3}, TMD_{g4} = are theoretical maximum density of aggregate types 1,2,3 and 4 (see table 6 for type of aggregates);
- TMD_s, TMD_f, TMD_b = theoretical maximum density of sand, filler and bitumen.

The theoretical maximum density of the 6% cloisite modified binder is a bit different than the TMD of the standard binder and it is computed as :

$$TMD_{cb} = \frac{P_c + P_b}{\frac{P_c}{TMD_c} + \frac{P_b}{TMD_b}} \quad (\text{Eq 8})$$

Where : TMD_{cb} = theoretical maximum density of cloisite modified bitumen;

P_c, P_b = proportion of cloisite modifier and bitumen in the modified binder respectively;

TMD_c, TMD_b = theoretical maximum density of cloisite modifier and bitumen respectively.

Using Equation 8, the computation of TMD_{cb} is summarized in table 7.

No.	Material	Theoretical maximum density (TDM)	Proportion(%)	$\frac{P}{TMD}$
1	Cloisite modifier	2600	6%	0,002307692
2	Bitumen 40/60	1035	94%	0,090821256
Sum	-	-	100%	0,093128948
TMD_{cb}	-	1073.8		

Table 7: Theoretical maximum Density of Cloisite modified bitumen

Using the above equations and input values, the computation of theoretical maximum density of the standard and 6% cloisite modified dense asphalt mixture is summarized in table 8

Component type	TMD	% of components	$\left[\frac{P}{TMD} \right]_s$	$\left[\frac{P}{TMD} \right]_c$
22.4 - 16	0,00%	0,0%	-	-
16 - 11.2	2774	10,8%	0,003910979	0,003910979
11.2 - 8	2762	9,9%	0,003586409	0,003586409
8 - 5.6	2765	10,8%	0,003923709	0,003923709
5.6 - 2 (8/4 and 6/2)	2781	19,6%	0,007055966	0,007055966
crushed sand	2677	36,8%	0,013743912	0,013743912
Wigro filler	2750	6,3%	0,002298456	0,002298456
Binder 40/60	1035	5,7%	0,005468964	
Binder 40/60 + 6%C	1073,7	5,7%		0,005271843
sum		100,00%	0,039988395	0,039791274
*TMD_m	2500,73			
*TMD_{cm}	2513,11			

* TMD_m, TMD_{cm} = theoretical maximum density of standard mixture and cloisite modified dense mixture respectively,

Table 8: Theoretical maximum Density of standard and 6% cloisite modified mixtures

Actual density (D_s):

The actual density of the specimen is the real density and it is specific for each specimen. In case of dense mixtures the actual density is computed as:

$$D_s = \frac{A}{B - C} \quad (\text{Eq 9})$$

Where: D_s = actual density of specimen;

A = dry weight of specimen in air;

B = surface dried (towel dried) weight of specimen in air;

C = weight of specimen in water.

The actual density is computed for each specimen and it is given in tabular form in the appendix B. Here the average density value of the different specimens selected for the different tests is reported.

Specimens of :	Average Actual Density	
	Standard Dense Mix	6% cloisite modified Dense MIX
Before sawing/polishing		
All	2440,7	2423,4
Dynamic creep test	2439,4	2422,0
Resilient modulus	2440,8	2420,1
indirect tensile test	2440,2	2426,8
fatigue resistance test	2442,2	2424,6
after sawing/polishing		
All	2442,6	2425,6
Dynamic creep test	2444,6	2430,1
Resilient modulus	2441,5	2420,3
indirect tensile test	2442,7	2427,5
fatigue resistance test	2441,9	2424,5

Table 9: Average Actual Density values of modified and unmodified specimens

3.3.2.3 Void content of specimens

Void content of the specimens is computed as given in equations below.

$$VC = \frac{V_m - V_{g+b}}{V_m} \quad (\text{Eq 10})$$

$$V_t = \frac{M}{D_s}, \quad V_{g+b} = \frac{M}{TMD} \quad (\text{Eq 11})$$

$$VC = \frac{\frac{M}{D_s} - \frac{M}{TMD}}{\frac{M}{D_s}} = \frac{1}{D_s} - \frac{1}{TMD} = \frac{TMD - D_s}{TMD} \quad (\text{Eq 12})$$

Where: VC = void content;
 Vm = volume of the mix;
 Vg+b = volume of aggregate + bitumen;
 M = mass of specimen, Ds and TMD as defined before.

The average void content is reported here, but the detailed part is given in the appendix B.

Specimens of :	Average void content (%)	
	Standard Dense Mix	6%cloisite modified Dense MIX
Before sawing/polishing		
All	2,40%	3,57%
Dynamic creep test	2,45%	3,63%
Resilient modulus	2,39%	3,70%
indirect tensile test	2,42%	3,43%
fatigue resistance test	2,34%	3,52%
after sawing/polishing		
All	2,32%	3,48%
Dynamic creep test	2,24%	3,30%
Resilient modulus	2,37%	3,69%
indirect tensile test	2,32%	3,41%
fatigue resistance test	2,35%	3,53%

Table 10: Average void content of modified and unmodified specimens

From table 10 it can be observed that the 6% cloisite modified dense mixture has higher void content values as compared to standard dense mixture.

3.3.3 Pre-treatment of specimens before test

After preparation of the marshall tablets, the specimens were sawed or sawed and polished to the required thickness before doing any test. The thickness and treatment types done for the specimens of each test type is summarized in table 11.

Test Type	Thickness(mm)	Treatment Type
Dynamic creep test	55	Sawing and polishing
Resilient modulus	35	Sawing
indirect tensile test	35	Sawing
fatigue resistance test	35	Sawing

Table 11: Pre-treatment of specimens before test

3.3.4 Testing program on dense asphalt mixtures

The tests performed on the modified and unmodified dense asphalt mixtures are: indirect tensile strength, resilient modulus test, dynamic creep test and fatigue resistance test. All these tests were performed in closed temperature controlled cabinets. In addition, all specimens selected for the different tests were stored in a temperature controlled cabinets to the target temperature for a minimum of three hours before commencing any test. Indirect tensile strength test, resilient modulus test and fatigue resistance test are performed by indirect tensile test with diametral load on the marshall tablets. The dynamic creep test is performed using cyclic uniaxial unconfined compression tests on cylindrical specimens.

3.3.4.1 General testing program

The generalized testing program on the modified and unmodified dense asphalt mixtures is summarized in table 12.

No.	Test Type	Number of specimens tested									Total	
		Temperature										
1	Dynamic Creep Test	40°C			50°C			60°C			27	
		Loading type			Loading type			Loading type				
		I	II	III	I	II	III	I	II	III		
		3	3	3	3	3	3	3	3	3		
2	Fatigue Resistance Test	Temperature									16	
		5°C				20°C						
		8				8						
3	Resilient Modulus Test	frequency = 8, 4,2 , 1 , 0.5Hz									15	
		Temperature										
		5°C		12,5°C		20°C		27,5°C		30°C		
		3		3		3		3		3		
4	Indirect Tensile Strength	Temperature									5	
		5°C		12,5°C		20°C		27,5°C		30°C		
		1		1		1		1		1		
Total											63	

Table 12: Number of specimens tested for the different tests

As can be seen from table 12, in total 63 specimens of standard dense asphalt mixture and 63 specimens of 6% cloisite modified dense asphalt mixture were tested.

3.3.4.2 Indirect tensile strength testing program

The indirect tensile strength test is performed with hydraulically controlled MTS (Material Testing System) machine which has a maximum loading capability of 50KN compressive force. The testing equipment is equipped with a software which is capable of scanning data of more than 100HZ(amount of data that can be measured or recorded per second).

The control and input parameters used in the indirect tensile strength testing program are given in table 13.

Control parameters	Type	Values/Description
Loading	mechanism	Static indirect tensile test
	control	Displacement controlled
	speed	Marshall speed :0.85mm/s
Measurement type	Load	Compressive force
	Displacement	Horizontal and vertical displ.
Specimen size	thickness	35mm
	diameter	101.6mm
Test temperature	-	5, 12.5, 20,27.5, 35°C
Failure type	-	Diametral crack
Test termination	-	After specimen failure

Table 13: Testing input and control parameters for indirect tensile strength

3.3.4.3 Resilient Modulus testing program

The resilient modulus test is performed using the UTM (Universal Testing Machine), which is servo-pneumatic testing device. The UTM is equipped with a cell which translates the measured signal to digital one and in addition it has a personal computer with software programs for test control, data acquisition and output result display. The load is distributed over the specimen by a metal strip with a width of 12.5mm.

The pulse load selected for the test is a half sine with a rest period to approach the practical situation and preconditioning is applied to make sure that the loading strip has a proper seat on the specimen before the test is performed. The nature of the preconditioning loading pulses is similar to the testing load pulses.

The load pulse width, rest period and the pulse period are related as:

Pulse period (Tt) = pulse width(Tp) + rest period (Rt) . Figure 15 shows the load pulse

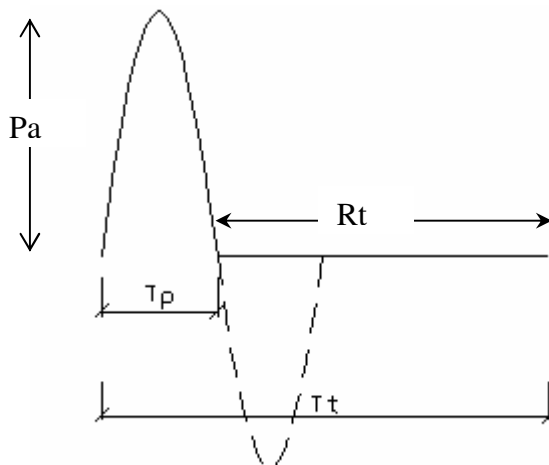


Figure15: half sine loading pulse in resilient modulus test using ITT

The control and input parameters used in the resilient modulus testing program are given in table 14.

Control parameters	Type	Values/Description
Loading	Mechanism	dynamic indirect tensile test
	Number of pulses	5
	Pulse form	Half sine with rest period
	Pulse width	63,125,250,500,1000ms
	Pulse period	*
	Pulse amplitude	**
Preconditioning pulses	-	Similar to loading pulses
Poisson' ratio	-	Assumed 0.35
Measurement type	Load	compressive force
	Displacement/strain	Recoverable horizontal disp./strain
Specimen size	Thickness	35mm
	Diameter	101.6mm
Test temperature	-	5, 12.5, 20,27.5, 35°C
Failure type	-	Non destructive
Test termination	-	After 5 pulses

* see table 15, ** see table 16

Table 14: Testing input and control parameters for Resilient modulus test using ITT

The values of T_p and T_t are selected in such a way that $T_t/T_p = 10$. The values of T_p and T_t used in the ITT test are given in table 15.

Frequency (Hz)	T_p (ms)	T_t (ms)
8	62.5	630
4	125	1250
2	250	2500
1	500	5000
0.5	1000	10000

Table 15: Loading pulse in resilient modulus test using ITT

The loading pulse amplitude (Pa) varies depending on the test temperature and type of asphalt mix. To avoid internal damage usually a value of about 10% of the specimen's indirect tensile strength is used. But this value can be increased or decreased a bit by looking into the loading signal. The amplitude of the load pulse is given in table 16.

Test temperature (°C)	Pulse amplitude, Pa (N)
5	2000-4000
12.5	1200-1400
20	600-850
27.5	250-350
35	100-150

Table 16: Loading pulse amplitude in resilient modulus test using ITT

3.3.4.4 Dynamic creep testing program

The dynamic creep test is performed using a uniaxial cyclic compression force at high temperature values (40, 50 and 60°C). The test is performed using UTM (Universal Testing Machine). Similar to the resilient modulus test, the test equipment is capable of performing tests at high frequency with pre-described and controlled load signals and the UTM is equipped with a cell and personal computer for signal conversion, test control, data acquisition and output result display.

The load is generated by pneumatic actuator and distributed over the specimen by a circular loading plate. A friction reduction is applied between the loading plates and the specimen to allow free compression of the specimen. The load is applied vertically through the sample and two axial LVDT's measure the vertical deflection of the samples.

The loading signal is half sine with a rest period and preconditioning pulses are applied to get proper contact between the loading plate and the specimen.

The control and input parameters used in the resilient modulus testing program are given in table 17.

Control parameters	Type	Values/Description
Loading	Mechanism	Cyclic uniaxial unconfined compression
	Number of pulses	variable
	Pulse form	Half sine with rest period
	Pulse width	200ms
	Pulse period	1000ms
	Pulse amplitude	*
Preconditioning pulses	Number	18
	Nature	Similar to loading pulses
Measurement type	Pulses	Number of pulse
	Load	compressive force
	Displacement	Axial displacement
Specimen size	Thickness	55mm
	Diameter	101.6mm
Boundary condition	-	Friction reduction applied at both ends
Test temperature	-	40,50,60°C
Failure type	-	deformation
Test termination	-	When LVDT get out of range or 7200pulses

* see table 18

Table 17: Testing input and control parameters for dynamic creep test

Again the pulse period is given as :

Pulse period (Tt) = pulse width(Tp) + rest period (Rt) and the loading pulse is shown in figure 16

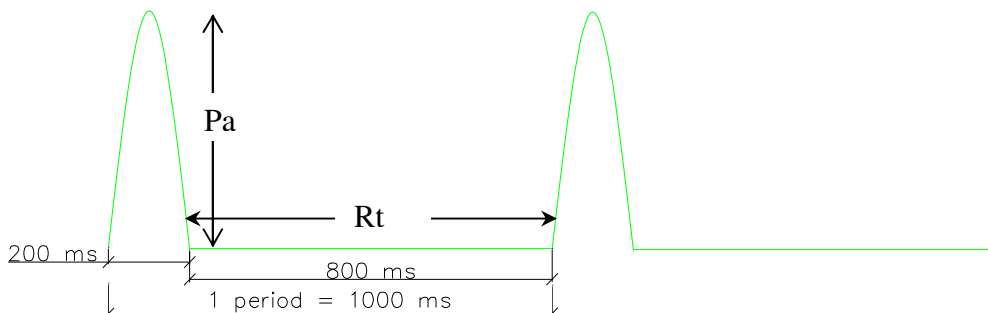


Figure16: half sine loading pulse in dynamic creep test

In this test pulse width and pulse period are constant and their values are as given in table 17 and figure 16.

Three different peak stresses (stress amplitudes) are considered for each testing temperature. The values of these peak values depend on the test temperature. This was done to get a reasonable number of repetitions in each test temperature. First the loading values for 40°C testing temperature were decided based on past experience with similar testing temperature and then based on the performance of the specimens @ 40°C for the different loading conditions, the loading values for the 50° and 60°C testing temperatures were determined. The load values considered in this testing program are given in table 18.

Test temperature(°C)	Peak Load (kpa)	Number of specimens
40	100	3
	300	3
	500	3
50	100	3
	200	3
	300	3
60	100	3
	150	3
	200	3

Table 18: Peak stress values in dynamic creep test

3.3.4.5 Fatigue resistance testing program

The fatigue resistance test is performed using indirect tensile test at two test temperatures (5 and 20 °C). Two types of test set-up were used. The first one was the UTM which was used for the tests at 20°C .The second one was MTS servo hydraulic set-up used for the test at 5°C . The MTS equipment had to be used for the 5°C tests because of limitations of the UTM with respect to the maximum compressive force that could be produced. sin its maximum compressive force capability. In both cases the testing equipments are provided with a data acquisition system and personal computer for test control, measurement data and result output display.

As mentioned before, the load is generated by pneumatic actuator in the case of the UTM where as in case of the MTS the load is generated by hydraulically controlled actuator. The load is distributed to the specimen by loading strip. Hard rubber with low potential of deformability is glued to the strip to avoid local shear failure near the loading strips. For the testing temperature of 20°C the rubber attachment was crucial to ensure cracking initiation at the center of the specimen. However, for the testing temperature of 5°C the rubber

attachment was not done because trial tests performed @5°C with out rubber proved that local shear failure near loading strip are very minimal.

The load is applied vertically through the sample and two axial LVDT's measure the vertical deflection of the samples. The load signal used with the 20°C test temperature is haversine with small rest period where as with the 5°C it is a continuous haversine signal. The provision of the rest period in the 20°C test temperature is because this is required when doing a repeated load test using UTM.

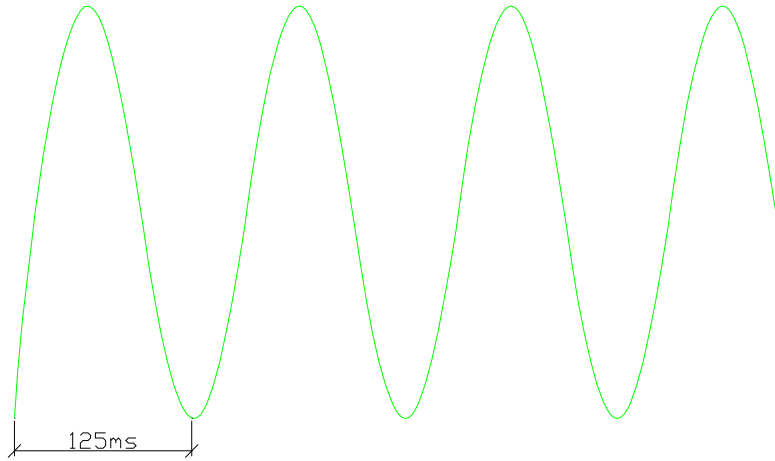
The control and input parameters used in the fatigue resistance testing program are given in table 19.

Control parameters	Type	Values/Description	
Test type	-	Stress controlled	
Loading	Mechanism	Continuous indirect tensile force	
	Number of pulses	variable	
	Pulse form	5°C	Continuous haversine sine
		20°C	Haversine with rest period
	Pulse width	125ms	
	Pulse period	5°C	125ms
		20°C	175ms
Pulse amplitude	*		
Measurement type	Pulses	Number of pulse	
	Load	compressive force	
	Displacement	Axial displacement	
Specimen size	Thickness	35mm	
	Diameter	101.6mm	
Test temperature	-	5, 20°C	
Failure type	-	Diametral cracking	
Test termination	-	When specimen fails by cracking	

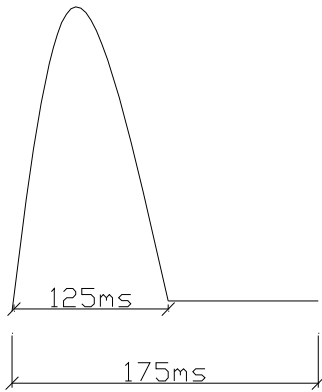
* see table 20

Table 19: Testing input and control parameters for fatigue resistance test

The pulse form and pulse period used with the two testing temperatures are shown in figure 17. In the fatigue resistance test, the values of the pulse width and pulse period remains constant for each test temperature. The peak force (amplitudes) differs for each specimen and for each testing temperature. The peak force value is selected in such a way that a reasonable number of load repetitions can be obtained with a reasonable amount of time. The peak compressive forces used in the two testing temperatures are given in table 20.



a) Loading pulse for 5°C



b) Loading pulse for 20°C

Figure 17: Haversine loading pulse in fatigue resistance test

Peak compressive force(KN)		
Test Number	5°C	20°C
1	4.3	0.9
2	5	1.05
3	6	1.25
4	7	1.5
5	8	1.75
6	9	2.0
7	10.5	2.4
8	12	2.75

Table 20: Peak stress values in fatigue resistance test

4 Tests and Characterization of Nanoclay Modifiers

The modification of asphalt binders with nanoclay is performed at nano-scale level. To understand the interaction of the nanoclay modifiers with the bitumen or other thermoplastic material, it is important to have good knowledge of the nanoclay modifiers at nano-scale level.

Understanding the nanoclay materials at particle size level is of great significance because the interaction of the nanoclay material with the binder is performed at particle size level. To achieve this, physical and chemical characterization of the nanoclay materials at particle size level was performed. The tests considered in this study work in relation to this were:

- microscopic analysis at nano/micro- scale;
- X- ray analysis

In addition, a consistency test is performed to get some engineering properties of the nanoclay modifiers. Determination of the plastic limit was considered for the consistency test.

4.1 Microscopic analysis of the nanoclay modifiers

To get an understanding about the arrangement and interaction of the nanoclay particles, about the particle size of the nanoclay, the particle shape and its aspect ratio, a microscopic analysis and imaging was performed on the nanoclay modifiers. The analysis was done using an electron microprobe. The nanoclay materials were glued on a carbon surfaced small disc and scattered by blowing and finally coated with a thin layer of gold. Using a highly energized electron beam, microscopic images of the particles was made. The microscopic images for the two nanoclay particles are shown in figure 18 and figure 19. The measurements shown on the pictures are actual measured values.

From the investigation of the two images, the following main points can be noted:

1. the particles of the two nanoclay particles have sizes in the range of 200 – 3000 nm;
2. the nanofill particles look more curly and randomly placed as compared to the the cloisite particles;
3. on average the size of the cloisite particles looks bigger than that of the nanofill particles;
4. both nanoclay particles have much bigger horizontal dimensions than their thickness (very big aspect ratio);
5. overall the particles of both materials are not uniformly arranged;
6. the random placement of the nanoclay particles can be due to the blowing effect used to disperse the particles for the microscopic analysis;
7. the particle sizes are not uniform for both nanoclay materials.

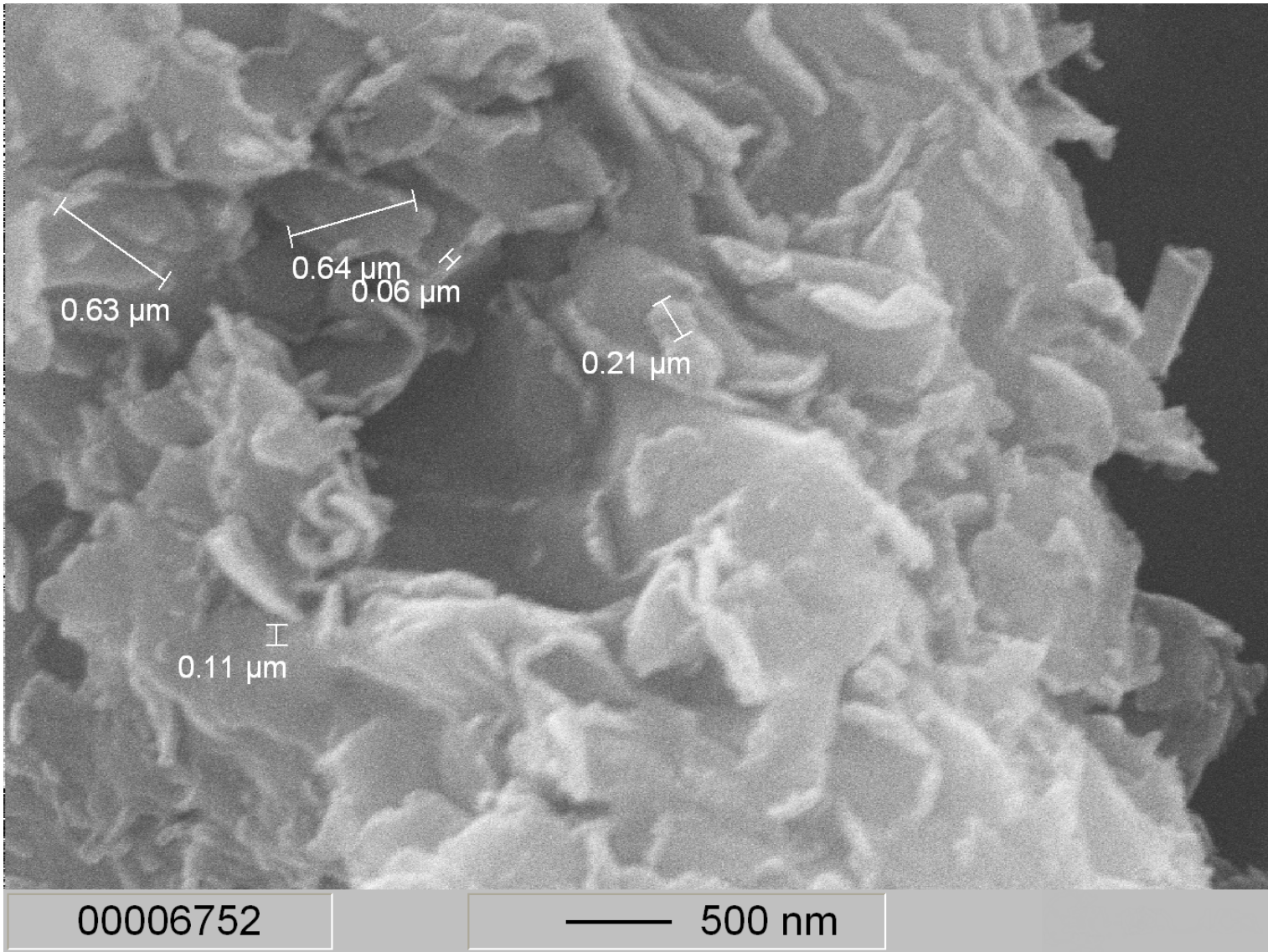


Figure18: Microscopic image of nanofill

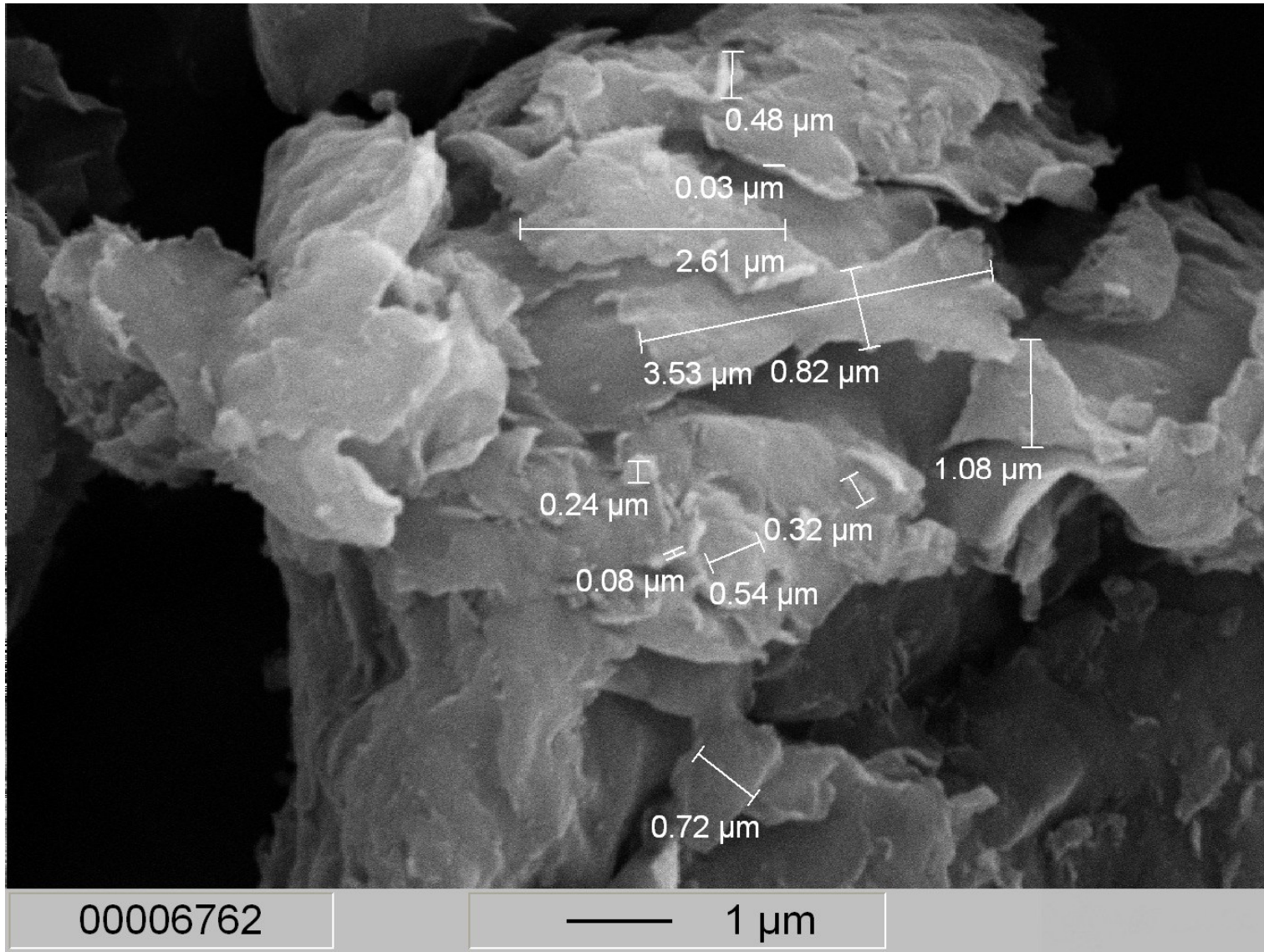


Figure 19: Microscopic image of cloisite

4.2 X-ray analysis of the nanoclay modifiers

In this study, X-ray analysis was performed for two main purposes being:

1. to know the elemental composition of the nanoclay materials
2. to know the chemical composition and if possible the chemical formula of the basic molecules of the nanoclay materials

To meet these requirements, two types of x-ray analyses were performed and discussed below.

4.2.1 Qualitative wavelength dispersive spot analyses

This type of X-ray analysis is normally performed to get qualitative information about the elemental composition of a material. The analysis was performed using crystal spectrometers: LDE1, TAP, PET and LIF. Each crystal analysis has a specific wavelength range. Each element within the material being tested emits an X-ray of a specific wavelength. Those elements with lower atomic number emit higher wave lengths where as those with higher atomic number emit lower wave lengths.

From this analysis it is difficult to get quantitative analysis of the elements. This is because the wave lengths emitted by the different elements in the specimen are analyzed by different crystal spectrometers which have different scale parameters.

The analysis results for the two nanoclay modifiers are shown in figure 20 and figure 21. The horizontal axis is wave length in angstrom (10^{-10} m).

The elements expected in the nanoclay modifiers are : Si, Al, O, H and possibly other metals and N (nitrogen) and carbon from the surfactants treatment.

From the analysis results the following discussion can be made:

- hydrogen is not reflected in the analysis though it was expected; the reason is that the analysis performed is not capable of detecting light elements like hydrogen;
- nitrogen is expected at a wave length of 30-35A, but it is not reflected there in the analysis of both materials; this analysis tells us that the presence of nitrogen is small as compared to the amount of other elements;
- gold is reflected in the analysis results of both materials; however, this does not mean that gold is part of the clay; the presence of gold is due the gold coating used in the analysis;
- a different amount of carbon content is shown between the two analysis results; the carbon reflected in the analysis can be either due to presence of carbon in the two materials or it can be due to the carbon material used as glue at the bottom of the materials tested.

A comparison of the two analysis results shows:

- the type of elements present in both nanoclay samples are the same (Si, O, Mg, Al, Fe, H and possibly carbon);
- a quantitative comparison of the elements between the two materials is not possible because the overall x-ray intensity depends on the amount (size) of specimen tested; the relative intensities between the elements of the same material do not depend on the size of the specimen;
- nitrogen is present in very small concentration or even absent.

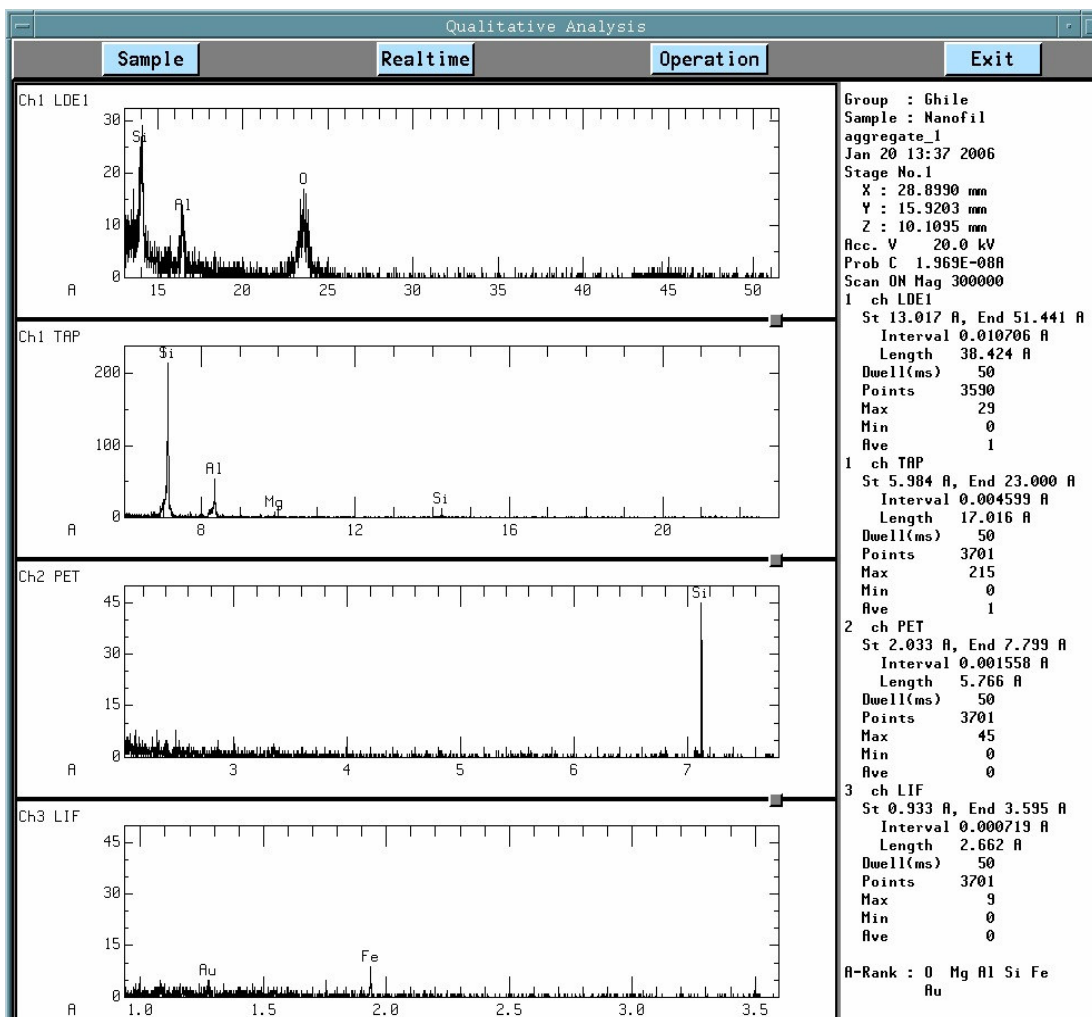


Figure 20: X-ray analysis with crystal spectrometer (Nanofill)

4.2.2 X-ray diffraction (XRD) analysis

The X-ray diffraction analysis was performed to determine the chemical composition of the molecules of the specimen. This was done by determining the crystal shape of the molecules by the X-ray analysis and finding a close match shape in the available library. In that way the chemical composition of the specimen can be estimated. However, from the XRD analysis performed on the nanoclay materials it was not possible to find an exact match and therefore

their exact chemical composition can not be presented here. The close match proposed by the program were Tosudite for the nanofill and loughlinitite for the cloisite.

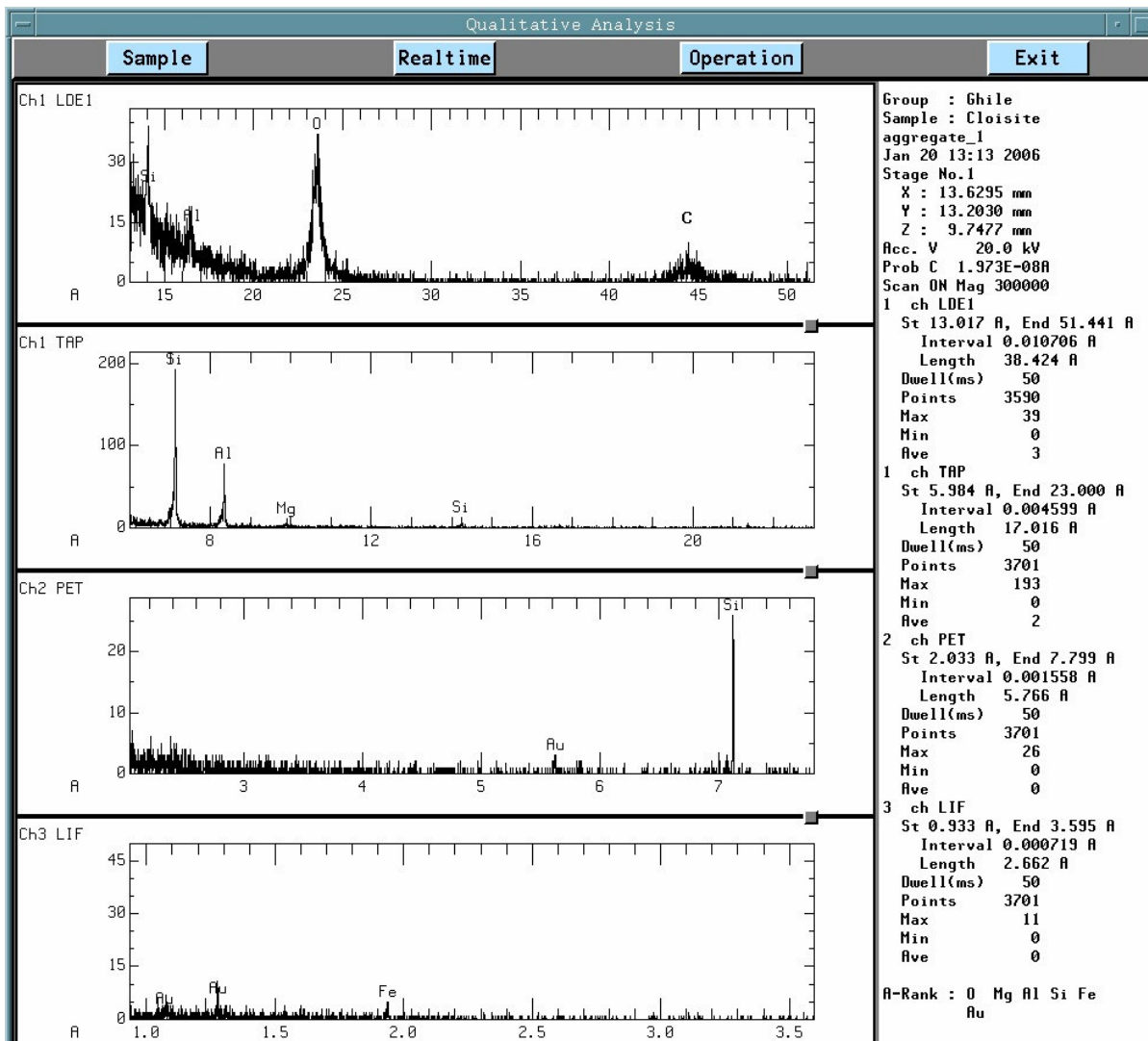


Figure 21: X-ray analysis with crystal spectrometer (Cloisite)

The X-ray diffraction analysis results are shown in figure 22 and 23. In the graphs the continuous line represents the crystal shape of the particles of the specimen where as the vertical lines with solid boxes on top of them belong to the possible matching material from the library. It can be clearly seen that there is some difference between the peaks of the specimens and the matching material.

The chemical composition given at the bottom of the graphs is not the chemical composition of the nanoclays, but it is the chemical composition of the matching material. The XRD analysis of both materials show broad peaks and this implies that the particle size of the nanoclays is very small and has a poor crystallinity. The nanofill specimen has less sharp peaks compared to the cloisite and this shows that the nanofill particles are relatively smaller and have relatively poorer crystalline shape as compared to the cloisite particles.

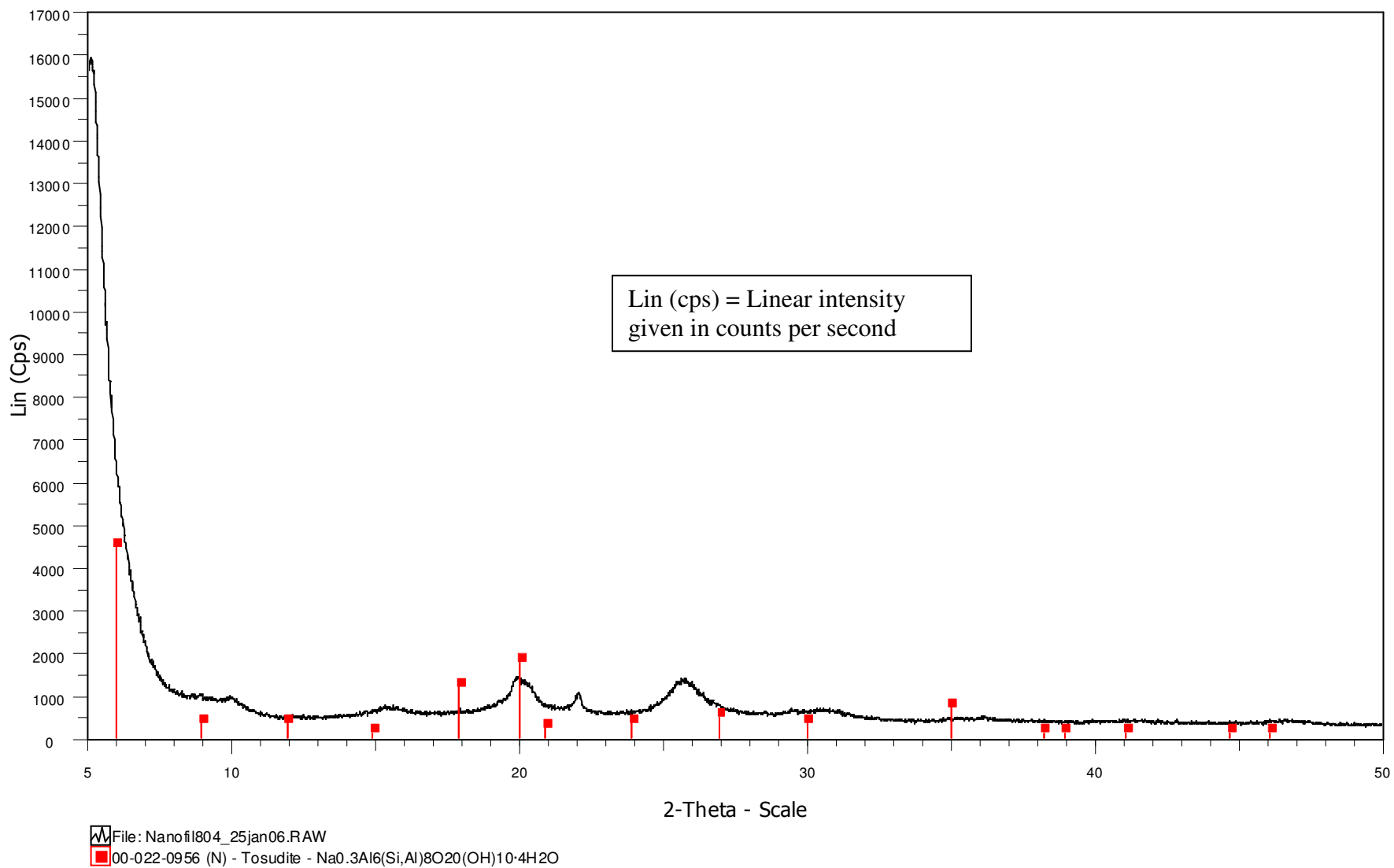


Figure 22: X-ray diffraction analysis (Nanofill)

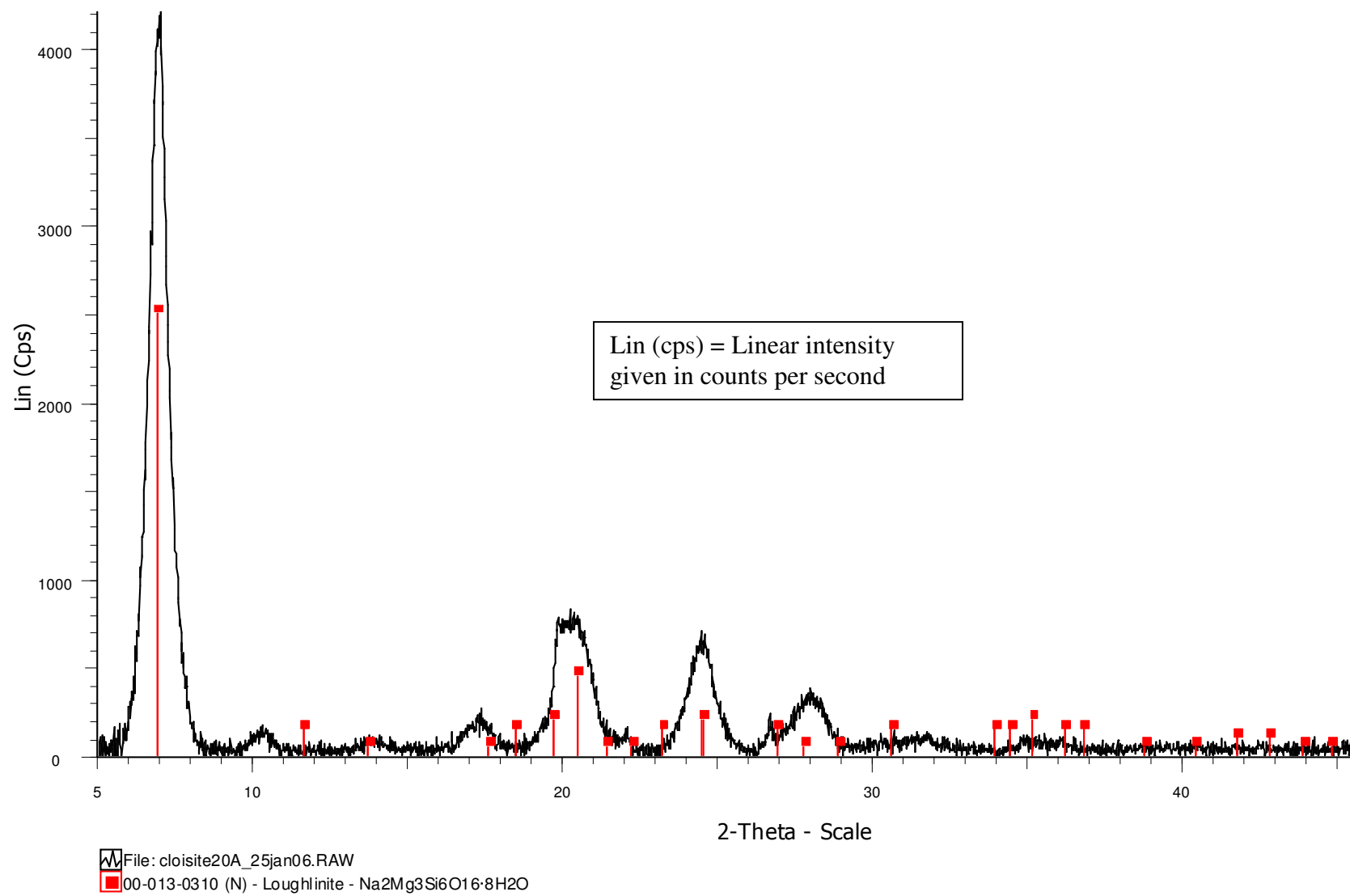


Figure 23: X-ray diffraction analysis (cloisite)

4.3 Plastic Limit of nanoclay modifiers

To get an idea on the consistency of the nanoclay materials a plastic limit test was performed on both materials and the measurement and analyses results are shown in table 21 and 22. The plastic limit was determined by rolling a thread of soil on a glass plate until the 1/8-inch(3mm) -diameter thread begins to crumble.

Test Number	1	2
weight of container + wet clay(gm)	23,85	25,96
weight of container + dry clay(gm)	20,92	21,86
weight of container (gm)	17,43	17,14
weight of water (gm)	2,93	4,1
weight of dry clay(gm)	3,49	4,72
moisture content (%)	83,95%	86,86%
plastic limit	85,41%	

Table 21: Plastic limit analysis for nanofill

Test Number	1	2
weight of container + wet clay(gm)	17,95	20,5
weight of container + dry clay(gm)	15,85	18,68
weight of container (gm)	13,45	16,6
weight of water (gm)	2,1	1,82
weight of dry clay(gm)	2,4	2,08
moisture content (%)	87,50%	87,50%
plastic limit	87,50%	

Table 22: Plastic limit analysis for cloisite

The liquid limit analysis was not performed due to limitation in amount of nanoclay materials.

From the results of the plastic limit the following points can be noted:

- the plastic limit of both nanoclay materials is more or less the same ;
- the plastic limit value of both clays is very high which tells us that the materials are part of the family of expansive soils (montmorillonite).

5 Rheological Tests on Modified and Unmodified asphalt binders

This chapter presents the rheological tests performed on the modified and unmodified binders, their analysis and discussion. The rheological tests done are of two types:

- i. *empirical rheological tests*: these comprise the penetration test and softening point test;
- ii. *fundamental rheological tests*: these comprise tests with the DSR.

The nanofill modifier is selected to modify 70/100 standard binder where as the cloisite is selected to modify 40/60 binder. The choice of the modifications is based on earlier researches done on the nanoclay modifiers. The nanofill modification showed relatively good performance in resistance to impact and abrasion tests done on porous asphalt mixtures and in ageing reduction of a 70/100 pen bitumen as used in PAC where as an increase in stiffness and strength of a dense asphalt mixtures was observed due to cloisite modification of the 40/60 pen bitumen used in that mixture.

5.1 Empirical rheological tests

In this section first the direct measurements of penetration and softening points is discussed and then it is followed by retained penetration and increment in softening point computations and discussion.

5.1.1 Penetration and softening point

The penetration and softening point tests were performed on fresh (un-aged), short term and long term aged samples of standard and modified binders. The results are shown in table 23.

Binder Type	Test type							
	Penetration @ 25 °C				Softening point test			
standard Bitumen 40/60	Fresh	short term RCAT aged	long term aged		Fresh	short term RCAT aged	long term aged	
			RCAT	PAV			RCAT	PAV
	58	39	23	-	49.6	54.0	59.8	-
standard Bitumen 70/100	Fresh	short term RCAT aged	long term aged		Fresh	short term RCAT aged	long term aged	
			RCAT	PAV			RCAT	PAV
	84	60	33		46.4	49.6	56.4	
Nanofill (6%) + Bitumen 70/100	Fresh	short term RCAT aged	long term aged		Fresh	short term RCAT aged	long term aged	
			RCAT	PAV			RCAT	PAV
	87	75	38		46.2	48.0	55.2	
Cloisite (3%) + Bitumen 40/60	Fresh	short term RCAT aged	long term aged		Fresh	short term RCAT aged	long term aged	
			RCAT	PAV			RCAT	PAV
	50	38	22	-	51.8	55.2	61.6	-
Cloisite (6%) + Bitumen 40/60	Fresh	short term RCAT aged	long term aged		Fresh	short term RCAT aged	long term aged	
			RCAT	PAV			RCAT	PAV
	45	33	20	-	57.6	61.2	65.6	-

Table 23: penetration and softening point tests on fresh and aged materials

Analysis and Discussion on test results:

From the empirical rheological test results on the fresh samples of the standard and modified binders, the following observations can be made.

Standard 70/100 and 70/100 + 6% nanofill binders

- the penetration has hardly changed due to the modification (84 versus 87);
- the softening point has hardly changed due to the modification (46.4 versus 46.2°C)

From these results the conclusion must be that nanofill modification does not bring any change on the penetration and softening point of the fresh 70/100 binder.

Standard 40/60 and 40/60 + 3% cloisite binders

- the penetration value has reduced with 8 points (from 58 to 50);
- the softening point has increased with 2.2°C (from 49.6 to 51.8°C)

The 3% cloisite modification shows relatively some increment on the softening point and decrement of penetration value of the fresh 40/60 binder.

Standard 40/60 and 40/60 + 6% cloisite binders

- the penetration value has reduced with 13 points (from 58 to 45);
- the softening point has increased with 8°C (from 49.6 to 57.6°C)

The 6% cloisite modification shows relatively higher increment in softening point and higher decrement in penetration value of the fresh 40/60 binder as compared to the other two modifications mentioned above.

5.1.2 Retained penetration and increment in softening point

Retained penetration

When bitumen gets aged it becomes harder and the increment in hardness due to ageing in relation to its fresh value can be assessed by the retained penetration and increment in softening point values. A lower retained penetration value and higher increment in softening point reflect more ageing of the binder.

The retained penetration and increment in softening point were computed and presented in figure 24 and figure 25 for the standard and modified binders in short term and long term ageing terms.

Analysis and Discussion of test results (fig24):

The assessment about ageing of the modified and unmodified 70/100 binders from the retained penetration and increment in softening point results is given below.

Short term aged - standard 70/100 and 70/100 + 6% nanofill binders

- the retained penetration is relatively higher for the 6% nanofill modified 70/100 binder than the standard one (86% for the modified versus 71% for the standard).

- the increment in softening point is relatively smaller for the modified binder in relation to the standard one (1.8°C for the modified , 3.2°C for the standard)

These analysis results show that the modification helps to some degree in improving the resistance to ageing of the 70/100 binder.

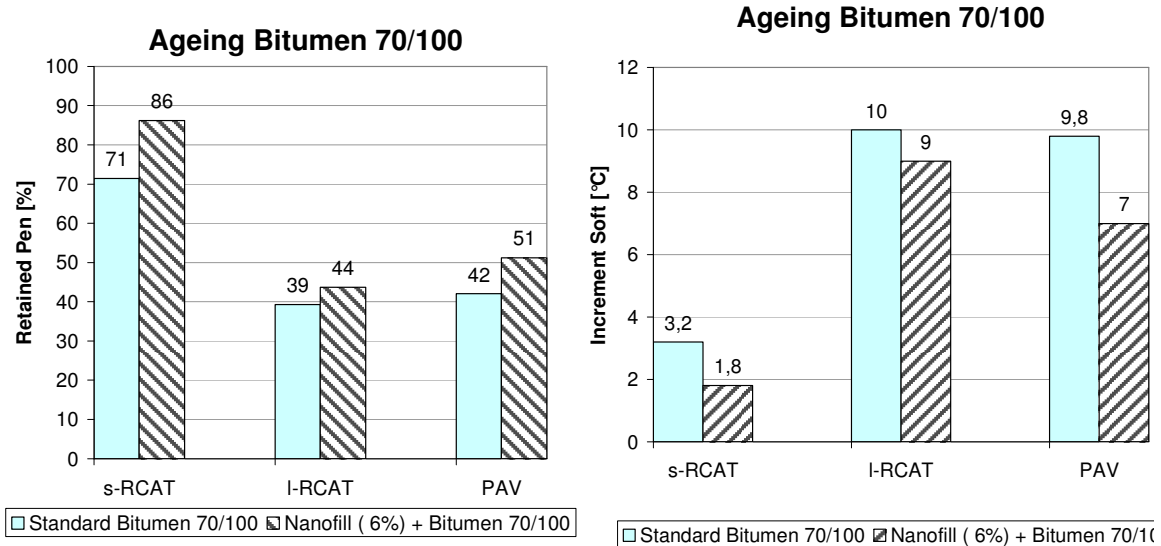


Figure 24: Retained penetration and increment in softening point for standard and modified 70/100 binder.

(s-RCAT = short term aged by RCAT, l-RCAT = long term aged by RCAT)

Long term aged (RCAT)- standard 70/100 and 70/100 + 6% nanofill binders

From the results of figure 24, the following observations can be made:

- the change in retained penetration value is very small due to the modification (44% for the modified versus 39% for the standard).
- the increment in softening point is also hardly changed due to the modification (9°C for the modified , 10°C for the standard)

The positive effect seen due to the nanofill modification in the short term ageing was not revealed in the long term ageing.

Long term aged (PAV) - standard 70/100 and 70/100 + 6% nanofill binders

From figure 24 it can be observed that:

- the retained penetration shows some changes due to the modification (51% for the modified versus 42% for the standard).
- the increment in softening point shows some changes too due to the modification (7°C for the modified , 9.8 °C for the standard)

From the PAV analysis it can be observed that there are some improvements in the resistance to ageing in the long term due to the nanofill modification.

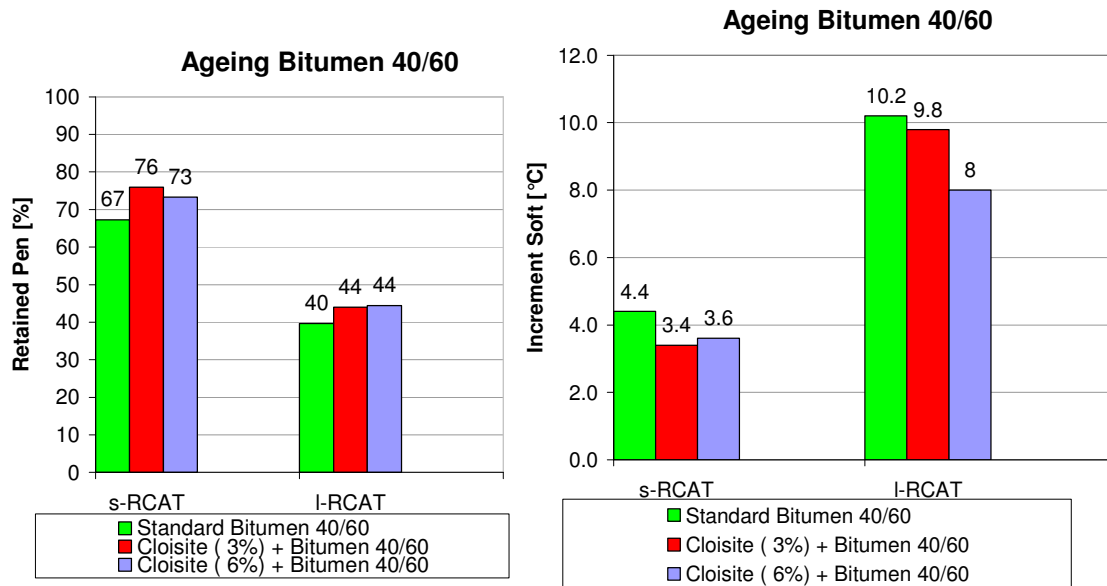


Figure 25: Retained penetration and increment in softening point for standard and modified 40/60 binder

(s-RCAT = short term aged by RCAT, l-RCAT = long term aged by RCAT)

Analysis and Discussion of test results (fig 25):

The assessment about ageing of the modified and unmodified 40/60 binders from the retained penetration and increment in softening point results is described below.

Short term aged-standard 40/60 , 40/60 + 3% cloisite and 40/60 + 6% cloisite binders

- the retained penetration is a little bit higher for the 3% cloisite modified binder than the standard one (76% for the modified versus 67% for the standard).
- the increment in softening point is a bit smaller for the 3% cloisite modified binder than the standard one (3.4°C for the modified , 4.4°C for the standard)
- the retained penetration as well as the increment in softening point has hardly changed due to an increment in the amount of modification from 3% to 6% cloisite.

Long term aged-standard 40/60, 40/60 + 3% cloisite and 40/60 + 6% cloisite binders

- Similar to the short term ageing results, the improvement of the resistance to ageing due to the modifications is very minimal as results of the retained penetration (40% for standard, 44% for the 3% and 6% cloisite) and increment in softening point (10.2°C for standard, 9.8°C for 3% cloisite and 8°C for 6% cloisite) reveal.

The analyses of the short term and long term ageing tell us that the modifications have hardly helped in improving resistance to ageing.

In addition the modified 40/60 material has a slightly higher viscosity than the regular 40/60 and therefore probably suffers less contact with hot air or hot oxygen. Hence, the small improvement can also be due to the influence of the viscosity instead of the influence of the modification.

5.2 DSR test results

The discussion on DSR test results comprises the following areas:

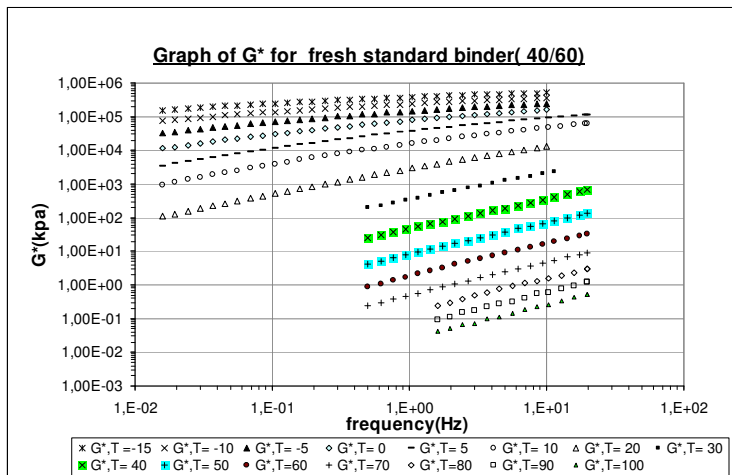
- ✓ A typical DSR test results analysis which comprises :
 - frequency sweep analysis;
 - master curve and black diagram.
- ✓ Comparison of the master curves of the stiffness of the modified and unmodified binders.
- ✓ Comparison of the master curves of phase angles of the modified and unmodified binders.
- ✓ Analysis of the change in ageing effect of the binder due to the modification.
- ✓ Analysis of the rutting and fatigue resistance parameters for the modified and unmodified binders.

5.2.1 Typical analysis of DSR test results

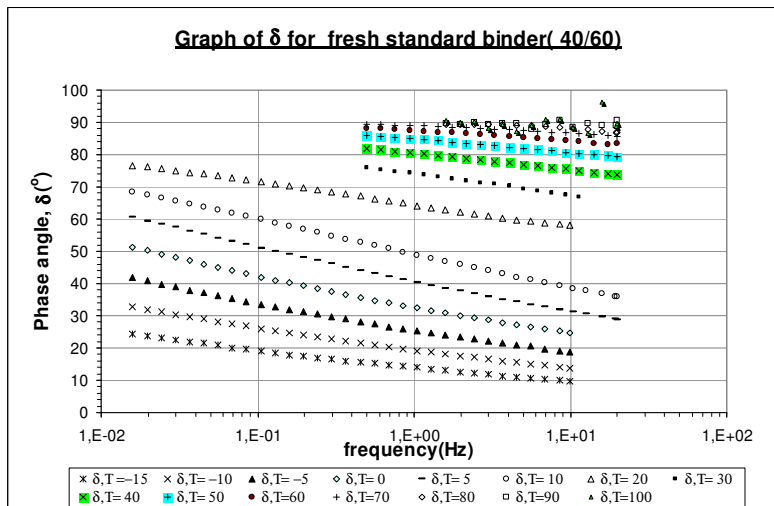
This part gives a typical example of frequency sweep DSR test results, a typical master curve of stiffness and phase angle and a typical example of a black diagram

5.2.1.1 Frequency sweep DSR test results

The frequency sweep results can be used in the construction of master curves and black diagrams. A typical example of frequency sweep of DSR test results of stiffness and phase angle is given in figure 26. The influence of temperature and frequency on the values of stiffness and phase is clearly depicted in the graph. From the figure it can be seen that the complex modulus (G^*) increases with a decrease in temperature and/or an increase in frequency where as the phase angle increases with an increase in temperature and/or a decrease in frequency. At high temperature ($>80^{\circ}\text{C}$) the testing is a bit problematic. This is due to the flow of bitumen out of the DSR plates at high temperature which results in reduction of binder thickness.



a) Stiffness versus frequency



b) Phase angle versus frequency

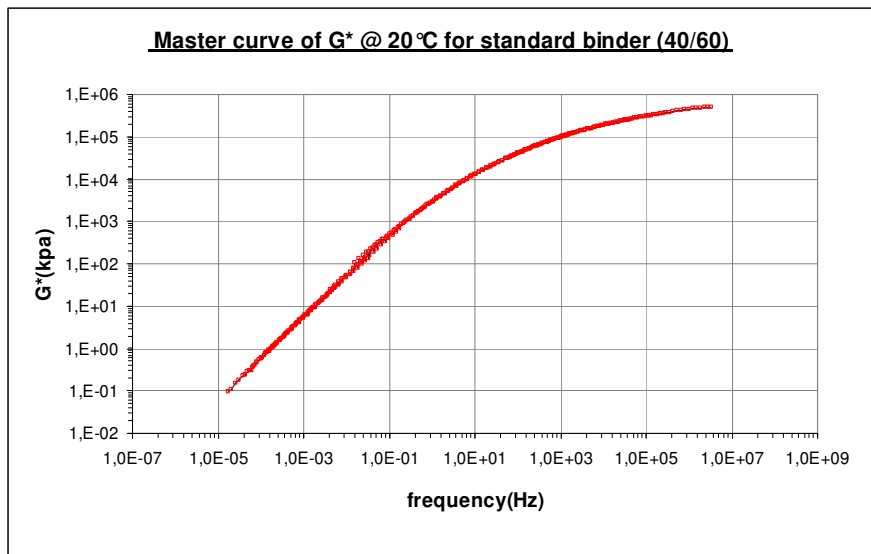
Figure 26: Frequency sweep of DSR test results (standard fresh 40/60 binder)

5.2.1.2 Master curve of stiffness and phase angle

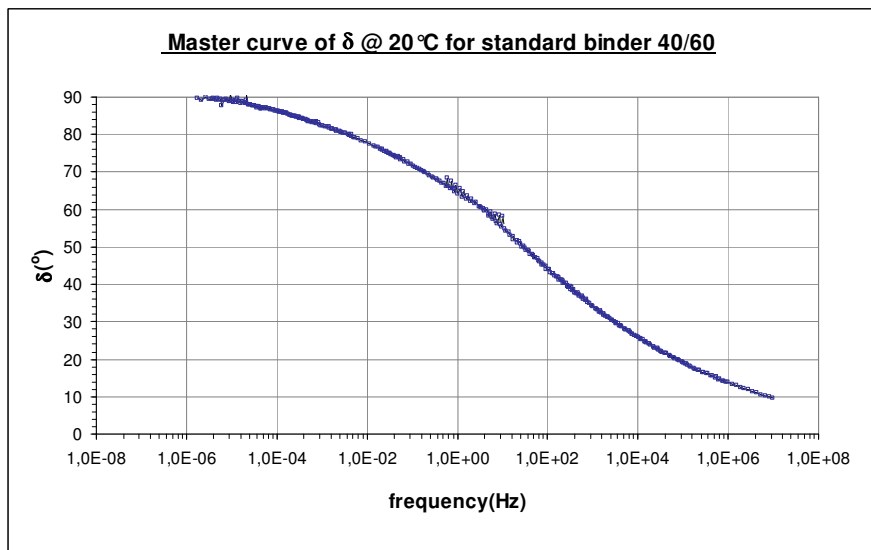
Construction of master curves of stiffness and phase angle is of great significance because:

- it can describe rheological properties of bitumen under a wide range of loading frequencies for a selected temperature value;
- a comparison of stiffness and phase angle values of the modified and unmodified binders is better described by master curve values than frequency sweep results;
- an effect of modification on the ageing effect of the binder can also be better explained and clarified using master curve values than the frequency sweep results.

A typical example of master curves of stiffness and phase angle is given in figure 27.



a) Master curve of stiffness



b) Master curve of phase angle

Figure 27: Master curve for standard fresh 40/60 binder

From figure 27 some common unique characteristics of the rheological properties of bitumen can be observed:

- At low temperatures or high frequencies asphalt binders tend to approach a limiting value of G^* of approximately 1.0 GPa and a limiting value of δ of 0 degrees.
- At high temperature or low frequencies δ approaches 90 degrees where as the values of G^* depends on the type of asphalt binder

5.2.1.3 Black diagram

The black diagram relates the complex modulus with the phase angle value and is unique for a selected binder type. The black diagram is seen as a fingerprint of the binder. It can tell us how the two values are related under wide temperature ranges. A typical example of a black diagram is given in figure 28.

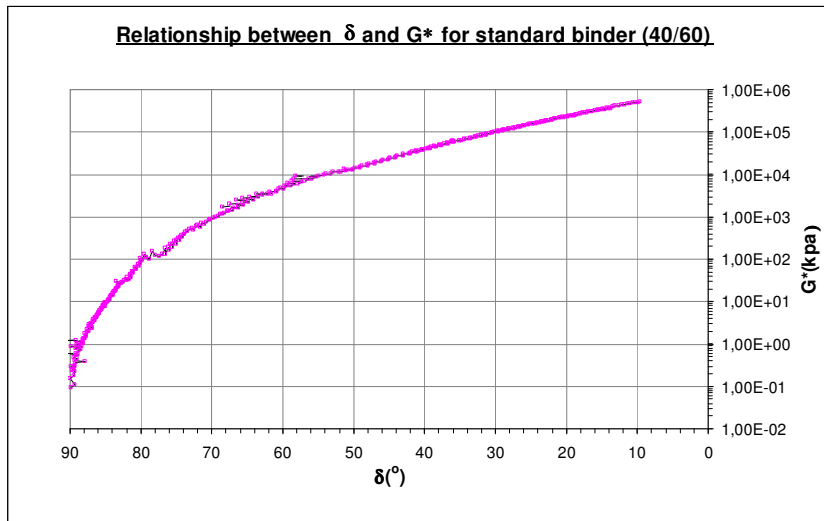


Figure28: Black diagram for standard fresh 40/60 binder

5.2.1.4 Frequency conversion

The master curve @20°C is used to compare stiffness and phase angle values of the standard and modified binders. In addition to the master curve, comparison of numerical values of stiffness and phase angle are given in tabular form for a selected frequency values at 20°C. The frequency ranges selected are mostly in the range of 10^{-3} Hz to 10^3 Hz. In order to get a matching frequency values at different temperature values, a frequency matching /conversion table for selected binder types is given in table 24.

The frequency matching table is prepared for stiffness values and a similar table can also be prepared for phase angle values. From the table it can be observed that for a given temperature, the matching frequency values for the three binder types are close to each other.

Binder	frequency	Frequency (Hz)						
	@20°C(Hz)	-10°C	0°C	10°C	30°C	40°C	50°C	60°C
standard 40/60 binder	1,00E-03	3,20E-08	1,82E-06	6,12E-05	1,53E-02	1,16E-01	6,19E-01	3,18E+00
	1,00E-02	3,20E-07	1,82E-05	6,12E-04	1,53E-01	1,16E+00	6,19E+00	3,18E+01
	1,00E-01	3,20E-06	1,82E-04	6,12E-03	1,53E+00	1,16E+01	6,19E+01	3,18E+02
	1,00E+00	3,20E-05	1,82E-03	6,12E-02	1,53E+01	1,16E+02	6,19E+02	3,18E+03
	1,00E+01	3,20E-04	1,82E-02	6,12E-01	1,53E+02	1,16E+03	6,19E+03	3,18E+04
	1,00E+02	3,20E-03	1,82E-01	6,12E+00	1,53E+03	1,16E+04	6,19E+04	3,18E+05
	1,00E+03	3,20E-02	1,82E+00	6,12E+01	1,53E+04	1,16E+05	6,19E+05	3,18E+06
nanofill 6% modified 70/100 binder		-10°C	0°C	10°C	35°C	45°C	55°C	60°C
	1,00E-03	3,39E-08	1,97E-06	5,93E-05	4,52E-02	3,25E-01	1,79E+00	4,08E+00
	1,00E-02	3,39E-07	1,97E-05	5,93E-04	4,52E-01	3,25E+00	1,79E+01	4,08E+01
	1,00E-01	3,39E-06	1,97E-04	5,93E-03	4,52E+00	3,25E+01	1,79E+02	4,08E+02
	1,00E+00	3,39E-05	1,97E-03	5,93E-02	4,52E+01	3,25E+02	1,79E+03	4,08E+03
	1,00E+01	3,39E-04	1,97E-02	5,93E-01	4,52E+02	3,25E+03	1,79E+04	4,08E+04
	1,00E+02	3,39E-03	1,97E-01	5,93E+00	4,52E+03	3,25E+04	1,79E+05	4,08E+05
1,00E+03	3,39E-02	1,97E+00	5,93E+01	4,52E+04	3,25E+05	1,79E+06	4,08E+06	
Cloisite 6% modified 40/60 binder		-10°C	0°C	10°C	30°C	40°C	50°C	60°C
	1,00E-03	3,52E-08	1,83E-06	5,89E-05	1,55E-02	1,17E-01	6,22E-01	3,28E+00
	1,00E-02	3,52E-07	1,83E-05	5,89E-04	1,55E-01	1,17E+00	6,22E+00	3,28E+01
	1,00E-01	3,52E-06	1,83E-04	5,89E-03	1,55E+00	1,17E+01	6,22E+01	3,28E+02
	1,00E+00	3,52E-05	1,83E-03	5,89E-02	1,55E+01	1,17E+02	6,22E+02	3,28E+03
	1,00E+01	3,52E-04	1,83E-02	5,89E-01	1,55E+02	1,17E+03	6,22E+03	3,28E+04
	1,00E+02	3,52E-03	1,83E-01	5,89E+00	1,55E+03	1,17E+04	6,22E+04	3,28E+05
1,00E+03	3,52E-02	1,83E+00	5,89E+01	1,55E+04	1,17E+05	6,22E+05	3,28E+06	

Table 24: Frequency matching table

5.2.2 Analysis and comparison of stiffness and phase angle values: standard 70/100 binder versus nanofill 6% modified 70/100 binder

Rheological properties can be represented either by the variation of G^* and δ as a function of frequency at a constant temperature commonly referred as master curve or by variation of G^* and δ with temperature at a selected frequency commonly called isochronal curve. However, the master curve is widely used for rheological properties representation and it is used as a means to compare the rheological properties of the modified and unmodified binders in this study work. All master curves used for comparison are constructed at 20°C. For ease of comparison all graphs of the modified and unmodified binders are shown on the same graph.

5.2.2.1 Comparison of stiffness (fresh)

The stiffness values of the standard and nanofill modified fresh samples for a selected value of frequency is given in table 25 and in addition it is given graphically for a wide range of frequencies in figure 29.

Analysis and discussion of test results

Looking into values of stiffness of fresh sample of the modified and unmodified binders in table 25 and figure 29, the following points can be observed.

- the nanofill modification helps to increase the stiffness of the standard 70/100 binder to some degree (by a factor of 1.3 at 10Hz to 1.7 at a frequency of 10^{-3} Hz).
- As frequency values increases the increment in stiffness values due to the modification gradually reduces and at very high frequency the stiffness of the modified and unmodified binders become more or less the same.

frequency Hz	Stiffness(Kpa)									
	Standard			Nanofill			Nanofill/ standard		increment in stiffness due to ageing(%)	
	fresh	Short term	differ ence	fresh	Short term	differen ce	fresh	aged	stand -ard	nanofill
100	24776	32039	7263	31158	28440	-2718	1,25	0,89	29%	-10%
10	6692	10139	3447	8598	7996	-602	1,3	0,79	52%	-7%
1	1387	2427	1040	1796	1753	-44	1,3	0,72	75%	-2%
0,1	226	419	194	302	310	7	1,3	0,74	86%	2%
0,01	27	48	21	45	40	-5	1,6	0,83	75%	-11%
0,001	3	6	3	5	4	-1	1,7	0,67	97%	-13%

Table 25: Stiffness values of standard and nanofill modified 70/100 binders (fresh and short term aged) @ 20°C

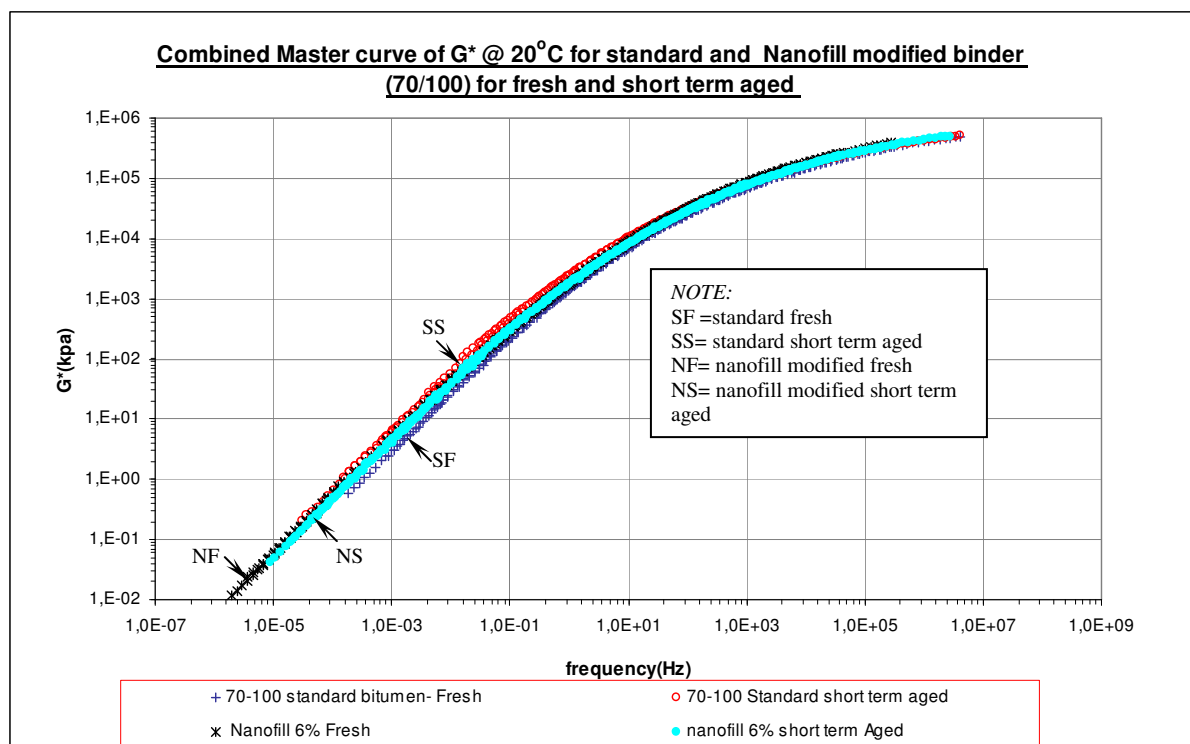


Figure 29: Master curve of stiffness for modified and unmodified 70/100 binder (fresh and short term aged)

5.2.2.2 Comparison of phase angle (fresh)

The value of phase angle for a fresh and short term aged samples of the modified and unmodified binders is given in table 26 and figure 30.

frequency Hz	phase angle						
	Standard			Nanofill			fresh Nanofill-standard
	fresh	short term	difference	fresh	Short term	difference	
10	55,6	55,5	0,1	59,1	53,4	5,8	3,6
1	65,6	61,6	4,0	66,2	62,9	3,3	0,6
0,1	73,1	67,8	5,3	72,9	71,0	1,8	-0,2
0,01	78,8	73,7	5,1	78,4	76,7	1,7	-0,4
0,001	83,1	79,0	4,1	83,0	81,5	1,5	-0,2

Table 26: Phase angle values of standard and nanofill modified 70/100 binders (fresh and short term aged) @ 20°C

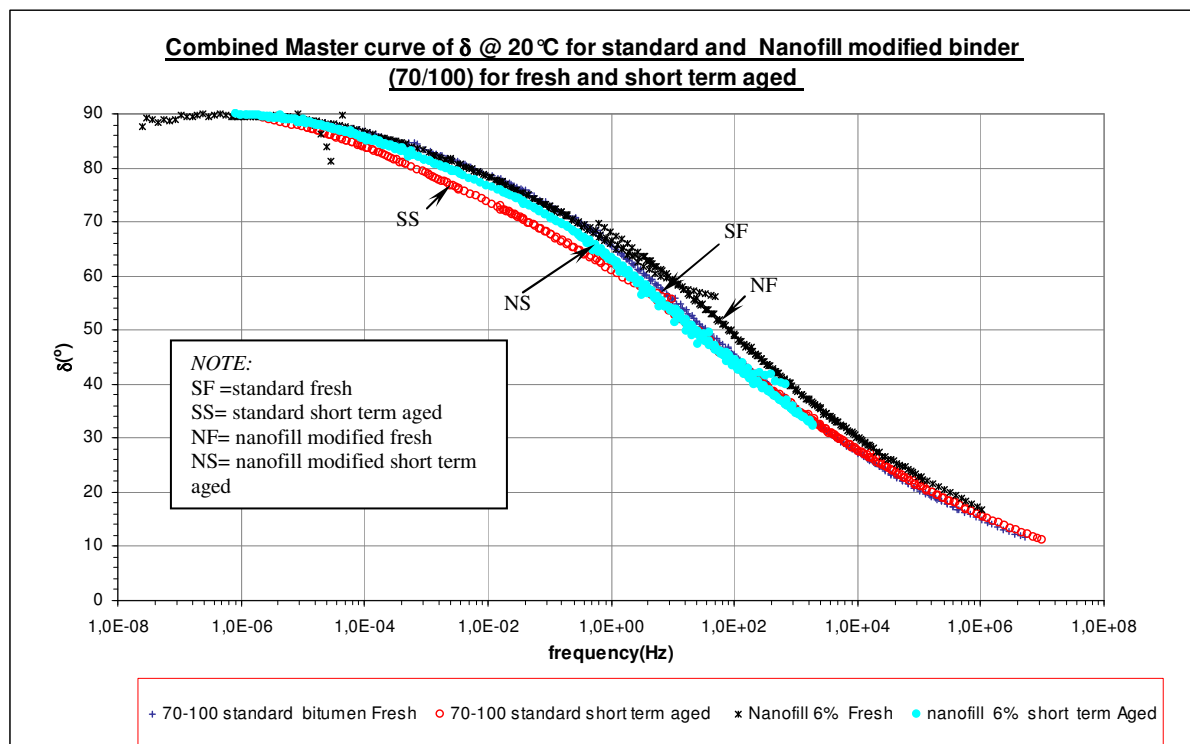


Figure30: Master curve of phase angle for modified and unmodified 70/100 binder (fresh and short term aged)

Analysis and discussion of test results:

From the assessment of the phase angle values of the fresh sample of the modified and unmodified binders in table 26 and figure 30, the following points can be observed.

- the nanofill modification hardly helps in decreasing the phase angle of the standard 70/100 binder at low frequency values (for instance, on average a phase angle difference of about -0.3° is obtained in frequency ranges between 0.1 to 10^{-3} Hz)

- at frequency values greater than 1Hz the phase angle value of the nanofill is somewhat higher than that of the standard binder (at frequency of 10Hz a phase angle difference of 3.6°). The higher phase angle of the nanofill modified material indicates that the elastic part of the deformation is smaller when compared to the reference bitumen. This was not expected because at these frequency levels the G^* of the nanofill modified material is higher.

5.2.2.3 Short term ageing effect analysis

The short term ageing effect analysis is performed based on the master curves of the stiffness and phase angle values which are given in figure 29 and 30 respectively and also on stiffness values and phase angles values given in table 25 and table 26.

From the stiffness values given in table 25 and figure 29, the following can be seen.

- After short term ageing, the stiffness value increases about 50% @ a frequency of 10Hz and almost 100% @ a frequency of 10^{-3} Hz for the standard binder. However, for the nanofill modified binder, the stiffness hardly increases even a small reduction in stiffness is observed.

Based on the stiffness increment analysis, the nanofill modification shows remarkable reduction in ageing effect of the binder in the frequency ranges 10^{-3} to 100Hz..

From the phase angle values given in table 26 and figure 30, the following can be seen.

- After short term ageing, the phase angle values decreases by about 4.6° for the standard binder and by 2° for the nanofill modified binder for a frequency ranges between 1Hz and 10^{-3} Hz.
- For frequencies ≥ 10 Hz the phase angle decrease due to ageing is bigger for the nanofill modified binder than the standard binder. This might be related to the high phase angle values of the fresh sample of the nanofill modified binder at high frequencies.

Based on the decrement of phase angle analysis, it can be concluded that the nanofill modification helped to reduce the ageing effect of the binder to some degree at low to medium frequency values (10^{-3} to 1Hz).

5.2.2.4 Long term ageing effect analysis

The increment in stiffness values due to long term ageing by RCAT is given in table 27 and figure 31. From the results the following can be noticed.

- The stiffness of the unmodified binder increases by about 225% and for the modified binder it increase by about 110% from their original values in the frequency ranges of 10^{-3} Hz to 1000Hz. This shows that the modification helps in improving resistance to ageing in the long term to some degree.

- At very high frequencies the increments in stiffness of both binders is getting smaller (percentage wise)

frequency Hz	Stiffness(kpa)							
	Standard			Nanofill			Increment in stiffness due to ageing(%)	
	fresh	Long term	difference	fresh	Long term	difference	standard	nanofill
1000	68398	89968	21570	84448	100035	15587	32%	18%
100	24776	40953,22	16178	31158	44523,52	13366	65%	43%
10	6692	13613.79	6922	8598	17122.05	8524	103%	99%
1	1387	4306.018	2919	1796	4483.42	2687	210%	150%
0.1	226	1021.824	796	302	854.6713	552	353%	183%
0.01	27	128.7404	101	45	96.52659	52	371%	116%
0.001	3	16.73334	14	5	12.87948	8	445%	153%
average							226%	109%

Table 27: stiffness values of standard and nanofill modified 70/100 binders (fresh and long term aged by RCAT) @20°C

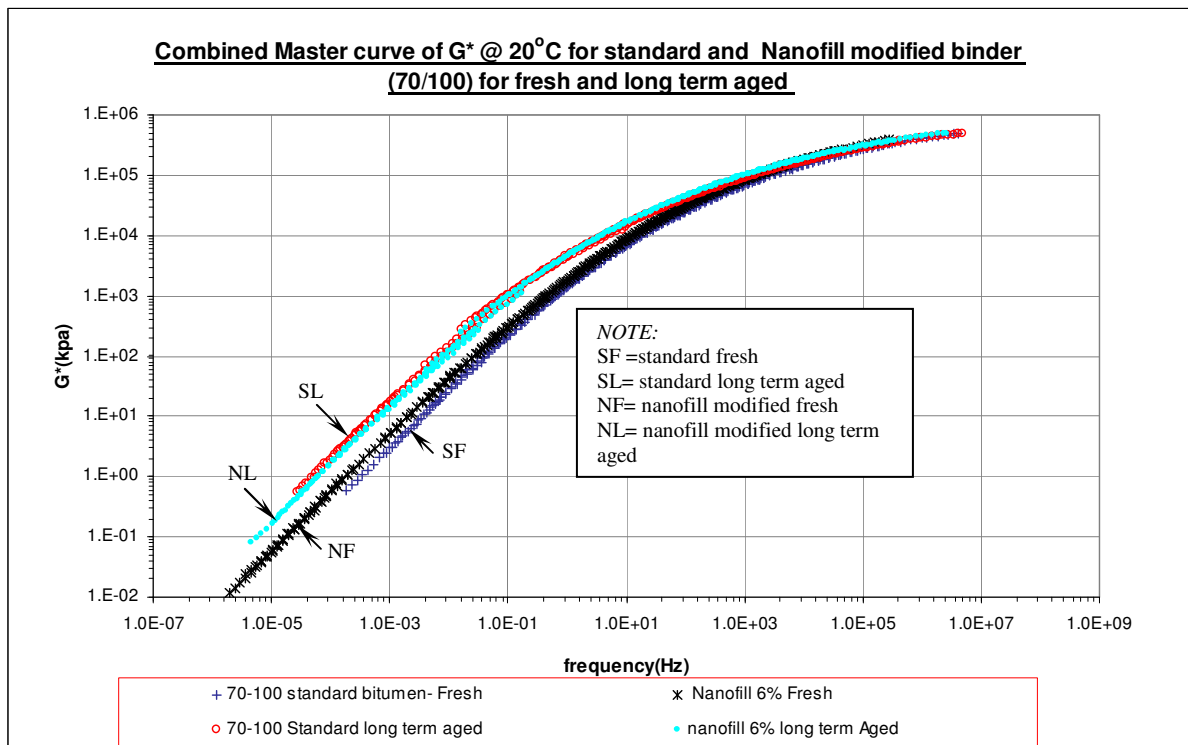


Figure 31: master curve of stiffness of modified and unmodified 70/100 binders (fresh and RCAT long term aged)

The decrement in phase angle values due to RCAT long term ageing effect is given in table 28 and figure 32. From the results the following can be observed.

- The phase angle for the standard binder is reduced on average by 12.0° where as for the modified binder it is reduced by 8.6° in frequency ranges of 10⁻³Hz to 1000Hz.

This also confirms that the modification helps to some degree in improving resistance to ageing of the binder.

- From graph 32, it can also be seen that the small improvement in ageing resistance due to the modification is also true in higher frequency ranges

frequency Hz	phase angle					
	Standard			Nanofill(6%)		
	fresh	Long term	difference	fresh	Long term	difference
1000	35.7	29.01	6.7	39.03	33.73	5.3
100	45.2	34.99	10.3	49.08	41.10	8.0
10	55.6	41.6	14.0	59.1	50.4	8.8
1	65.6	50.4	15.2	66.2	56.1	10.1
0.1	73.1	59.2	13.9	72.9	62.5	10.3
0.01	78.8	66.1	12.7	78.4	69.0	9.4
0.001	83.1	71.9	11.2	83.0	74.8	8.2
average			12.0			8.6

Table 28: Phase angle values of standard and nanofill modified 70/100 binders at selected frequency (fresh and long term aged)

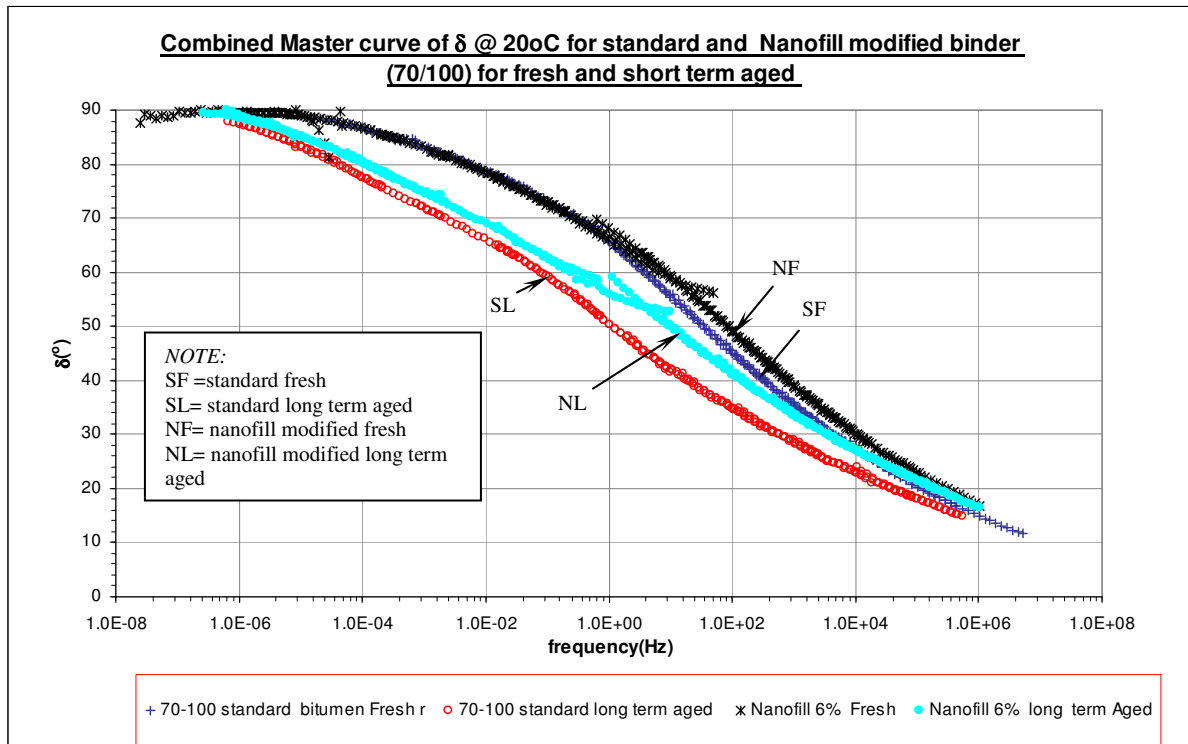
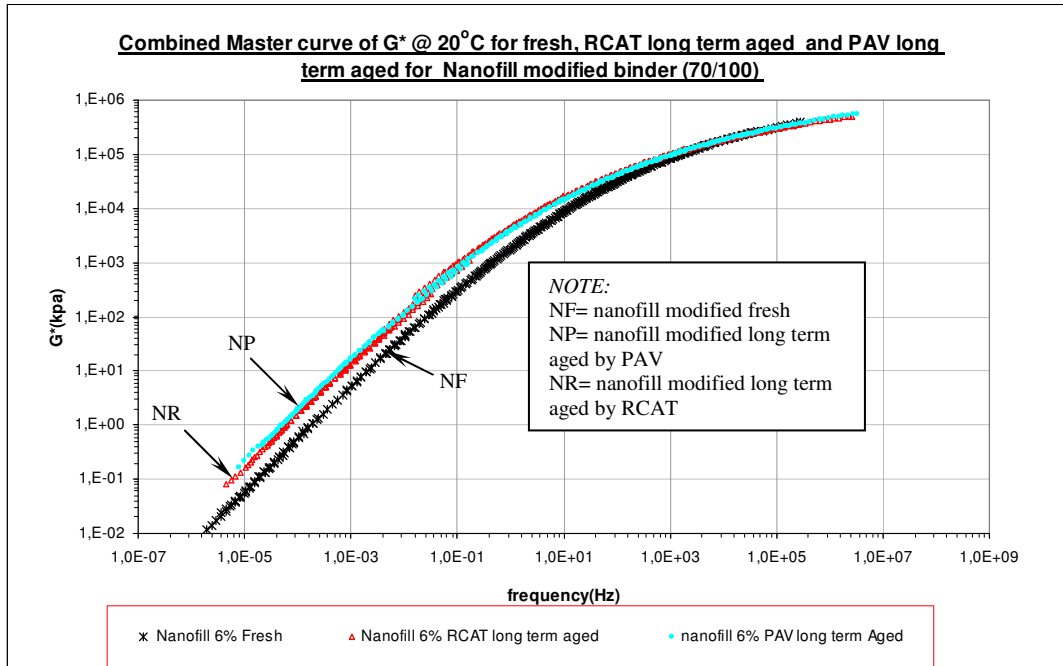


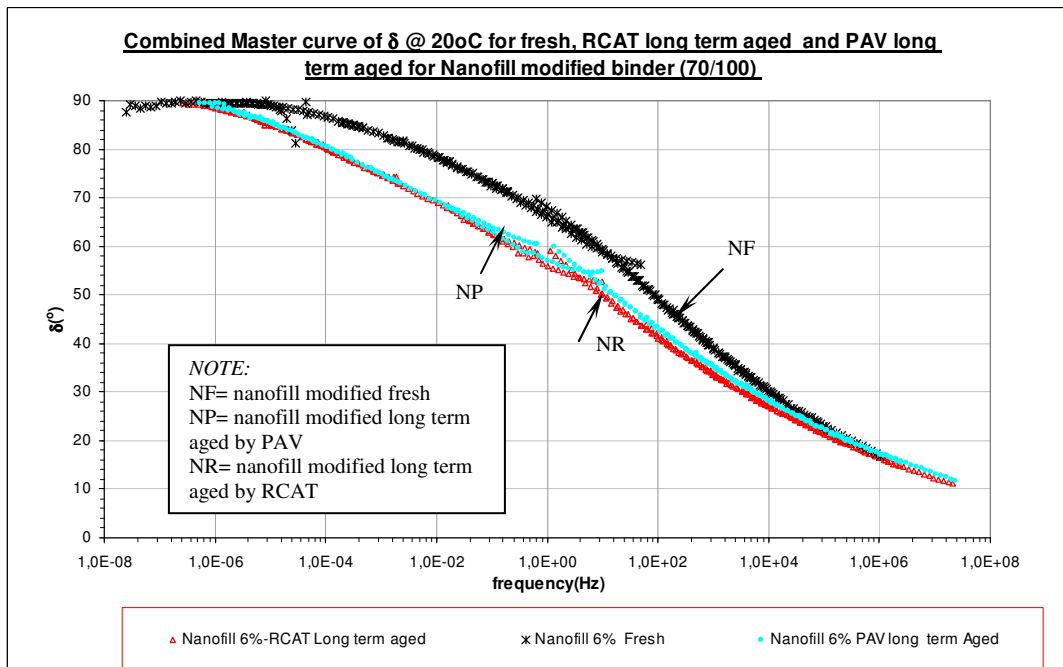
Figure 32: master curve of phase angle for modified and unmodified 70/100 binder (fresh and long term aged)

Long term ageing was also performed using the pressure ageing vessel (PAV). A comparison of master curves of the modified and unmodified samples, which are long term aged by

RCAT and PAV, was performed to see the effect of the ageing equipment on the ageing process. The test result is shown in figure 33 and table 29.



a) Master curve of stiffness



b) Master curve of phase angle

Figure33: master curve of stiffness and phase angle for long term aged modified and unmodified 70/100 binders (using RCAT and PAV)

frequency Hz	stiffness(kpa)			phase angle(°)		
	PAV	RCAT	ratio	PAV	RCAT	difference
1000	16.3306	12.87948	0.788672	74.87734	74.77443	-0.1029077
100	113.5863	96.52659	0.849809	69.35295	69.03801	-0.3149337
10	738.3863	854.6713	1.157485	63.20982	62.527	-0.6828168
1	3832.924	4483.42	1.169713	57.09058	56.14577	-0.9448111
0.1	14247.95	17122.05	1.20172	52.03055	52.661	0.63045354
0.01	40422.45	44523.52	1.101455	42.79096	41.65889	-1.1320673
0.001	93185.26	100035.4	1.073511	35.11086	33.72567	-1.3851951

Table 29: comparison of stiffness and phase angle of PAV and RCAT long term aged nanofill modified 70/100

As can be seen from figure 33 and table 29, the stiffness and phase angle values of the RCAT aged samples are more or less the same as those aged by the PAV. From the results of stiffness and phase angle, on average the binder aged by RCAT is a little bit more aged than the one aged by PAV. The difference is however small.

5.2.3 Analysis and comparison of stiffness and phase angle values: standard 40/60 binder versus cloisite 3% modified 40/60 binder

The same approach of comparison as used with the 70/100 binder is adopted to see the effect of the cloisite modification on the rheology and ageing effect of the 40/60 binder.

5.2.3.1 Comparison of stiffness (fresh)

The master curves of the stiffness of the standard and 3% cloisite modified 40/60 binders is given in figure 34. In addition, values of stiffness for some selected frequency values is given in table 30.

frequency Hz	Stiffness(Kpa)								
	Standard			Cloisite(3%)			Ratio: fresh	increment in stiffness due to ageing(%)	
	fresh	Short term	Differ- ence	fresh	Short term	differ- ence	Clois.3%/ standard	stand- ard	Clois. 3%.
1000	95639	111366	15727	112054	119011	6957	1.17	16%	6%
100	39095	49442	10348	47524	53688	6164	1.22	26%	13%
10	12566	17560	4994	16412	20098	3686	1,3	40%	22%
1	2794	4720	1926	3754	5129	1375	1,3	69%	37%
0,1	436	912	476	629	962	333	1,4	109%	53%
0,01	49	105	56	73	109	36	1,5	115%	49%
0,001	6	14	8	9	14	5	1,6	142%	57%

Table 30: Stiffness values of standard and cloisite 3% modified 40/60 binders (fresh and short term aged) @20°C

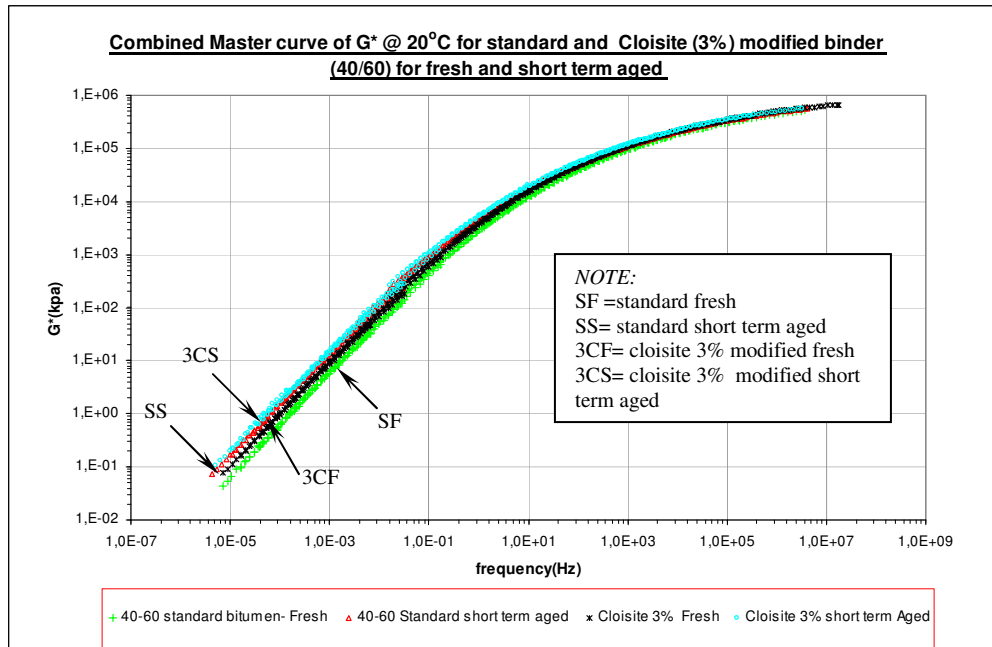


Figure 34: master curve of stiffness of modified and unmodified 40/60 binders (fresh and short term aged)

Analysis and discussion of test results:

From the stiffness results the following points can be observed:

- The cloisite 3% modification helps to increase the stiffness of the standard 40/60 binder to some degree (by a factor of 1.2 at 1000Hz to 1.6 at a frequency of 10^{-3} Hz)
- At higher frequency values the ratio of increment of stiffness values due to modification becomes small.

5.2.3.2 Comparison of Phase angle (fresh)

The master curves of the phase angle of the standard 40/60 binder and 3% cloisite modified binders is shown in figure 35. In addition, values of phase angle for some selected frequency values are provided in table 31.

frequency Hz	phase angle						
	Standard			Cloisite (3%)			fresh Cloisite 3%- standard
	fresh	short term	difference	fresh	Short term	difference	
1000	34.0	31.0	3.1	34.9	32.2	2.6	0.8
100	43.8	39.3	4.6	44.4	40.7	3.6	0.5
10	56,3	50,5	5,8	55.4	52.8	2.6	-0.9
1	63,9	57,6	6,3	63,3	58,4	4,8	-0,6
0,1	71,7	64,9	6,8	68,5	64,4	4,1	-3,2
0,01	77,5	71,1	6,4	74,4	70,9	3,4	-3,1
0,001	82,2	76,6	5,6	79,3	76,6	2,7	-2,8

Table 31: Phase angle values of standard and cloisite 3% modified 40/60 binders at selected frequencies (fresh and short term aged)

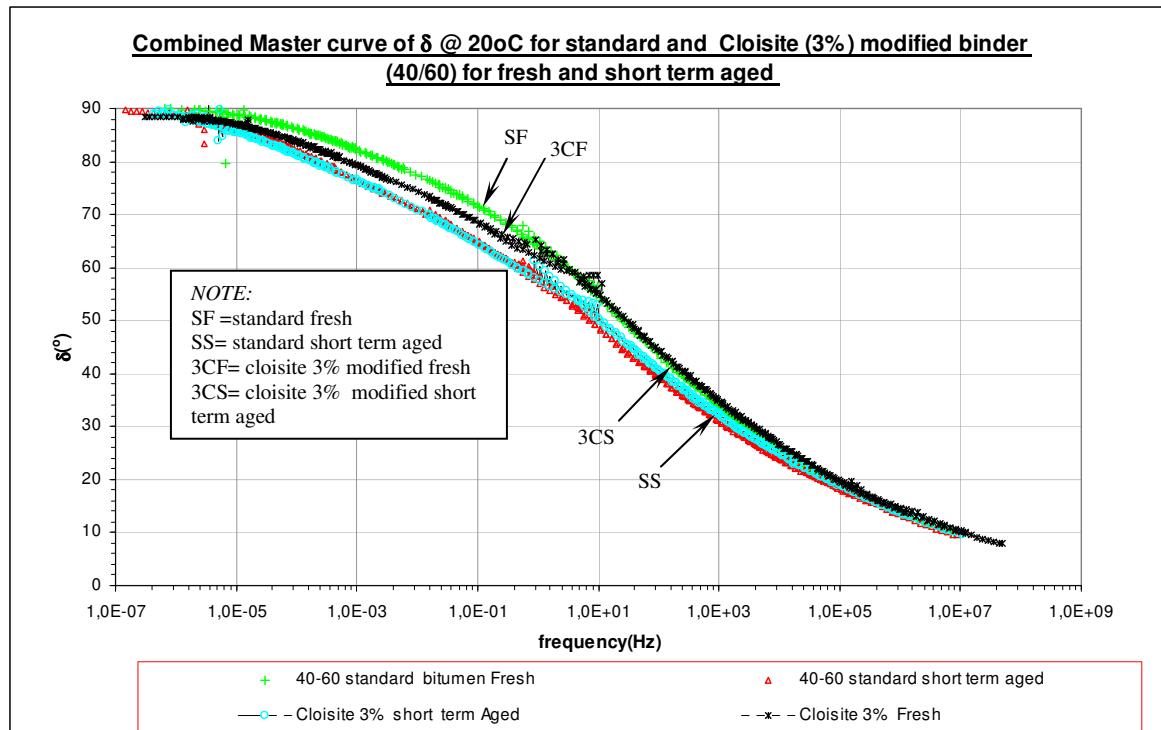


Figure 35: master curve of phase angle of modified and unmodified 40/60 binder (fresh and short term aged)

Analysis and discussion of test results:

The phase angle values of the modified and unmodified 40/60 binder show the following.

- The cloisite 3% modification helps in decreasing the phase angle of the standard 40/60 binder to some degree (for instance a difference of -0.6° is obtained @ 1Hz and about -3° @ 10^{-3} Hz)
- At frequencies >10 Hz the phase angle of the standard 40/60 and the 3% cloisite modified binder are more or less the same.

5.2.3.3 Short term ageing effect analysis

The short term ageing effect comparison is performed based on the master curves of figure 34 and figure 35 and the analysis done on stiffness in table 30 and the analysis done on phase angle in table 31.

From the stiffness values given in table 30 and figure 34 the following can be seen.

- The increment in stiffness is relatively bigger for the standard binder as compared to the modified binder after short term ageing (the stiffness value increases about 16% @ a frequency of 1000Hz and almost 140% @ a frequency of 10^{-3} Hz for the standard binder where as for the cloisite modified binder the stiffness increases about 6% @ a frequency of 1000Hz and almost 60% @ a frequency of 10^{-3} Hz)

- At higher frequency values the increment in stiffness values due to ageing becomes less in both binders (% wise).

From the phase angle values given in table 31 and figure 35 the following can be observed.

- After short term ageing, the phase angle values decreases by about 6.2° on average for the standard binder and by 3.5° for the cloisite 3% modified binder for a frequency ranges between 10Hz and 10⁻³ Hz.
- For frequency >10 Hz the decrease in phase angle due to ageing becomes more or less the same for the standard and cloisite 3% modified binders.

In order to understand the practicability of the frequencies ranges (@20°C) mentioned above and in order to make the conclusion more practical, table 32 gives comparison of G* and phase angle for some selected frequencies and temperature values after short term ageing.

	Increment in Stiffness (%)				decrement in phase angle(°)			
	freq.(Hz)/ temp(°C)	-10°C	20°C	60°C	freq.(Hz)/ temp(°C)	-10°C	20°C	60°C
Cloisite 3%	0,1Hz	9%	53%		0,1Hz	-1,97	-4,10	-
	10Hz	3%	22%	44%	10Hz	-0,68	-2,60	-2,35
	20Hz	-	18%	56%	20Hz	-	2,53	-2,12
standard 40/60	0,1Hz	27%	109%		0,1Hz	-3,41	-6,80	
	10Hz	13%	40%	76%	10Hz	-1,04	-5,80	-3,45
	20Hz	-	33%	79%	20Hz	-	-5,94	-3,66

Table 32: stiffness and phase angle analysis after short term ageing for modified and unmodified binders

From table 32 the following can be observed.

- The increment in stiffness is bigger for the standard binder as compared to the 3% cloisite modified binder
- The decrement in phase angle values is lower for the 3% cloisite modified binder in relation to the standard binder.

The assessment of the increment of the stiffness and decrement of phase angle values due to the short term ageing process on modified and unmodified binders proves that the cloisite 3% modification helped to reduce the ageing effect of the binder.

5.2.3.4 Long term ageing effect analysis

The increment in stiffness values due to long term ageing by RCAT for the 3% cloisite modified and standard binder is given in table 33 and figure 36. From the results, the following can be observed.

- The stiffness of the unmodified binder increases by about 340% and for the modified binder it increase by about 260% from their original values in the frequency ranges

between 10^{-3} Hz to 1000Hz. This shows us that the modification helps a bit in improving the resistance to ageing in the long term.

- The ratio of increment in stiffness value due to long term ageing effect gets smaller in higher frequency values.

frequency Hz	Stiffness(kpa)							
	Standard			Cloisite (3%)			Increment in stiffness due to ageing(%)	
	fresh	Long term	difference	fresh	Long term	difference	standard	Clois. 3%
1000	95639	117098	21459	112054	122643	10590	22%	9%
100	39095	60667	21572	47524	62246	14722	55%	31%
10	12566	26189	13622	16412	23005	6593	108%	40%
1	2794	9522	6728	3754	8683	4929	241%	131%
0,1	436	2380	1944	629	2379	1750	446%	278%
0,01	49	360	311	73	490	417	635%	567%
0,001	6	56	50	9	81	72	874%	793%
average							340%	264%

Table 33: stiffness values of standard and cloisite 3% modified 40/60 binders (fresh and long term aged by RCAT) @20°C

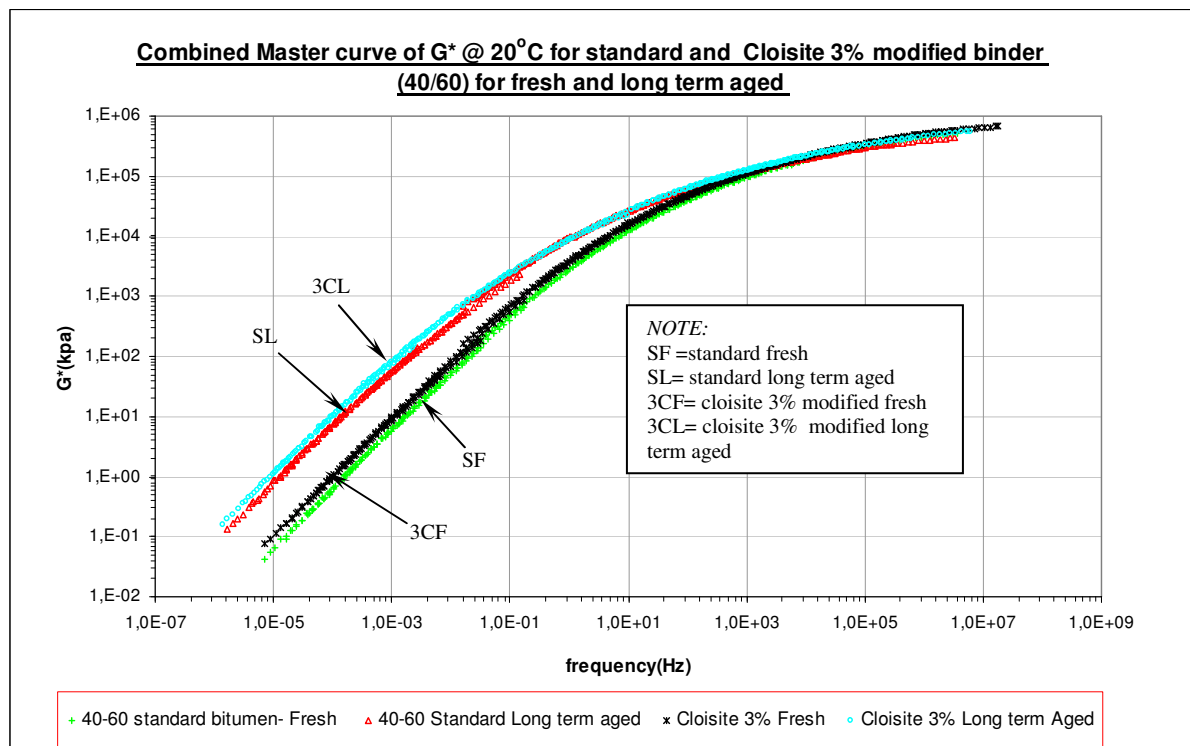


Figure 36: master curve of stiffness of cloisite 3% modified 40/60 binder and unmodified 40/60 binders (fresh and RCAT long term aged)

The decrement in phase angle due to RCAT long term ageing is given in table 34 and figure 37. The results show that:

- The phase angle for the standard binder is reduced on average by 13.5° where as for the modified binder it is reduced by 11.8° in frequency ranges between 10⁻³Hz to 0.1Hz. This shows that the modification hardly changes the value of the phase angle in low frequency ranges (10⁻³Hz to 0.1Hz).
- From graph 37 and table 34, it can also be seen that at higher frequency values (>1Hz) the modified binder is more aged than the standard 40/60 binder.

frequency Hz	phase angle					
	Standard			Cloisite(3%)		
	fresh	Long term	difference	fresh	Long term	difference
1000	34.0	26.8	7.3	34.9	22.4	12.5
100	43.8	33.4	10.5	44.4	28.2	16.2
10	56,3	41,3	15,0	58,3	33,1	25,2
1	63,9	50,4	13,5	63,3	43,2	20,0
0,1	71,7	57,0	14,8	68,5	54,4	14,1
0,01	77,5	63,8	13,6	74,4	62,7	11,6
0,001	82,2	70,1	12,1	79,3	69,7	9,6

Table 34: Phase angle values of standard and cloisite 3% modified 40/60 binders (fresh and long term aged) @20°C

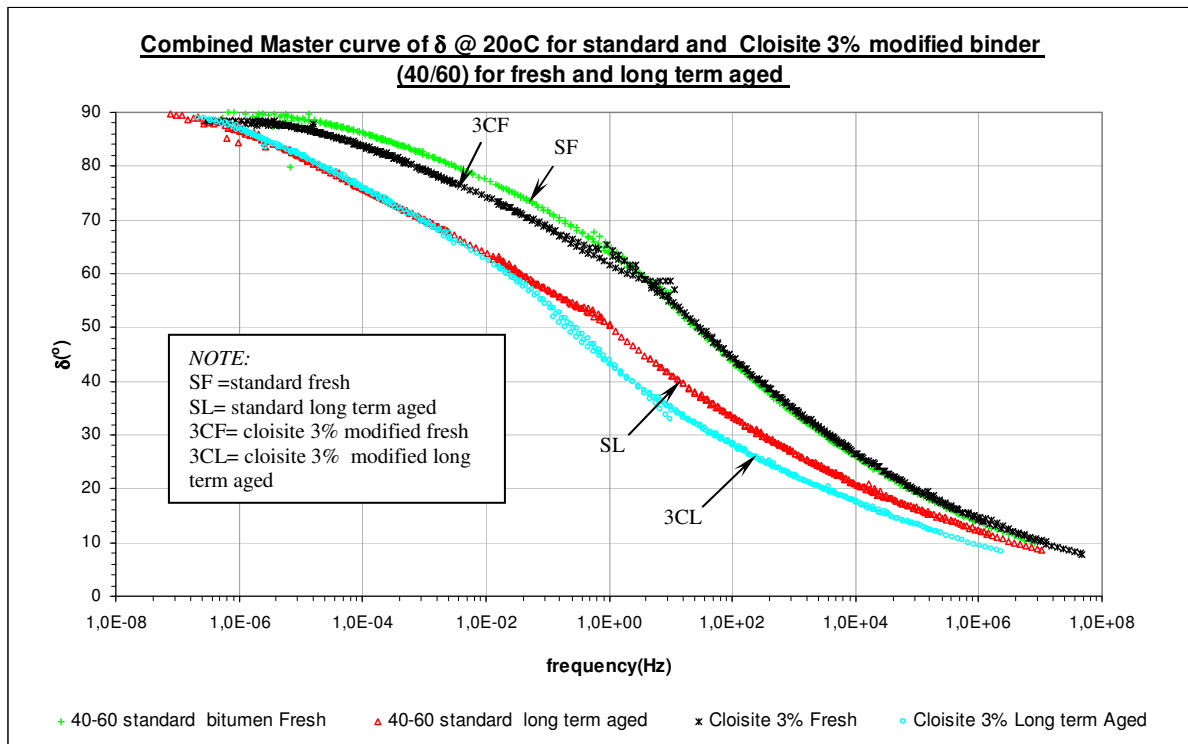


Figure 37: master curve of phase angle of modified and unmodified 40/60 binder (fresh and long term aged)

5.2.4 Analysis and comparison of stiffness and phase angle values: standard 40/60 binder versus cloisite 6% modified 40/60 binder

The effect of 6% cloisite modification on increment of stiffness and decrement of phase angle of an aged 40/60 binder is first discussed. In addition the effect of 6% cloisite modification on short term and long term ageing effect is investigated and reported.

5.2.4.1 Comparison of stiffness (fresh)

The master curve of the stiffness of the standard and modified binders is shown in figure 38. Furthermore, values of stiffness for some selected frequency values is given in table 35.

frequency Hz	Stiffness (Kpa)								
	Standard			Cloisite(6%)			Ratio: fresh	increment in stiffness due to ageing(%)	
	fresh	Short term	differ- ence	fresh	Short term	differ- ence	Clois. 6% / standard	standard	Clois. 6%
1000	95639	111366	15727	123051	140258	17207	1.3	16%	14%
100	39095	49442	10348	53467	65221	11754	1.4	26%	22%
10	12566	17560	4994	18103	24369	6265	1,4	40%	35%
1	2794	4720	1926	4540	6840	2301	1,6	69%	51%
0,1	436	912	476	788	1342	554	1,8	109%	70%
0,01	49	105	56	94	161	67	1,9	115%	72%
0,001	6	14	8	13	24	12	2,2	142%	94%
0,0001	0,60	1,58	0,98	1,51	2,99	1,48	2,5	163%	98%

Table 35: Stiffness values of standard and 6% cloisite modified 40/60 binders (fresh and short term aged)@20°C

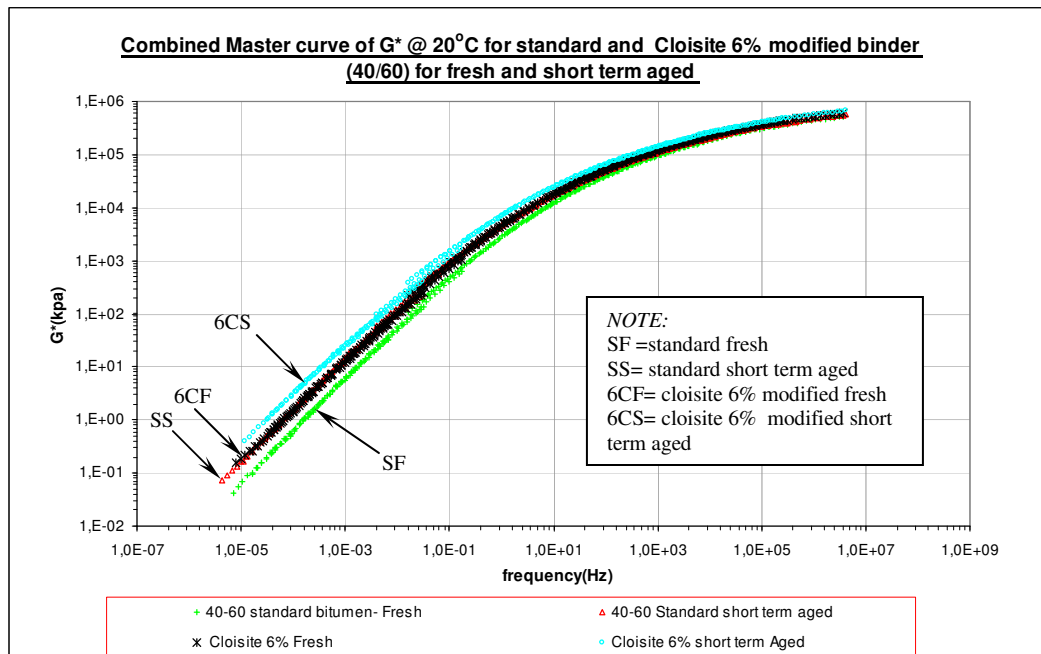


Figure 38: master curve of stiffness of standard and 6% cloisite modified binder (fresh and short term aged)

Analysis and discussion of test results:

From the stiffness results the following conclusions can be drawn.

- The cloisite 6% modification increases the stiffness of the standard 40/60 binder at low to medium frequency ranges (by a factor of 1.3 at 1000Hz to 2.5 at a frequency of 10^{-4} Hz)
- The cloisite 6% modification increases the stiffness of the standard 40/60 binder some what better than the 3% cloisite modification (for instance @ 10^{-3} Hz the 3% cloisite modification increases stiffness 1.6 factor where as the 6% cloisite by 2.2 factor)

5.2.4.2 Comparison of Phase angle (fresh)

The master curve of the phase angle of the standard and modified binders is given in figure 39 and values of phase angle for some selected frequency values are provided in table 36.

frequency Hz	phase angle						
	Standard			Cloisite (6%)			fresh Clois.6%-standard
	fresh	short term	difference	fresh	Short term	difference	
1000	34.0	31.0	3.1	31.9	31.7	0.2	-2.2
100	43.8	39.3	4.6	41.0	40.1	1.0	-2.8
10	56,3	50,5	5,8	51,5	49,2	2,3	-4,8
1	63,9	57,6	6,3	61,8	58,9	2,9	-2,1
0,1	71,7	64,9	6,8	66,7	62,5	4,2	-5,0
0,01	77,5	71,1	6,4	71,8	67,5	4,3	-5,7
0,001	82,2	76,6	5,6	76,4	71,9	4,6	-5,8
0,0001	86,2	81,8	4,4	78,7	76,0	2,7	-7,5
average			5,4			2.8	-4.5

Table 36: Phase angle of standard and modified binders (aged and un-aged) @20°C

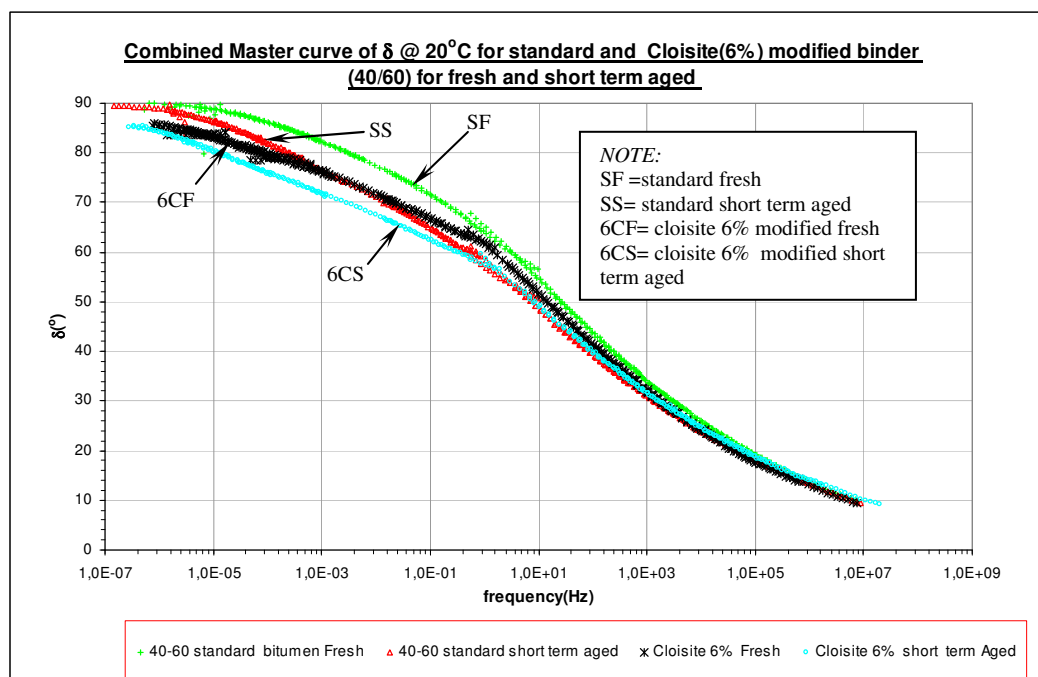


Figure39: master curve of phase angle of standard and modified binders (aged and un-aged)

Analysis and discussion of test results:

From the phase angle values of the modified and unmodified 40/60 binders, the following can be observed.

- The cloisite 6% modification helps in decreasing the phase angle of the standard 40/60 binder (for instance a difference of -4.8° is obtained @ 10Hz and about -7.5° @ 10^{-4} Hz)
- The decrease in the phase angle of the standard 40/60 binder due to cloisite 6% modification is much bigger than the 3% cloisite modification (for instance @ 10^{-3} Hz the 3% cloisite modification decreases phase angle by 2.8° where as the 6% cloisite by 5.8°)

5.2.4.3 Short term ageing effect analysis

The short term ageing effect comparison is performed based on the master curves of figure 38 and figure 39 and the analysis done on stiffness in table 35 and the analysis done on phase angle in table 36.

From the stiffness values given in table 35 and figure 38, the following can be observed.

- The increment in stiffness due to the short term ageing is relatively bigger for the standard binder as compared to the modified binder (the stiffness value increases about 16% @ a frequency of 1000Hz and almost 160% @ a frequency of 10^{-4} Hz for the standard binder where as for the cloisite modified binder the stiffness increases about 14% @ a frequency of 1000Hz and almost 100% @ a frequency of 10^{-4} Hz)
- Based on the analysis of the stiffness, the increment of the modification from 3% to 6% hardly improves the resistance to short term ageing.

From the phase angle values given in table 36 and figure 39 it can be seen that:

- After short term ageing, the phase angle values decreases by about 5.4° on average for the standard binder and by 2.8° for the cloisite 6% modified binder for a frequency ranges between 1000Hz and 10^{-4} Hz.
- From the analysis done on the phase angle, the increment of the modification from 3% to 6% cloisite further improves the resistance to short term ageing a bit.

The assessment of stiffness and phase angle values after the short term ageing process proves that the cloisite 6% modification helped to reduce the ageing effect of the binder at low to medium frequency (10^{-3} to 10Hz) values to some degree. However, the increment from 3% cloisite to 6% cloisite hardly changes the resistance to short term ageing effect.

5.2.4.4 Long term ageing effect analysis

The RCAT long term ageing effect on stiffness of 6% cloisite modified and standard binders is given in table 37 and figure 40. From the stiffness analysis the following can be observed.

- The stiffness of the unmodified binder increases by about 335% and for the 6% cloisite modified binder it increases by about 235% from their original values in the frequency ranges between 10^{-3} Hz to 1000Hz. This shows us that the improvement due to the 6% cloisite modification in long term ageing resistance is not big.
- The increment of cloisite from 3% to 6% hardly changes the resistance to ageing effect in the long term.

frequency Hz	stiffness							
	Standard			Cloisite (6%)			Increment in stiffness due to ageing(%)	
	fresh	Long term	difference	Fresh	Long term	difference	standard	Clois. 6%
1000	95639	117098	21459	123051	136472	13421	22%	11%
100	39095	60667	21572	53467	77087	23620	55%	44%
10	12566	26189	13622	18103	26241	8137	108%	45%
1	2794	9522	6728	4540	10958	6418	241%	141%
0,1	436	2380	1944	788	3010	2222	446%	282%
0,01	49	360	311	94	622	528	635%	564%
0,001	6	56	50	13	83	70	874%	556%
average							335%	235%

Table 37: stiffness values @20°C of standard and cloisite 6% modified 40/60 binders (fresh and long term aged by RCAT)

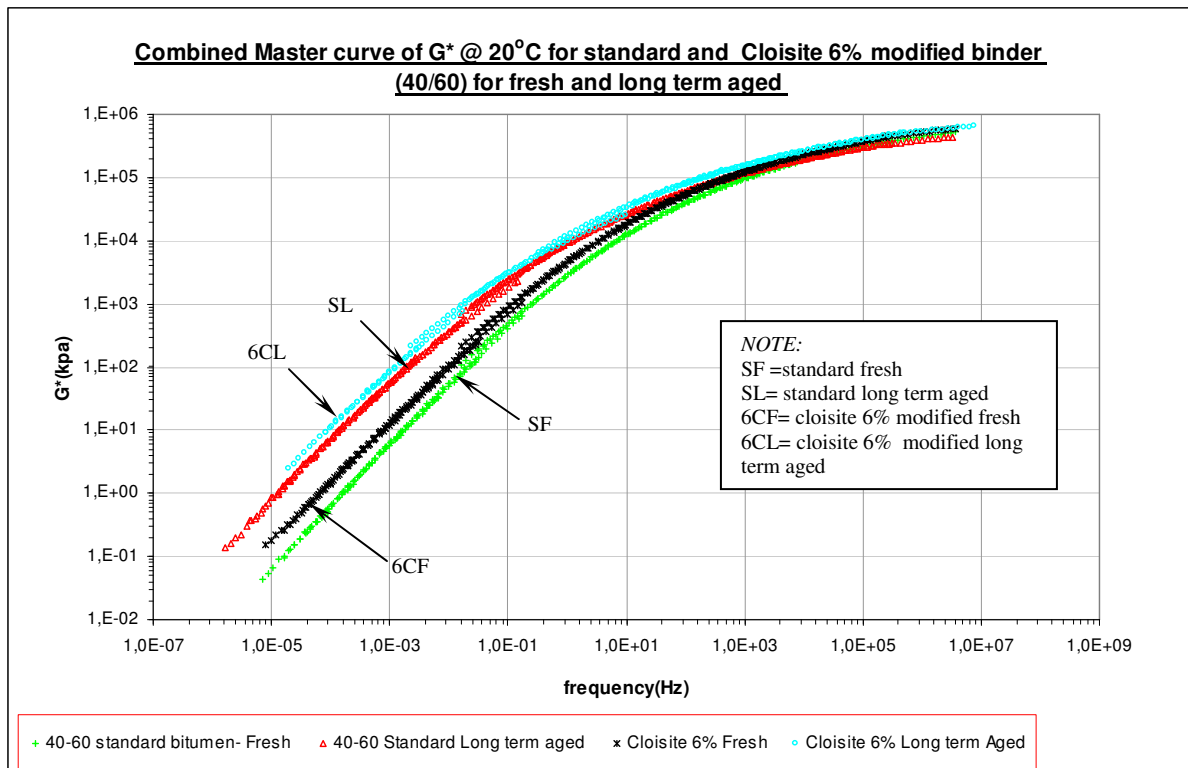


Figure 40: master curve of stiffness of cloisite 6% modified 40/60 binder and unmodified 40/60 binders (fresh and RCAT long term aged)

RCAT long term ageing effect on the phase angle of standard and 6 % cloisite modified binders is given in table 38 and figure 41. The results show that:

- The phase angle for the standard binder is reduced on average by 13.5° where as for the modified binder it is reduced by 11.7° in frequency ranges between 10⁻³Hz to 0.1Hz. This shows that the modification hardly increases the resistance to ageing in low frequency ranges (10⁻³Hz to 0.1Hz).
- In frequency ranges > 1Hz the decrement in phase angle is even a bit higher for the 6% cloisite modification as compared to the standard binder.

frequency Hz	phase angle					
	Standard			Cloisite(6%)		
	fresh	Long term	difference	fresh	Long term	difference
1000	34.0	26.8	7.3	31.9	25.3	6.6
100	43.8	33.4	10.5	41.0	27.1	13.9
10	56,3	41,3	15,0	51,5	32,3	19,2
1	63,9	50,4	13,5	61,8	42,5	19,3
0,1	71,7	57,0	14,8	66,7	52,7	14,0
0,01	77,5	63,8	13,6	71,8	60,6	11,2
0,001	82,2	70,1	12,1	76,4	66,7	9,8

Table 38: Phase angle values @20°C of standard and cloisite 6% modified 40/60 binders (long term aged)

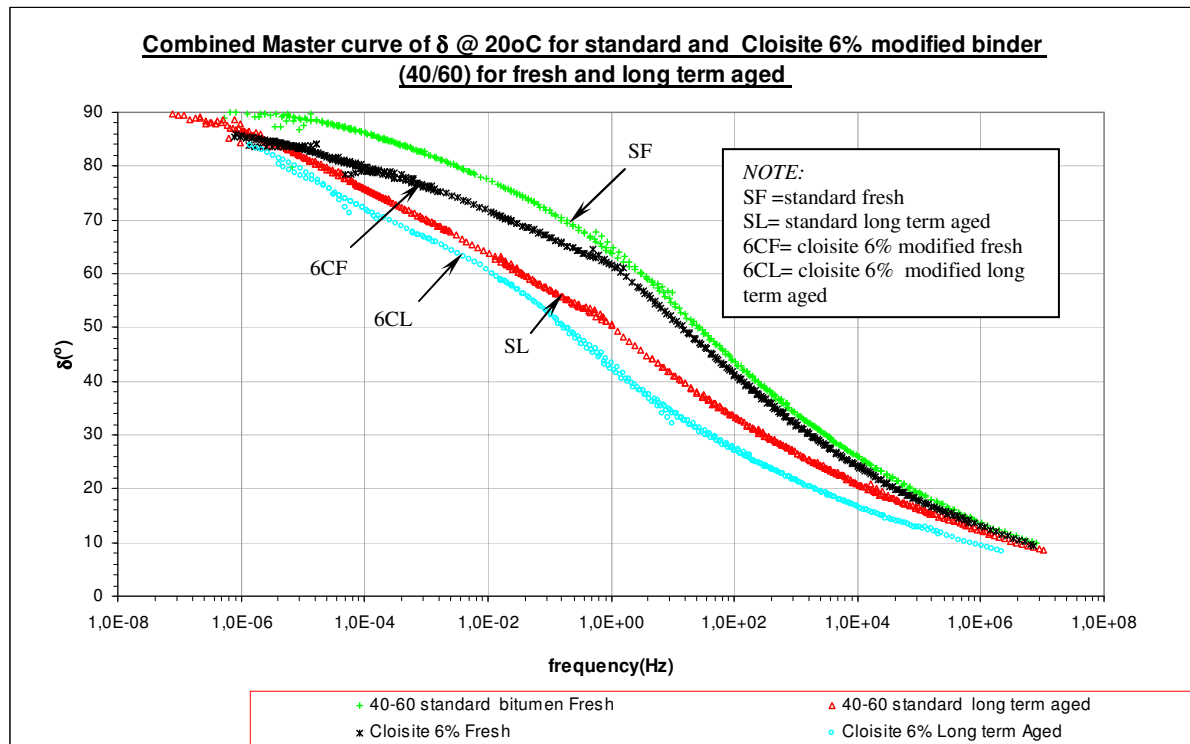


Figure 41: master curve of phase angle of 6% cloisite modified 40/60 binder and unmodified 40/60 binders (fresh and RCAT long term aged)

5.3 Permanent deformation and fatigue analysis from DSR results

The complex shear modulus and phase angle of a binder, which are indicators of bitumen resistance to shear deformation in the visco-elastic region, help to predict the potential rutting and fatigue resistance of hot asphalt mixture.

5.3.1 Rutting Parameter

Rutting is assumed to be the primary result of deformations within the surface layer. Rutting is considered to be a stress-controlled, cyclic loading phenomenon. During each cycle of traffic loading a certain amount of work is being done to deform the surface layer. Part of the work done is recovered in the elastic rebound of the surface layer, while the remaining work is dissipated through permanent deformation and heat. To minimize rutting the work dissipated during each loading cycle should be minimized [10,17]. The work dissipated per cycle (W_c) is calculated in terms of stress (σ) and strain (ϵ) as :

$W_c = \pi \sigma \epsilon \sin \delta$ and for stress controlled condition $\sigma = \sigma_o$. Therefore, $W_c = \pi \sigma_o \epsilon \sin \delta$

$$\text{Since } \epsilon = \frac{\sigma_o}{G^*} \longrightarrow W_c = \pi \sigma_o^2 \left(\frac{1}{G^*/\sin \delta} \right) \quad (\text{Eq13})$$

From Equation 13 it can be seen that an increase in G^* and decrease in $\sin \delta$ will both decrease the amount of work dissipated per loading cycle within a pavement's surface layer. This relationship follows the validation that a binder with a high G^* value is stiffer, which increases its resistance to deformation, and a binder with a low $\sin \delta$ value is more elastic, whereby its ability to recover part of the deformation is increased. Hence, a binder with bigger value of $G^*/\sin \delta$ shows better rutting resistance than another one with small value of $G^*/\sin \delta$.

To relate G^* and δ with actual traffic loading condition, a loading time of 0.1 sec which is related to a pass of a truck tire traveling at 80 km/h (50 mi/h) is selected as a loading frequency. With sinusoidal loading, 0.1 second corresponds to 10 rad/s (1.6 Hz).

To see the effect of high temperature on rutting performance, high temperature values (40-80°C) are selected and the rutting parameter ($G^*/\sin \delta$) is calculated at 10rad/s (1.6Hz). Table 39 and figure 42 show the comparison between modified and unmodified; aged and unaged 40-60 binders. The minimum limit of $G^*/\sin \delta$ is 1.0 kPa for unaged binder and 2.2 kpa for RTOFT aged asphalt cements and the limiting temperature corresponds to the highest temperature in which the binder is actually expected to serve. Normally temperature values like 58°C, 64°C and 70°C are used for moderate temperature regions.

		$G^* / \sin \delta$			ratio - $G^*/\sin \delta$ (Modified/standard)		
Binder	Temperature (°C)	unaged	short term aged	long term aged	unaged	short term aged	long term aged
standard 40/60	40	72.28	161.98	417	1.00	1.00	1.00
	50	12.99	28.88	76.6	1.00	1.00	1.00
	60	2.99	5.90	14.77	1.00	1.00	1.00
	70	0.79	1.51	3.89	1.00	1.00	1.00
	80	0.24	0.45	1.05	1.00	1.00	1.00
Cloisite 3% + 40/60	40	112.92	176.70	442	1.6	1.09	1.06
	50	20.66	33.25	87.4	1.6	1.2	1.1
	60	5.27	6.66	19.02	1.8	1.1	1.3
	70	1.35	1.97	4.07	1.7	1.3	1.0
	80	0.43	0.63	1.15	1.8	1.4	1.1
Cloisite 6% + 40/60	40	144.53	255.25	561	2.0	1.6	1.3
	50	28.42	50.05	113.3	2.2	1.7	1.5
	60	6.86	11.71	25.79	2.3	2.0	1.7
	70	1.74	3.13	7.19	2.2	2.1	1.8
	80	0.66	1.03	2.07	2.7	2.3	2.0

Table 39: comparison of $G^*/\sin \delta$ of modified and unmodified 40/60 binders

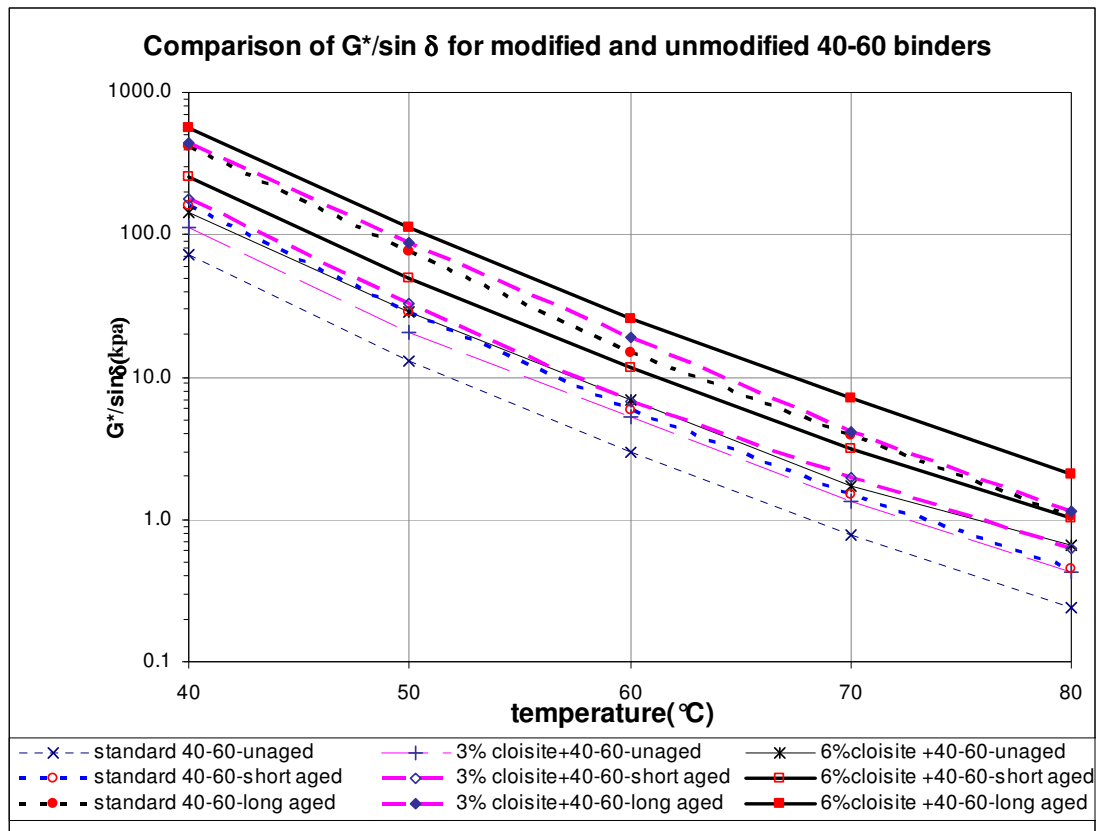


Figure 42: Comparison of $G^*/\sin \delta$ of modified and unmodified 40-60 binders

Analysis and discussion of test results:

The analysis result of figure 42 and table 39 shows

- The rutting parameter , $G^*/\sin \delta$, of 6% cloisite modified un aged 40-60 binder is 2 to 3 times higher than that of the standard unaged 40-60 binder. In addition, it is 1.6 to 2.3 times higher in short term ageing and 1.3 to 2 times higher in long term ageing.
- The rutting parameter , $G^*/\sin \delta$, of 3% cloisite modified un aged 40-60 binder is 1.6 to 1.8 times higher than that of the standard unaged 40-60 binder. In addition, it is 1.1 to 1.4 times higher in short term ageing and 1.0 to 1.3 times higher in long term ageing.

Taking into account the binder effect on rutting, the 6% cloisite modified 40-60 binder performs much better than standard 40-60 binder.

The comparison of the rutting parameter $G^*/\sin \delta$ of the modified and unmodified 70-100 binders is given in table 40 and figure 43.

Binder	Temperature (°C)	$G^*/\sin \delta$				ratio - $G^*/\sin \delta$ (Modified/standard)			
		unaged	short term aged	long term aged		unaged	short term aged	long term aged	
				RCAT	PAV			RCAT	PAV
standard 70/100	40	40.75	77.45	182	204	1.00	1.00	1.00	1.00
	50	7.81	14.40	37.8	34.1	1.00	1.00	1.00	1.00
	60	1.81	3.30	8.10	7.67	1.00	1.00	1.00	1.00
	80	0.21	0.20	0.55	0.56	1.00	1.00	1.00	1.00
nanofill 6% + 70/100	40	70.33	56.58	164	143	1.7	0.73	0.90	0.70
	50	12.43	10.66	29.7	25.8	1.6	0.74	0.79	0.76
	60	1.95	2.52	6.68	5.79	1.1	0.76	0.82	0.75
	80	0.20	0.22	0.51	0.44	1	1.09	0.92	0.79

Table 40: comparison of $G^*/\sin \delta$ of modified and unmodified 70/100 binders

Analysis and discussion of test results:

The analysis result of figure 43 and table 40, the following can be observed.

- The rutting parameter , $G^*/\sin \delta$, of the 6% nanofill modified un aged 70-100 binder is about 1.6 times higher than that of the standard unaged 70-100 binder in temperature ranges of 40 to 50°C. However, this improvement was not shown in temperature values > 60°C.
- The rutting parameter , $G^*/\sin \delta$, of the 6% nanofill modified aged 70-100 binder is less than that of the standard aged 70-100 binder (85% in RCAT short term and long term ageing, 75% in PAV long term ageing). This is because the nanofill modified binder is less aged as compared to the standard 70-100 binder.

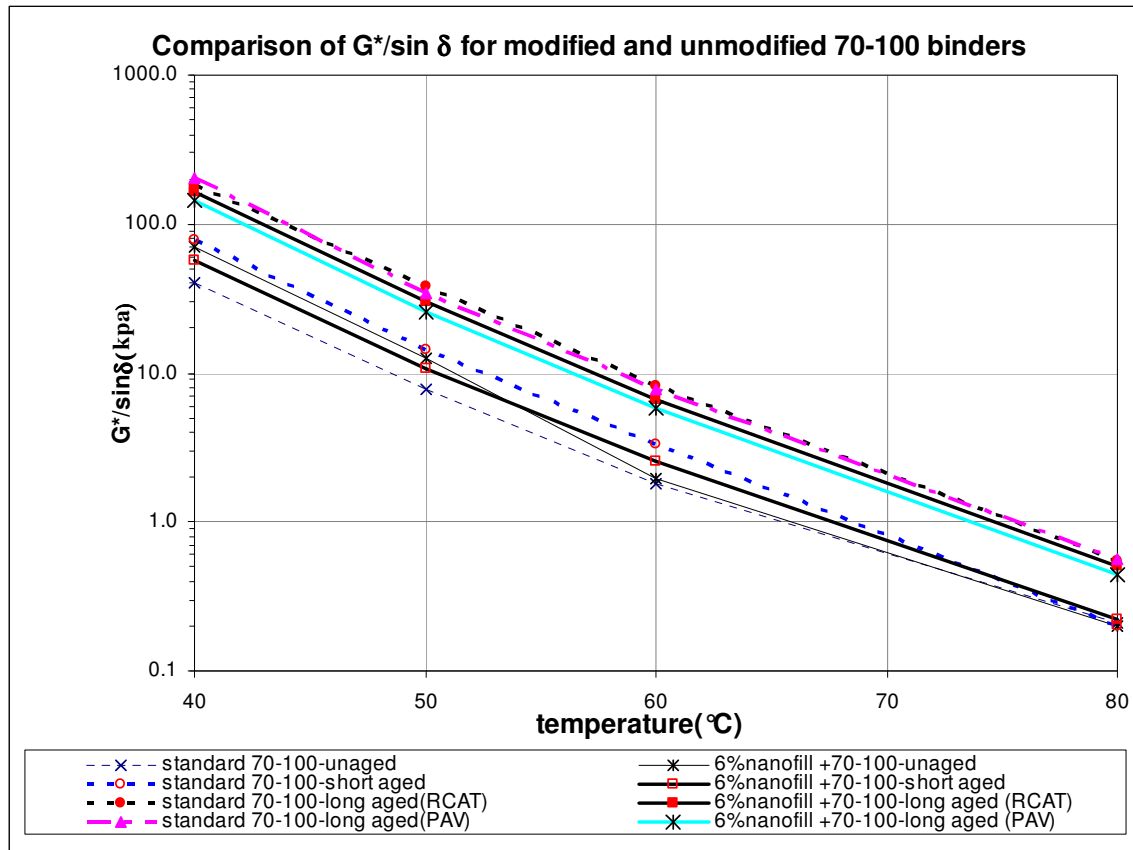


Figure 43: Comparison of $G^*/\sin \delta$ of modified and unmodified 70-100 binders

The maximum temperature values at which the minimum limit of $G^*/\sin \delta$ is still satisfied is given in table 41.

Binders	Temperature (°C)	
	unaged- $G^*/\sin \delta = 1 \text{ kpa}$	short aged- $G^*/\sin \delta = 2.2 \text{ kpa}$
standard 70-100	65.0	63.4
6% nanofill + 70-100	65.2	62.8
standard 40-60	69.0	68.4
3% cloisite + 40-60	73.8	69.5
6% cloisite + 40-60	76.8	74.4

Table 41: Temperature values at minimum limits of $G^*/\sin \delta$

The results of table 41 shows that the 6% cloisite modified binder shows much better rutting resistance than the standard and the 3% cloisite modified 40-60 binders

5.3.2 Fatigue resistance parameter

Fatigue cracking is the primary pavement distress at intermediate service temperatures. Pavement fatigue cracking is considered a strain controlled distress in thin pavement layers. The work done during a loading cycle can be dissipated by cracking, crack propagation, heat,

and plastic flow. To improve fatigue life the work dissipated during each loading cycle should be minimized [10,17]. The work dissipated per cycle (W_c) is calculated in terms of stress (σ) and strain(ϵ) as :

$$W_c = \pi \sigma \epsilon \sin \delta \text{ for stress controlled } \epsilon = \epsilon_0. \text{ Hence, } W_c = \pi \sigma \epsilon_0 \sin \delta$$

$$\sigma = \epsilon_0 * G^* \longrightarrow W_c = \pi \epsilon_0^2 G^* \sin \delta \quad (\text{Eq14})$$

Eq.14 shows that by limiting the $G^* \sin \delta$ parameter, decreasing G^* and/or $\sin \delta$, the energy dissipated per cycle is limited as well. This limiting parameter follows the underlying principle that a binder with a low G^* is softer, which allows it to deform without developing high stresses, and a binder with a low $\sin \delta$ will be more elastic, which enables the pavement structure to return to its original condition without dissipating energy.

Similar to rutting resistance analysis a loading frequency of 10rad/s(1.59Hz) is considered to approach practical loading time. Low to medium temperature values (0 to 20°C) are selected for fatigue resistance comparison.

The maximum limit of $G^* \sin \delta$ is 5.0 MPa for PAV aged asphalt binders and the limiting temperature according to SHRP is 4°C above the mid point between the highest and the lowest design temperatures of the pavement. Normally values between 10 to 25°C are common values.

Table 42 and figure 44 show the comparison of fatigue parameter ($G^* \sin \delta$) between modified and unmodified 40-60 binders.

Binder	Temperature(°C)	$G^* \times \sin \delta$			ratio - $G^* \times \sin \delta$ (Modified/standard)		
		unaged	short term aged	long term aged	unaged	short term aged	long term aged
standard 40/60	0	46853.80	53425.27	47751.3	1.00	1.00	1.00
	5	28031.30	34120.35	30672.2	1.00	1.00	1.00
	10	14562.30	19343.56	19360.0	1.00	1.00	1.00
	20	3516.40	4959.63	5860.0	1.00	1.00	1.00
Cloisite 3% + 40/60	0	53230.00	53537.33	53672.7	1.1	1.00	1.12
	5	32850.00	33981.12	37617.5	1.2	1.00	1.2
	10	18300.00	19337.80	23888.8	1.3	1.00	1.2
	20	4395.00	5674.42	7145.5	1.2	1.14	1.2
Cloisite 6% + 40/60	0	54720.00	59463.76	64735.4	1.2	1.1	1.4
	5	34160.00	38941.67	46685.4	1.2	1.1	1.5
	10	18660.00	22646.94	30386.13	1.3	1.2	1.5
	20	5079.20	7646.04	8045.20	1.4	1.5	1.4

Table 42: comparison of $G^* \times \sin \delta$ of modified and unmodified 40/60 binders

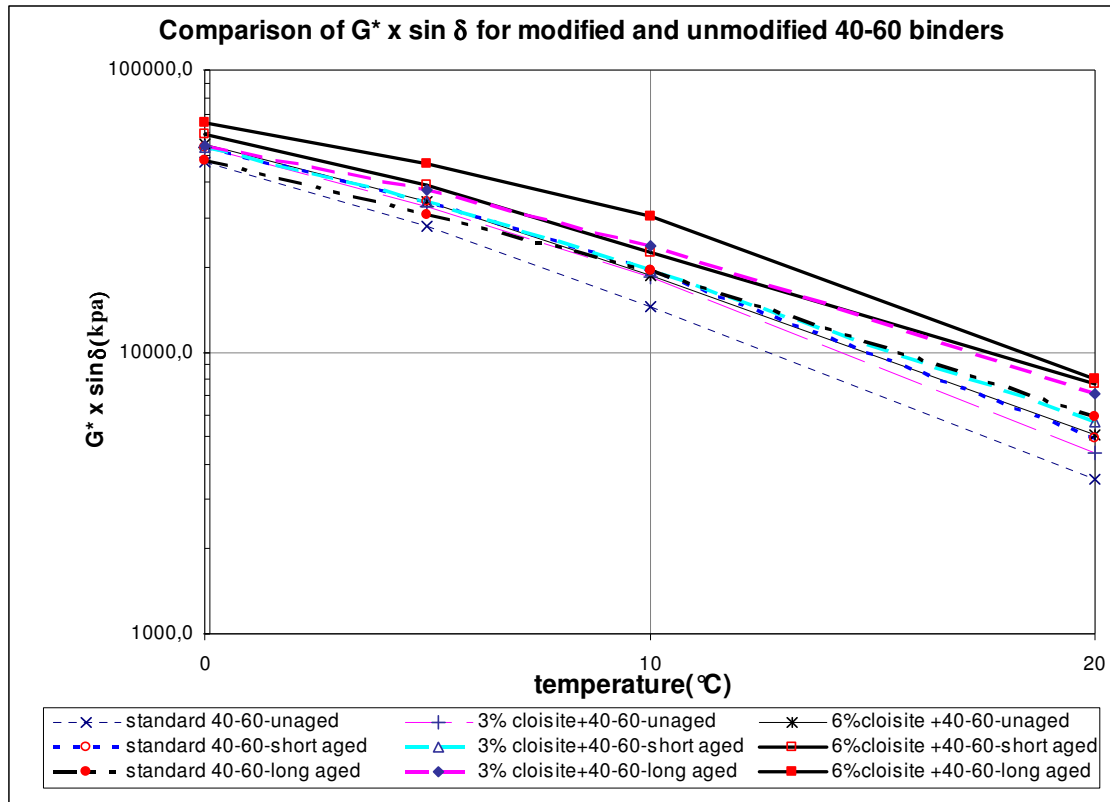


Figure 44: Comparison of $G^* \times \sin \delta$ of modified and unmodified 40-60 binders

Analysis and discussion of test results:

From the assessment of figure 44 and table 42 the following points can be observed.

- The fatigue resistance parameter, $G^* \sin \delta$, of the 6% cloisite modified unaged 40-60 binder is 1.2 to 1.4 times higher than the standard unaged 40-60 binder. Similarly, it is 1.1 to 1.5 times higher after short term ageing and 1.4 to 1.5 times higher after long term ageing.
- The fatigue resistance parameter, $G^* \sin \delta$, of the 3% cloisite modified unaged 40-60 binder is 1.1 to 1.3 times higher than the standard unaged 40-60 binder. Similarly, it is 1.0 to 1.1 times higher after short term ageing and 1.1 to 1.2 times higher after long term ageing.

This analysis shows that in the low to medium temperature ranges the cloisite modifier reduces the fatigue life of the 40-60 binder and the reduction in fatigue life is bigger when the amount of cloisite in the binder increases.

The comparison of modified and unmodified 70-100 binders is given in table 43 and figure 45.

Binder	Temperature (°C)	$G^* \times \sin \delta$				ratio - $G^* \times \sin \delta$ (Modified/standard)			
		unaged	short term aged	long term aged		unaged	short term aged	long term aged	
				RCAT	PAV			RCAT	PAV
standard 70/100	0	37919	41115	44484	41349	1.00	1.00	1.00	1.00
	5	20472	23956	28388	26199	1.00	1.00	1.00	1.00
	10	9718	12552	16434	15104	1.00	1.00	1.00	1.00
	20	1736	2818	4057	5012	1.00	1.00	1.00	1.00
nanofill 6% + 70/100	0	44124	40444	46281	45672	1.2	0.98	1.04	1.10
	5	23875	22558	29152	28194	1.2	0.94	1.03	1.08
	10	11632	11143	16678	15674	1.2	0.89	1.01	1.04
	20	2278	2128	4816	4116	1	0.76	1.19	0.82

Table 43: comparison of $G^* \times \sin \delta$ of modified and unmodified 70/100 binders

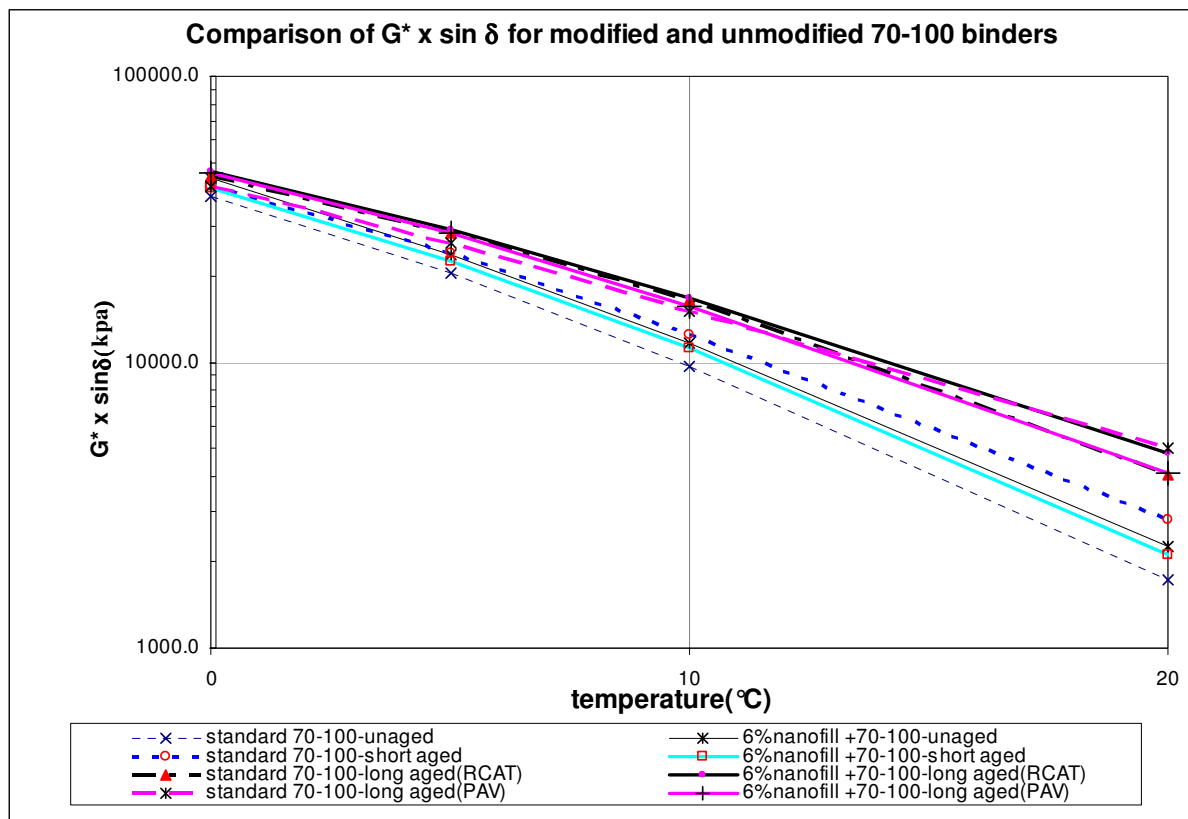


Figure 45: Comparison of $G^* \times \sin \delta$ of modified and unmodified 70-100 binders

Analysis and discussion of test results:

From the analysis done in figure 45 and table 43 the following observations can be made.

- The energy dissipation factor, $G^* \sin \delta$, for 6% nanofill modified unaged 70-100 binder is 1.2 to 1.3 times higher than the standard 70-100 unaged binder.
- The energy dissipation factor, $G^* \sin \delta$, for 6% nanofill modified aged 70-100 binder is more or less the same as the standard 70-100 aged binder.

This analysis shows that in the low to medium temperature ranges, the nanofill modification reduces the fatigue life of the unaged 70/100 binder. However, after being aged the nanofill modified binder shows the same fatigue life as the standard binder and this is because of the ageing resistance improvement by the nanofill.

The minimum temperature values at which the maximum limit of $G^* \sin \delta$ is satisfied is given in table 44.

Binders	Temperature (°C)
	long aged- $G^* \sin \delta = 5000 \text{ kpa}$
standard 70-100 (RCAT)	19,2
6% nanofill + 70-100(PAV)	20.0
6% nanofill + 70-100(RCAT)	19,8
6% nanofill + 70-100(PAV)	19.2
standard 40-60	22,1
3% cloisite + 40-60	24,0
6% cloisite + 40-60	25,2

Table 44: Temperature values at minimum limits of $G^* \sin \delta$

The results of table 44 further confirms that the cloisite modified 40/60 binder has less fatigue life than the standard 40/60 binder where as the nanofill modified binder shows more or less the same fatigue life as the standard 70/100 binder in the long term aged samples.

6 Performance Tests on Modified and Unmodified Dense Asphalt Mixtures

This chapter discusses about tests performed on 6% cloisite modified and standard dense asphalt mixtures and the comparison of the test results to see the effect of the clay modification on the performance of the asphalt mixtures. The performance tests selected for comparison are:

- i. *Indirect tensile strength test*
- ii. *Resilient modulus test*
- iii. *Dynamic creep test*
- iv. *Fatigue resistance test*

Based on the suggestions made by Dr.Hartmut, from TNO, it was decided that the dense asphalt mixture be modified by 6% cloisite modified binder.

6.1 Indirect Tensile Strength Test

The section on indirect tensile strength discusses on:

- ✓ a typical indirect tensile strength test result ;
- ✓ test result analysis and comparison of indirect tensile strength values of the modified and unmodified dense asphalt mixtures;
- ✓ comparison of the fracture energy of the modified and unmodified asphalt mixtures.

6.1.1 Purpose of performing the test

Indirect tensile strength is performed for two main purposes:

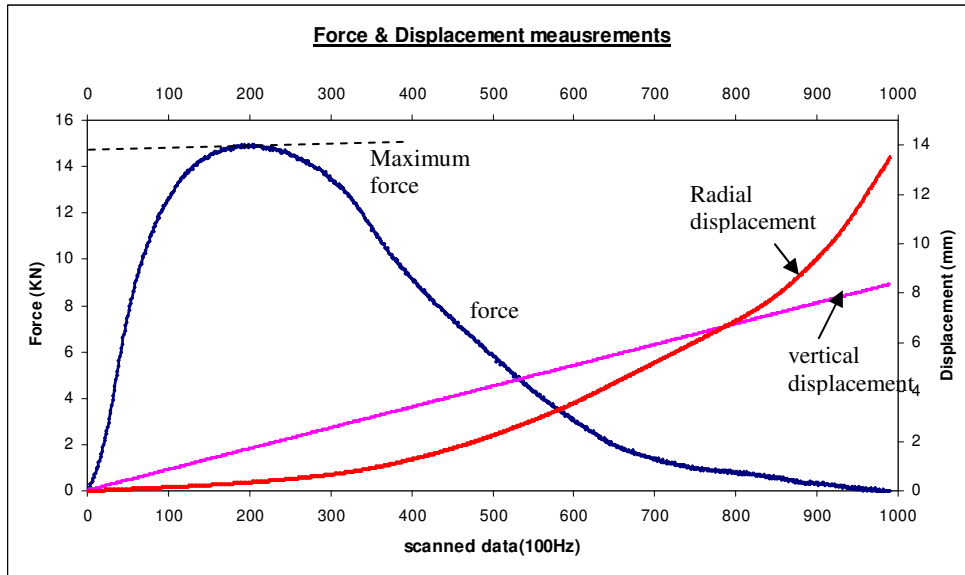
- ❖ to determine the loading values for resilient modulus test and fatigue resistance tests. (normally the loading values of these tests are a certain percentage of the ITS);
- ❖ to compare the indirect tensile strength as well as fracture energy of the modified and unmodified dense mixtures.

6.1.2 Typical Indirect tensile strength test result

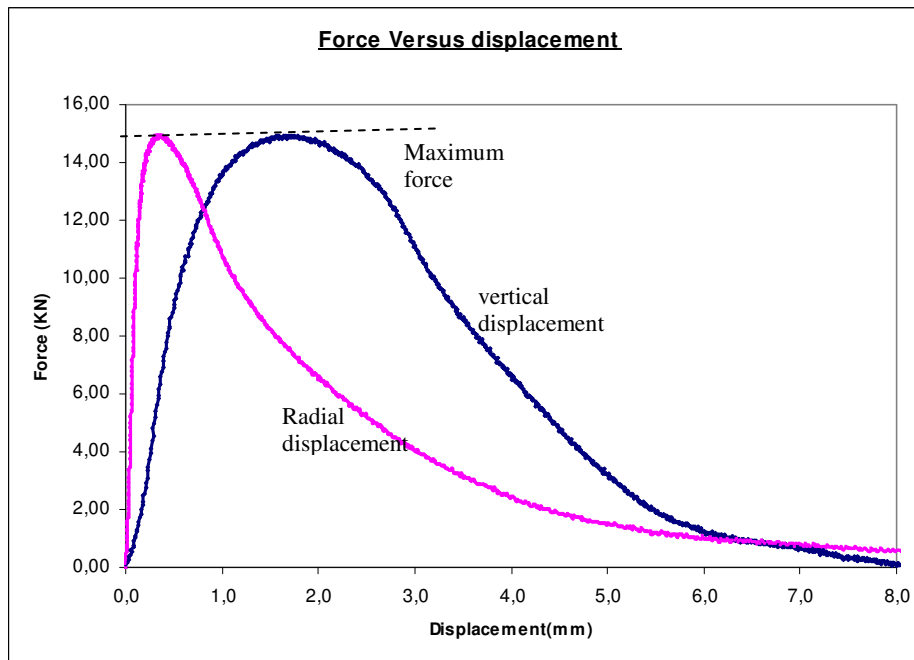
A typical indirect tensile strength test result comprises measurement of the compressive load, vertical and radial displacements. A typical result output is given in graphical form in figure 46. Part a) of the figure shows force and displacement measured versus time (data scanned). The data scanning rate is 100 per second. Hence, the x –axis of part a) of figure 46 implies that the measurement was taken with period of 1/100 second. Part b) of the figure correlates the applied compressive force with the vertical and radial displacements.

The maximum value of the force shown in figure 46 is used to compute indirect tensile strength of the specimens tested. In addition, from the relationship between compressive

force and vertical displacement as shown in part b) of figure 46, the fracture energy of the specimens is determined. Two fracture energy types are computed which are explained later in this section.



a) Force, displacement measurements versus scanned data



b) Force measurement versus displacements

Figure 46: typical test result output of indirect tensile strength (ITS) test

6.1.3 Test result analysis

The indirect tensile strength test (ITS) is performed on standard dense asphalt mixture and on 6% cloisite modified dense mixture. The tests were conducted on five different temperatures and the indirect tensile strength is computed from the maximum compressive force measured during the test using Eq.4. The measured data and the indirect tensile strength values of the modified and unmodified dense asphalt mixtures are given in table 45 and table 46.

Test Type : Dry Indirect Tensile Strength(ITS _{dry})								
Mixture Type	Specimen nr.	height(mm)	Temperature(°C)			Displacement at peak Force value(mm)		Failure type
				Peak Force(KN)	ITS (Mpa)	Vertical	Radial	
Standard Dense Mix	DACS-II-10	34,6	5	24,74	4,48	1,70	0,15	A
	DACS-II-1	34,3	12,5	14,94	2,73	1,72	0,36	A
	DACS-II-91	34,5	20	8,58	1,56	1,99	0,45	A
	DACS-II-21	34,5	27,5	3,98	0,72	2,90	0,64	A
	DACS-II-94	34,4	35	2,08	0,38	2,59	0,90	C

Table 45: Indirect tensile strength test results and analysis (standard dense mix)

Test Type : Dry Indirect Tensile Strength(ITS _{dry})								
Mixture Type	Specimen nr.	height(mm)	Temperature(°C)			Displacement at peak Force value(mm)		Failure type
				Peak Force(KN)	ITS (Mpa)	Vertical	Radial	
Cloisite 6% modified Dense Mix	DAC-6%C-26	35,2	5	27,08	4,82	1,79	0,10	A
	DAC-6%C-1	35,5	12,5	18,48	3,26	2,15	0,17	A
	DACS-6%C-107	34,3	20	10,01	1,83	2,45	0,28	A
	DACS-6%C-81	35,5	27,5	5,20	0,92	3,40	0,50	A
	DACS-6%C-19	35,2	35	2,97	0,53	2,84	0,57	A

Table 46: Indirect tensile strength test results and analysis (cloisite 6% modified dense mix)

Note: The diameter of all the specimens tested for ITS is 101.6mm

In the above tables a failure type of each specimen tested is shown. The different failure mechanisms possible with ITS test are:

- type A: where pure crack is observed in the diametrical line
- type B : where no clearly visible tensile failure line exists
- type C: where larger deformation near the loading strip occurs and at the same time there exists limited crack line.

The failure types are shown graphically in figure 47.

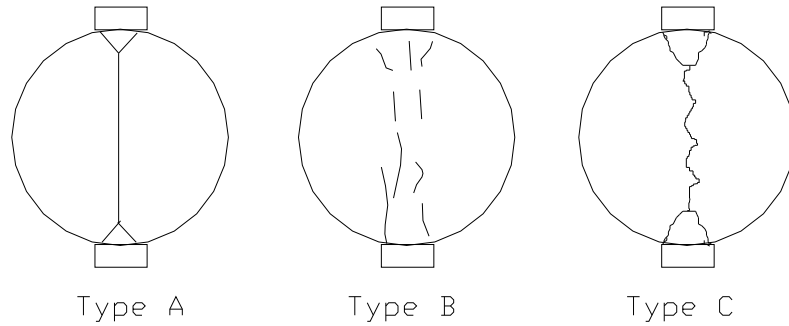


Figure 47: Failure mechanism in ITS

6.1.4 Test results Comparison

Based on the analysis results given above a comparison of ITS values of the modified and unmodified dense specimens is summarized in table 47 and figure 48.

Temperature(°C)	Indirect Tensile Strength (Mpa)		difference in ITS (MPA)	Percentage increment
	Standard	6% Cloisite modified		
5	4,48	4,82	0,34	8%
12,5	2,73	3,26	0,53	20%
20	1,56	1,83	0,27	17%
27,5	0,72	0,92	0,20	27%
35	0,38	0,53	0,15	40%

Table 47: ITS comparison between modified and unmodified dense mixes

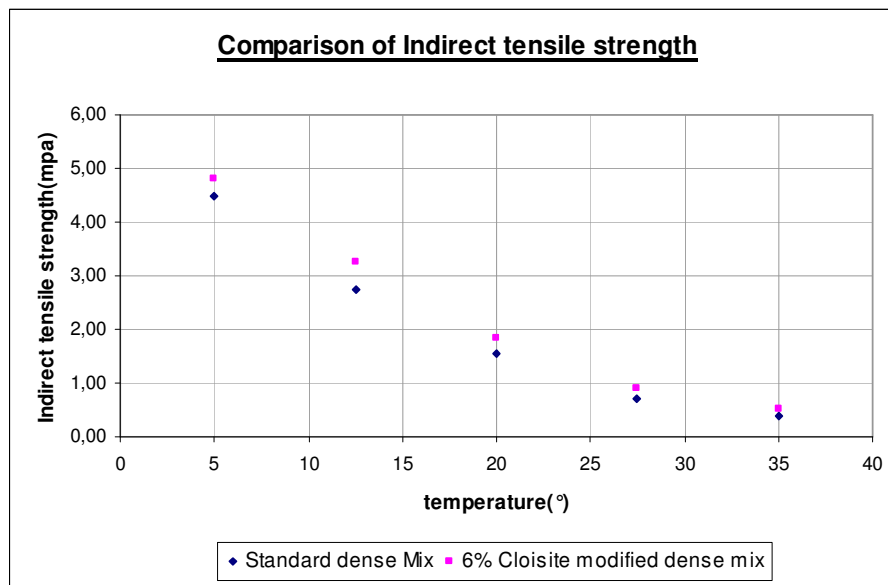


Figure 48: Comparison of ITS results of modified and unmodified dense mixes

The percentage increment in table 47 is computed as:

$$\frac{\text{Modified ITS} - \text{standard ITS}}{\text{standard ITS}} \quad (\text{Eq.15})$$

A comparison of the ITS results of the modified and unmodified dense mixtures show that:

- the ITS results of the modified specimens is higher than the ITS of standard mixtures at all test temperatures;
- percentage increment in ITS values due to the modification varies from 8% to 40% and the percentage of increment is higher for the higher testing temperature;
- at 35 °C the specimen of the modified mixture fails due to pure crack where as the specimen of the standard mixture fails due to crack and deformation.

6.1.5 Fracture Energy analysis and comparison

The area under force versus vertical displacement curve in ITS test provides us the energy dissipated to crack or fracture the specimen. As described below, two fracture energy values can be identified in the analysis:

- 1) *Fracture energy until failure*: this represents the energy dissipated before the specimen starts failing and this is given by the shaded area of part a) of figure 49.
- 2) *Total Fracture energy*: this represents the total energy dissipated to totally destroy the specimen and it is given by the shaded area of part b) of figure 49.

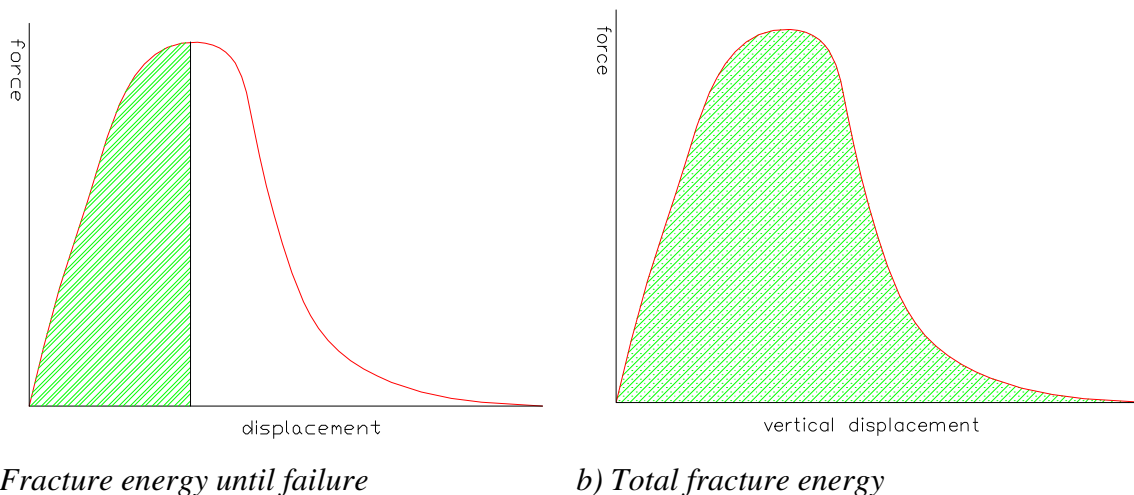


Figure 49: Fracture Energy from ITS

A comparison of fracture energy values between the standard dense mixture and cloisite 6% modified dense mixture is provided in table 48 and figure 50.

Temperature(°C)	Total fracture energy(N.m)			Fracture energy until failure(N.m)		
	Standard dense mix	6% cloisite modified mix	Ratio of modified to standard mix	Standard mix	6% cloisite modified mix	Ratio of modified to standard mix
5	32,8	35,7	1,1	15,4	24,5	1,6
12,5	53,4	65,5	1,2	18,2	25,1	1,4
20	40,9	50,5	1,2	12,8	17,7	1,4
27,5	17,0	22,6	1,3	6,1	8,5	1,4
35	9,6	15,7	1,6	2,7	5,1	1,9

Table 48: Fracture energy values of standard and modified dense mix

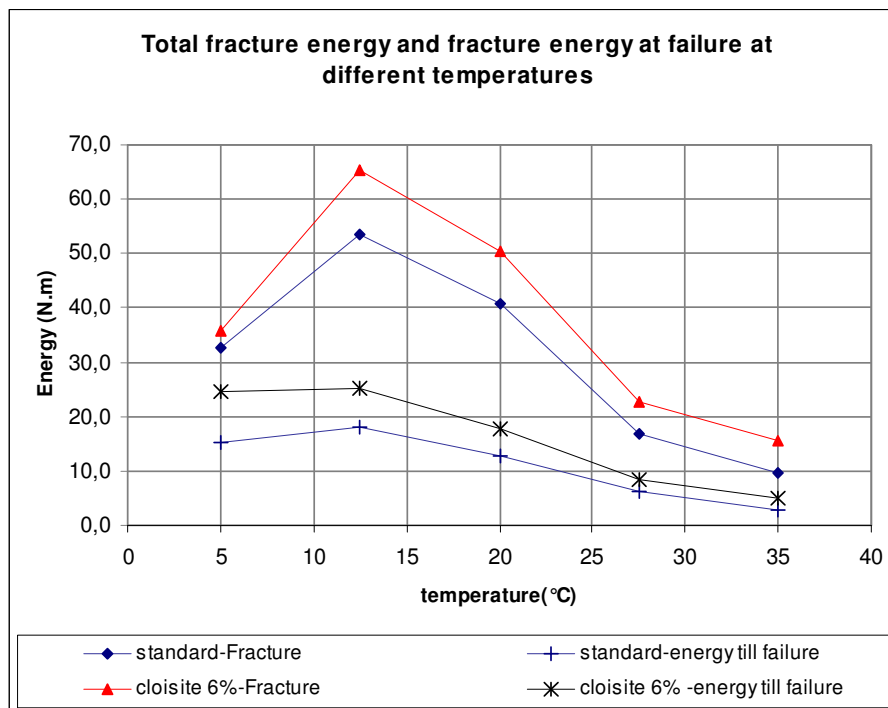


Figure 50: Fracture energy values of standard and modified dense mix

From the analysis results the following points can be noticed:

- the modified mixture has a larger total fracture energy and fracture energy until failure in all test temperatures as compared to standard mix;
- 40% to 90% increment in fracture energy until failure is observed due to the modification and the increment depends on the test temperature;
- the modified mixture shows 10% to 60% increment in total fracture energy which also depends on test temperature;
- at 5°C it can be seen that, compared to standard mixture, more energy is required to start the initiation of cracks in the modified mixture, however once the cracks get started then less energy is required to destroy the specimen.(energy till failure :

modified = 24.5, standard 15.4 and energy after crack initiates : modified = 35.7-24.5 ~11 , standard = 32.8-15.4 ~17)

6.2 Resilient Modulus

In this section discussions are presented on:

- ✓ typical resilient modulus test result;
- ✓ test result analysis and comparison of resilient modulus values of the modified and unmodified dense asphalt mixtures for different frequency and temperature values;
- ✓ construction of master curve and comparison of the master curve of the modified and unmodified dense mixtures.

6.2.1 Purpose of performing the test

The resilient modulus test is performed to :

- ❖ determine the elastic moduli of the modified and standard dense mixtures and develop master curves for each mix;
- ❖ make a comparative analysis of resilient modulus values between the standard and modified dense mixtures.

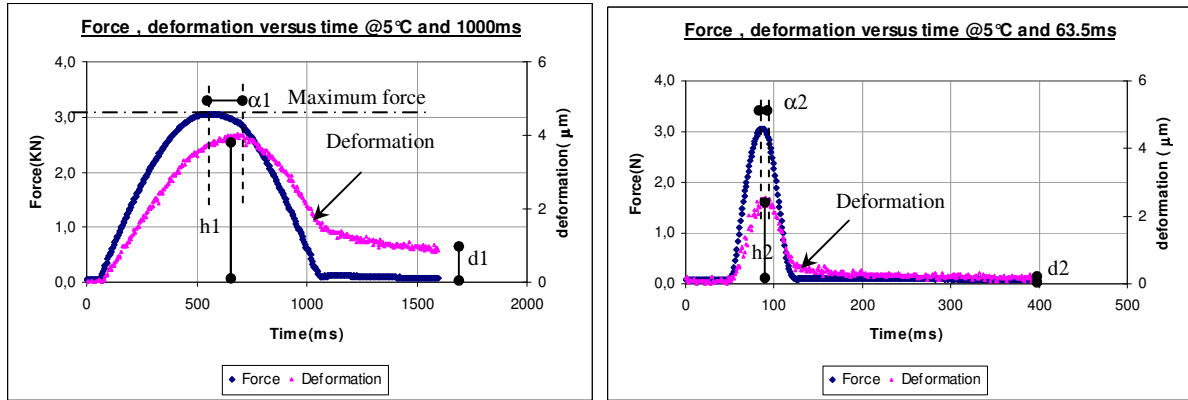
6.2.2 Typical resilient modulus test result

In indirect tensile test (ITT) resilient modulus test, the applied compressive load and the total radial deflection are measured for each applied pulse load. Data scanning rate is automatic and it varies between 250 to 1000Hz depending on the loading frequency value. A typical resilient modulus test output result at different frequencies and temperatures is given in figure 51.

From the typical resilient modulus test results @ 5°C and 35°C and at loading times of 63.5ms and 1000ms in figure 51 the following observations can be made.

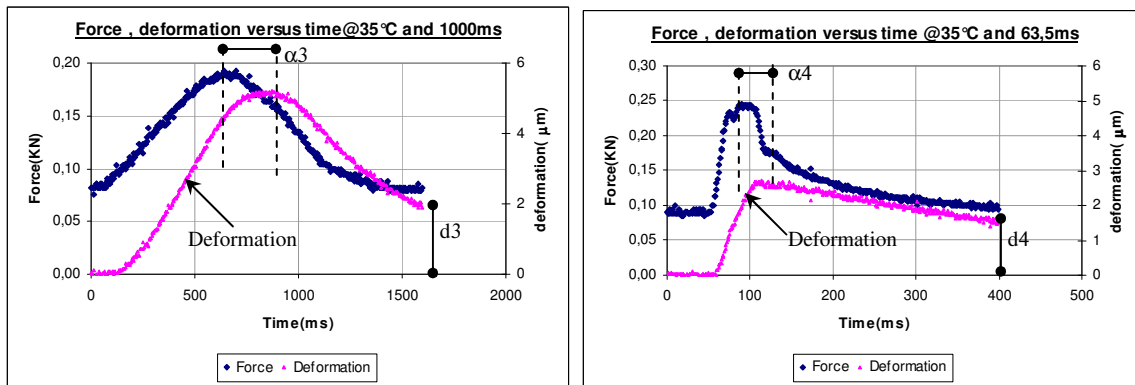
- in all test result outputs there is a phase lag between deformation and the applied force;
- the phase lag depends on the test temperature and the loading time; the lower the test temperature value is, the smaller the phase lag while the smaller the loading time is the smaller the phase lag (i.e. $\alpha_2 < \alpha_1 < \alpha_4 < \alpha_3$) (see figure 51);
- after each pulse is applied a small amount of permanent deformation is accumulated and its value depends on the test temperature and the loading time;
- the accumulated permanent deformation is larger if the test temperature is higher and loading time is larger (i.e. $d_3 > d_4 > d_1 > d_2$) (see figure 51);
- the accumulated permanent deformation becomes smaller if the rest period is larger

- on average for all test temperatures and loading times the accumulated permanent deformation after each pulse is very small since the applied load is small;
- keeping test temperature and applied load constant, the deformation increases when loading time increases (example: $h_1 > h_2$) (see figure 51).



a) @5°C and 1000ms

b) @5°C and 63.5ms



c) @35°C and 1000ms

d) @35°C and 63.5ms

Figure 51: typical resilient modulus output results

6.2.3 Test result analysis

The mixtures selected for resilient modulus test are 6% cloisite modified dense mixture and a standard dense mixture. The resilient modulus test is performed at 5 different temperature values. The computation of resilient modulus value is made using Equation 5 (chapter 2) and the input values are maximum applied force, recoverable deformation which are obtained from the test results as shown in figure 51 and the thickness of the specimen which is predetermined. For all the test temperature values and loading frequencies a Poisson's ratio of 0.35 is assumed.

The resilient modulus values for the different specimens of the standard and 6% cloisite modified dense mixtures for the selected test temperatures and loading frequency values are given in table 49

		6% Cloisite Modified Dense Mix				Standard Dense Mix			
		Resilient Modulus(Mpa)				Resilient Modulus(Mpa)			
Temperature (°C)	Loading time(ms)	*1 st Specimen	*2 nd Specimen	*3 rd Specimen	Average Value	*1 st Specimen	*2 nd Specimen	*3 rd Specimen	Average Value
5	Specimen	DACC-28	DACC-44	DACC-97		DACS-35	DACS-49	DACS-57	
	Void content	3,42%	3,98%	3,50%	3,63%	2,4%	2,6%	2,1%	2,4%
	1000	13515,0	12917,0	13853,0	13428,3	11575,4	10938,8	12531,4	11681,9
	500	15524,0	15088,0	15919,0	15510,3	13732,8	12985,2	14584,8	13767,6
	250	17802,0	17318,0	18032,0	17717,3	15509,2	14503,4	16500,4	15504,3
	125	19563,0	19147,0	20198,0	19636,0	17676,2	16827,6	18770,8	17758,2
	63	21560,0	20983,0	22121,0	21554,7	19110,8	18277,6	19869,0	19085,8
12,5	Specimen	DACC-31	DACC-35	DACC-59		DACS-5	DACS-43	DACS-101	
	Void content	3,29%	3,76%	4,11%	3,72%	2,2%	2,3%	2,6%	2,4%
	1000	6643,0	6407,0	6618,0	6556,0	5267,6	5647,2	5228,4	5381,1
	500	8136,0	7904,0	7762,0	7934,0	6705,4	7128,4	6716,6	6850,1
	250	9855,0	9695,0	9317,0	9622,3	8259,6	8613,8	7944,4	8272,6
	125	12115,0	11642,0	11516,0	11757,7	10278,8	10531,4	9811,6	10207,3
	63	14425,0	13675,0	13926,0	14008,7	12035,4	12379,2	11561,4	11992,0
20	Specimen	DACC-12	DACC-18	DACC-24		DACS-3	DACS-37	DACS-69	
	Void content	3,65%	3,27%	3,88%	3,60%	2,1%	2,4%	2,7%	2,4%
	1000	2235,0	2365,0	2412,0	2337,3	2145,4	2313,0	2267,0	2241,8
	500	3069,0	3218,0	3306,0	3197,7	2951,0	3234,4	3205,4	3130,3
	250	4159,0	4287,0	4430,0	4292,0	4071,4	4221,0	4179,2	4157,2
	125	5526,0	5692,0	5831,0	5683,0	5292,8	5468,8	5592,6	5451,4
	63	7257,0	7273,0	7680,0	7403,3	6326,8	7610,6	7654,2	7197,2
27,5	Specimen	DACC-21	DACC-45	DACC-47		DACS-17	DACS-24	DACS-88	
	Void content	3,59%	3,43%	4,31%	3,78%	2,4%	2,4%	2,3%	2,4%
	1000	840,0	844,0	882,0	855,3	728,9	687,5	918,4	778,3
	500	1122,0	1130,0	1134,0	1128,7	993,6	984,0	1095,0	1024,2
	250	1522,0	1580,0	1562,0	1554,7	1233,8	1212,6	1346,0	1264,1
	125	2162,0	2026,0	2077,0	2088,3	1757,6	1697,2	1945,0	1799,9
	63	2941,0	2726,0	2929,0	2865,3	2589,6	2779,8	2846,0	2738,5
35	Specimen	DACC-9	DACC-79	DACC-38		DACS-15	DACS-38	DACS-92	
	Void content	3,84%	3,60%	3,77%	3,74%	2,4%	2,2%	2,4%	2,3%
	1000	486,0	427,0	402,0	438,3	349,0	378,0	462,0	396,3
	500	586,0	510,0	502,0	532,7	416,0	464,0	580,0	486,7
	250	727,0	617,0	648,0	664,0	526,0	591,0	622,0	579,7
	125	931,0	781,0	829,0	847,0	670,0	781,0	795,0	748,7
	63	1264,0	1093,0	1175,0	1177,3	964,0	1097,0	1079,0	1046,7

Table 49: Resilient modulus of standard and 6% cloisite modified dense mixes

For each test temperature 3 specimens are tested. One specimen is tested for 5 loading frequencies (loading times). In the resilient modulus test for each selected test temperature and loading frequency, five loading pulses are considered. From each loading pulse a resilient modulus is obtained and an average of 5-pulse resilient modulus values make up the

resilient modulus of a specimen for a given test temperature and loading frequency. The resilient modulus of the mixture at a selected test temperature and loading frequency is determined from the average resilient modulus of the three specimens.

6.2.4 Test result Comparison

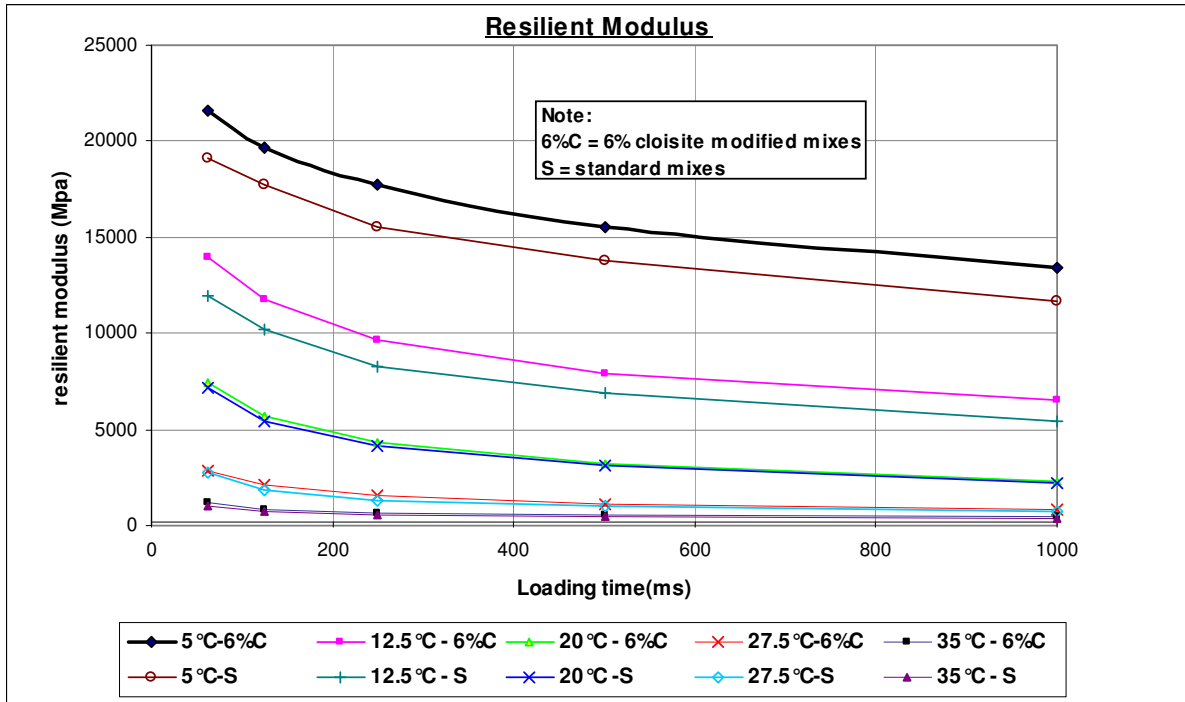
A comparison of the average resilient modulus between 6% cloisite modified mixture and standard dense mixture is performed for each test temperature and loading frequency. The comparison done is based on the analysis result given in table 49. The comparison made is given in table 50 and figure 52.

Temperature (°C)	Resilient Modulus(Mpa)					
	Loading time(ms)	6%Cloisite Dense Mix	standard Dense Mix	Modified - Standard	Increment (%)	Average increment(%)
5	1000	13428.3	11681.9	1746.5	15%	13%
	500	15510.3	13767.6	1742.7	13%	
	250	17717.3	15504.3	2213.0	14%	
	125	19636.0	17758.2	1877.8	11%	
	63	21554.7	19085.8	2468.9	13%	
12.5	1000	6556.0	5381.1	1174.9	22%	17%
	500	7934.0	6850.1	1083.9	16%	
	250	9622.3	8272.6	1349.7	16%	
	125	11757.7	10207.3	1550.4	15%	
	63	14008.7	11992.0	2016.7	17%	
20	1000	2337.3	2241.8	95.5	4%	3%
	500	3197.7	3130.3	67.4	2%	
	250	4292.0	4157.2	134.8	3%	
	125	5683.0	5451.4	231.6	4%	
	63	7403.3	7197.2	206.1	3%	
27.5	1000	855.3	778.3	77.0	10%	13%
	500	1128.7	1024.2	104.4	10%	
	250	1554.7	1264.1	290.5	23%	
	125	2088.3	1799.9	288.4	16%	
	63	2865.3	2738.5	126.9	5%	
35	1000	438.3	396.3	42.0	11%	12%
	500	532.7	486.7	46.0	9%	
	250	664.0	579.7	84.3	15%	
	125	847.0	748.7	98.3	13%	
	63	1177.3	1046.7	130.7	12%	

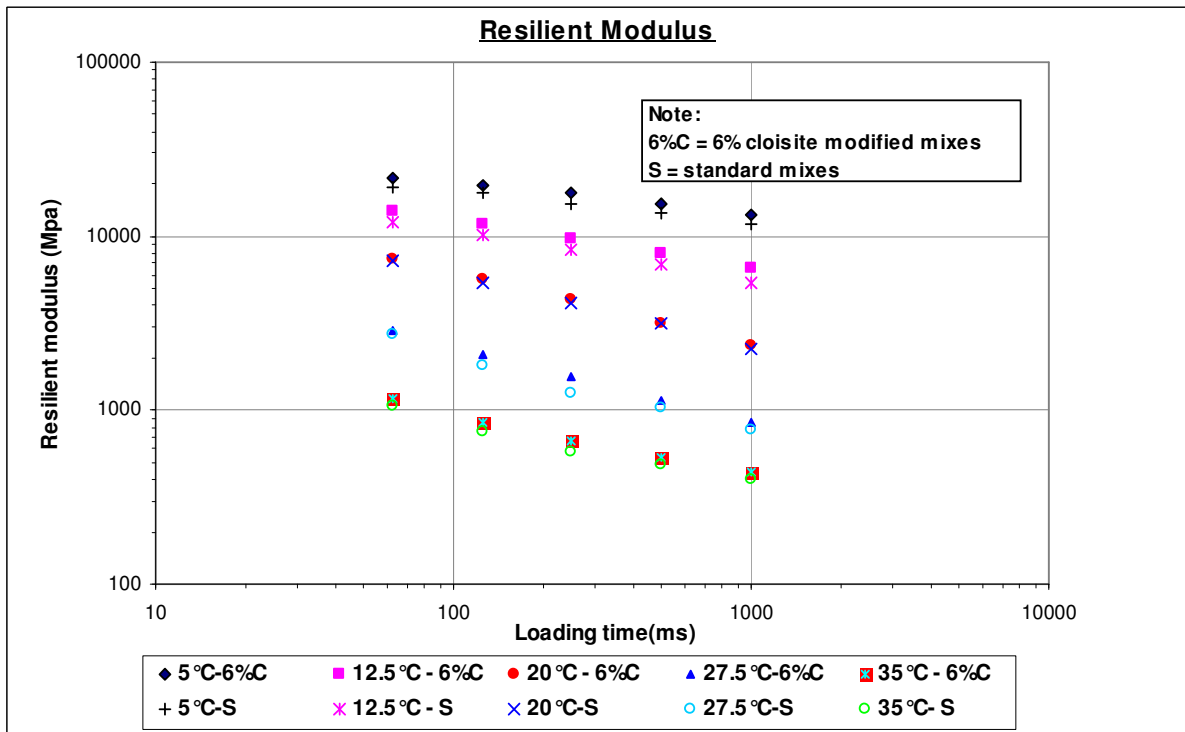
Table 50: Resilient modulus comparison of standard and 6% cloisite modified dense mixes

The increment in stiffness (%) in table 47 is computed as:

$$\frac{\text{Modified stiffness} - \text{standard stiffness}}{\text{standard stiffness}} \times 100 \quad (\text{Eq.16})$$



a) Linear scale



b) Logarithmic scale

Figure 52: Comparison of resilient modulus values of standard and 6% cloisite modified dense mixes

A comparison of the average resilient modulus between 6% cloisite modified mixture and standard given in table 50 and figure 51 shows that:

- the 6% cloisite modified dense mixture has greater stiffness than the standard dense mixture at all test temperatures;
- there is increment in stiffness due to the 6% cloisite modification and the increment varies from 3% to 17% and the value varies depending on the test temperature;
- percentage wise the increment in stiffness due to the modification is minimum @ 20°C though the actual stiffness increment value is more or less similar to that of the 27.5°C and greater than that of 35°C
- the increment in stiffness due to the modification varies depending on the test temperature and the loading frequency and no pattern of increment is noticed from the analysis results though in most cases the increment values are more or less the same within the same testing temperature.
- an overall average of about 12% increment in stiffness is obtained due to the 6% cloisite modification for the frequencies and testing temperatures considered.

6.2.5 Master curve construction and comparison

The master curve at the reference temperature of 20°C is constructed from the resilient modulus results obtained at different test temperatures and loading frequencies. The shift factor is determined using WLF and Arrhenius equations and the curve fitting is done using sigmoidal model. The equations of WLF and Arrhenius are given in section 2.3.2. The sigmoidal model is given as:

$$S_{\text{model}} = S_{\text{min}} + \frac{(S_{\text{max}} - S_{\text{min}})}{\left[1 + \left(\frac{t_c}{t_{\text{red}}}\right)^k\right]^{m_e/k}} \quad (\text{Eq.17})$$

Where :

S_{model} = mixture stiffness ,(Mpa),

S_{min} = minimum mixture stiffness (Mpa),

S_{max} = maximum mixture stiffness (Mpa),

t_c = location parameter with dimension of time(ms),

t_{red} =reduced time (ms)

k, m_e = shape parameters, dimensionless

$$t_{\text{red}} = \frac{t_{\text{loading}}}{a_T} \quad (\text{Eq 18})$$

at = shift factor

t_{red} = reduced time (ms),

t_c = Actual loading time(ms).

The procedures followed in constructing the best fit master curve are:

1. assume reasonable values for the constants in the shift factor models (WLF and Arrhenius);
2. compute initial shift factor values and compute initial reduced time (t_{red});
3. assume reasonable values for constants in the sigmoidal model and use the computed values of t_{red} (from step 2) and compute initial stiffness values of the model;
4. use solver program (non linear regression analysis) to find values of all the constants in the shift factor models and sigmoidal model so as the summation of the squares of the difference of the actual stiffness and stiffness of the model is minimized.

Following these procedures, master curves are constructed using WLF and Arrhenius approaches. The values of the master curves from both approaches are given in table 51. The values of the constants of the sigmoidal model, WLF and Arrhenius are given in table 52.

Cloisite 6% Modified Dense Mix						Standard dense mix					
Arrhenius			WLF			Arrhenius			WLF		
Red. Loading time(ms)	Smixture _d -data	Smix _m -Model	Red. Loading time(ms)	Smix _d -data	Smix _m -Model	Red. Loading time(ms)	Smix _d -data	Smix _m -Model	Red. Loading time(ms)	Smix _d -data	Smix _m -Model
4.2E-01	21554.7	21600.0	4.1E-01	21554.7	21591.1	5.0E-01	19085.8	19640.1	4.9E-01	19085.8	19110.1
8.3E-01	19636.0	19648.4	8.3E-01	19636.0	19646.3	1.0E+00	17758.2	17620.4	9.9E-01	17758.2	17258.0
1.7E+00	17717.3	17596.8	1.7E+00	17717.3	17612.1	2.0E+00	15504.3	15586.1	2.0E+00	15504.3	15368.2
3.3E+00	15510.3	15487.0	3.3E+00	15510.3	15524.8	4.0E+00	13767.6	13570.8	3.9E+00	13767.6	13470.8
5.4E+00	14008.7	13980.5	5.6E+00	14008.7	13922.7	6.0E+00	11992.0	12437.0	5.9E+00	11992.0	12361.1
6.7E+00	13428.3	13369.9	6.6E+00	13428.3	13429.0	8.0E+00	11681.9	11611.1	7.9E+00	11681.9	11600.5
1.1E+01	11757.7	11892.5	1.1E+01	11757.7	11854.6	1.2E+01	10207.3	10526.3	1.2E+01	10207.3	10524.3
2.2E+01	9622.3	9895.6	2.3E+01	9622.3	9869.8	2.4E+01	8272.6	8730.3	2.4E+01	8272.6	8774.7
4.4E+01	7934.0	8045.0	4.5E+01	7934.0	8020.6	4.8E+01	6850.1	7083.3	4.8E+01	6850.1	7149.6
6.3E+01	7403.3	7155.4	6.3E+01	7403.3	7207.0	6.3E+01	7197.2	6486.4	6.3E+01	7197.2	6549.1
8.7E+01	6556.0	6386.9	9.0E+01	6556.0	6353.2	9.5E+01	5381.1	5614.1	9.5E+01	5381.1	5682.4
1.3E+02	5683.0	5611.2	1.3E+02	5683.0	5638.5	1.3E+02	5451.4	5092.6	1.3E+02	5451.4	5152.1
2.5E+02	4292.0	4301.1	2.5E+02	4292.0	4298.0	2.5E+02	4157.2	3901.8	2.5E+02	4157.2	3946.9
5.0E+02	3197.7	3230.4	5.0E+02	3197.7	3197.2	5.0E+02	3130.3	2919.3	5.0E+02	3130.3	2945.3
6.4E+02	2865.3	2915.1	5.8E+02	2865.3	2991.9	5.8E+02	2738.5	2729.2	5.8E+02	2738.5	2756.0
1.0E+03	2337.3	2387.9	1.0E+03	2337.3	2330.6	1.0E+03	2241.8	2139.2	1.0E+03	2241.8	2146.8
1.3E+03	2088.3	2146.2	1.2E+03	2088.3	2173.4	1.2E+03	1799.9	1992.1	1.2E+03	1799.9	2000.2
2.5E+03	1554.7	1571.0	2.3E+03	1554.7	1563.3	2.3E+03	1264.1	1436.1	2.3E+03	1264.1	1431.1
5.1E+03	1128.7	1156.1	4.6E+03	1177.3	1134.7	4.7E+03	1024.2	1035.8	4.6E+03	1024.2	1024.5
5.8E+03	1177.3	1095.1	4.6E+03	1128.7	1129.0	4.9E+03	1046.7	1014.5	4.8E+03	1046.7	1007.8
1.0E+04	855.3	867.1	9.2E+03	847.0	838.1	9.3E+03	778.3	761.6	9.3E+03	778.3	750.3
1.2E+04	847.0	825.5	9.3E+03	855.3	834.3	9.8E+03	748.7	747.5	9.6E+03	748.7	739.4
2.3E+04	664.0	644.9	1.8E+04	664.0	646.0	2.0E+04	579.7	574.7	1.9E+04	579.7	570.1
4.6E+04	532.7	527.6	3.7E+04	532.7	527.3	3.9E+04	486.7	469.1	3.8E+04	486.7	470.6
9.2E+04	438.3	453.4	7.3E+04	438.3	457.4	7.8E+04	396.3	408.4	7.7E+04	396.3	416.2

Table 51: values of the master curves of stiffness for standard and modified dense mixes

	WLF		Arrhenius	
	Parameter	Value	Parameter	Value
Standard dense mix	C1	36.62	H	218.23
	C2	276.19	R	8.31
	Smax	39130.28	Smax	43417.46
	Smin	368.10	Smin	345.68
	tc	27201732	tc	2347802
	k	-0.1962	k	-0.1913
	me	-4.7758	me	-2.9768
6% cloisite modified dense mix	C1	26.03	H	226.5625
	C2	194.24	R	8.31
	Smax	37596.46	Smax	36116.74
	Smin	375.33	Smin	342.02
	tc	6494.1	tc	415.16
	k	-0.24	k	-0.3
	me	-1.43	me	-0.93

Table 52: values of constants of sigmoidal, WLF and Arrhenius models

The summation of the absolute values of the difference of the actual stiffness and the model stiffness is computed for both shifting factor models and is summarized in table 53.

$(\sum \text{abs}(S_{\text{mix}_d} - S_{\text{mix}_m}))$		
	Arrhenius	WLF
Standard dense mix	4837	4772
6% cloisite modified dense mix	1695	1480

Table 53: summation of difference between model stiffness and actual stiffness

The master curves are given in figure 53.

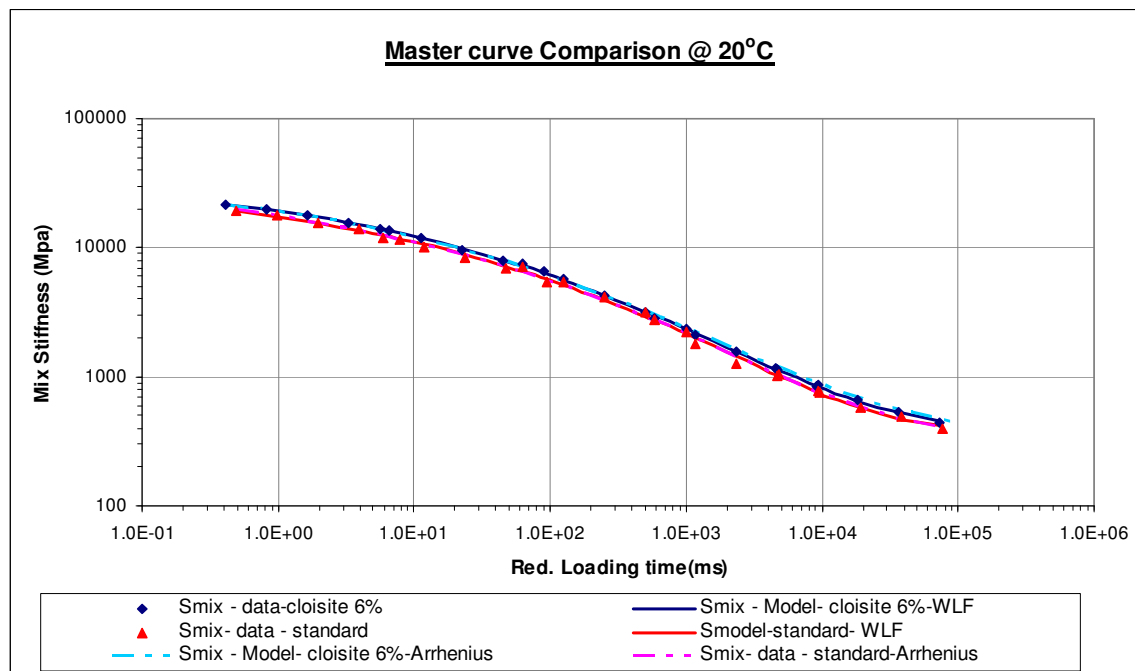


Figure 53: Master curves of standard and 6% cloisite modified dense mixes

From the results of the master curves of both dense asphalt mixtures it can be observed that:

- for any loading frequency (loading time) ,the stiffness of the 6% cloisite modified mixture is higher (on average about 12%) than the standard dense mixture (fig 53 and table 51);
- both WLF and Arrhenius models give good fit of master curves with both dense asphalt mixtures;
- the fitting of the two models is a little bit better for the 6% cloisite modified mixture than the standard mixture.

6.3 Dynamic creep tests

This section discusses about the dynamic creep tests performed on standard dense mixtures and 6% cloisite modified dense mixture. The discussion includes:

- ✓ typical dynamic creep test result;
- ✓ dynamic creep test result analysis and comparison of the modified and unmodified dense asphalt mixtures at different test temperatures and loading conditions.

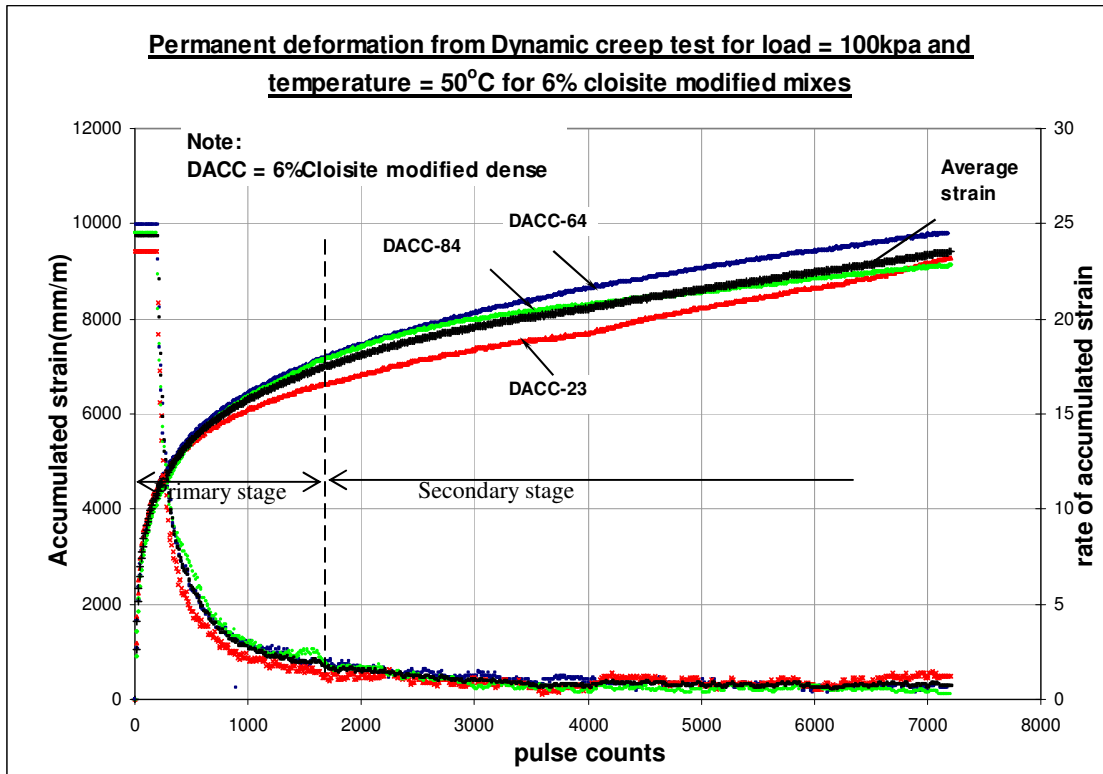
6.3.1 Purpose of performing the test

Dynamic creep test is performed to:

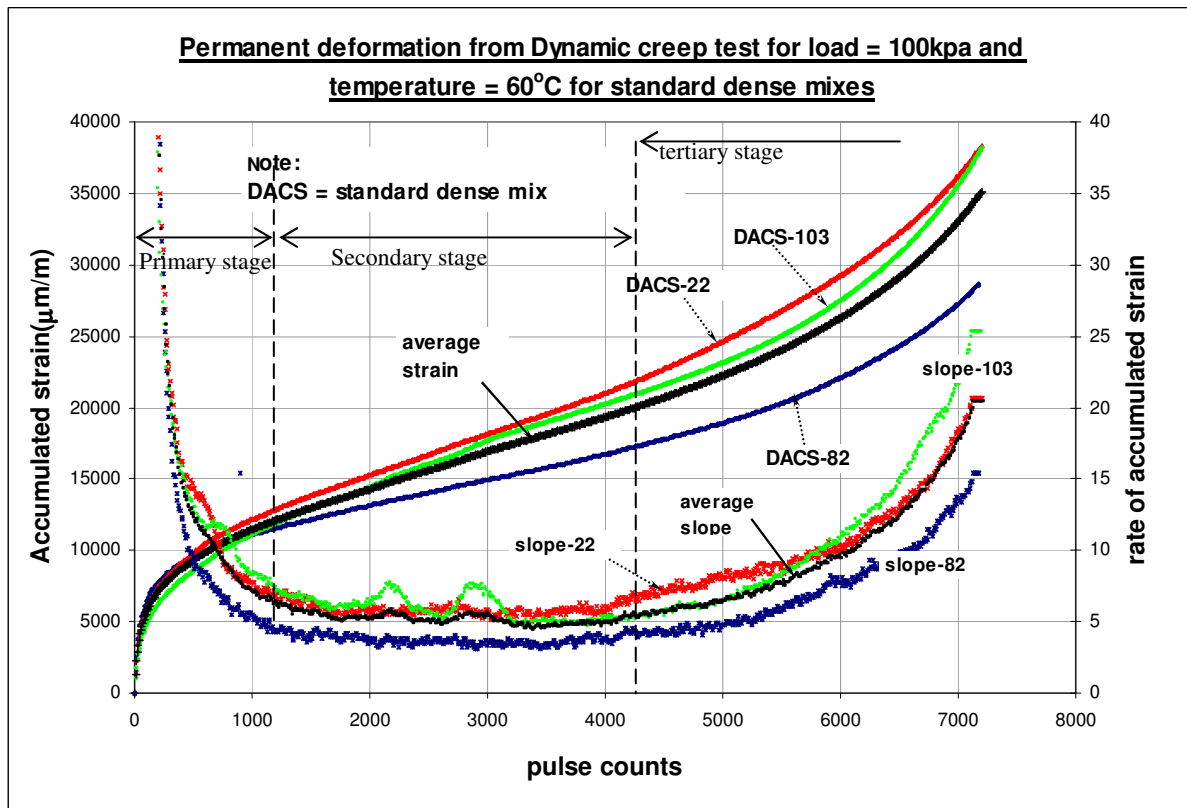
- ❖ determine the resistance to permanent deformation of the standard and 6%cloisite modified dense mixtures at high temperatures and make a comparative analysis;
- ❖ investigate the effect of variation of temperature and level of applied pressure on the permanent deformation resistance response of the modified and standard dense mixes.

6.3.2 Typical dynamic creep test result

A repetitive uniaxial compression test was used to evaluate the permanent deformation of the standard and modified dense mixtures. In this test, a constant repetitive load is applied and the resulting permanent deformation is measured in relation to time (pulse counts). The pulse form selected is half sine with a duration of 200ms and a rest period of 800ms; hence one pulse period is 1second. Two axial LVDT's are used to measure the axial displacement and the average of the two gives the average permanent deformation. Normally the permanent strain (accumulated permanent strain) is reported which is computed as average permanent deformation divided by specimen thickness. A typical dynamic creep test result at different test temperatures and level of applied pressure is given in figure 54.



a) typical permanent deformation curve without tertiary stage



b) typical permanent deformation curve with tertiary stage

Figure 54: typical permanent deformation test result

In figure 54 two typical dynamic creep test results are given. Part a) of the figure shows a typical permanent deformation curve where no shear deformation (accelerated permanent deformation) occurs. This type of test result occurs when the test temperature and /or the level of applied load are small. Part b) of the figure is the common type of permanent deformation test result and it occurs when the temperature and/or the applied load are high.

In both types of curves the rate of the accumulated strain with time is also given by the curves at the bottom of the figure. Part a) of the figure only shows the primary stages and secondary stages of the permanent deformation development. Part b) of the figure shows three stages of permanent deformation development. In primary stage the rate of permanent deformation decreases rapidly; in secondary stage the rate of permanent deformation is more or less constant and in tertiary stage the rate of permanent deformation increases rapidly.

As can be seen in figure 54, the representative permanent deformation curve for a given test temperature and level of applied load is obtained by averaging the permanent deformation curves of three different specimens.

6.3.3 Results of the dynamic creep tests

The average permanent deformation for a given temperature and level of applied load is determined by the procedure given in section 6.3.2. Below the test results at the different test temperatures and loading conditions are given.

6.3.3.1 40°C test temperature

Figure 55 shows the results of dynamic creep test at temperature of 40°C. From the figure the following points can be observed:

- for applied load levels of 100kpa and 300kpa, both types of dense mixtures don't reach the tertiary stage after 7200 load repetition;
- for applied load levels of 500kpa the standard dense mixture reached the tertiary stage at about 4000 pulses where as the cloisite modified dense mixture did not reach the tertiary stage after 7200 pulses;
- at 500kpa on average the standard dense mixture specimens failed by excessive deformation before the 7200 maximum pulse limit is reached where as the cloisite modified dense mixture specimens did not show shear deformation failure till 7200 pulse;
- at all applied load levels , the primary deformations of the standard dense mixture samples are bigger as compared to those of the cloisite modified dense mixture samples.

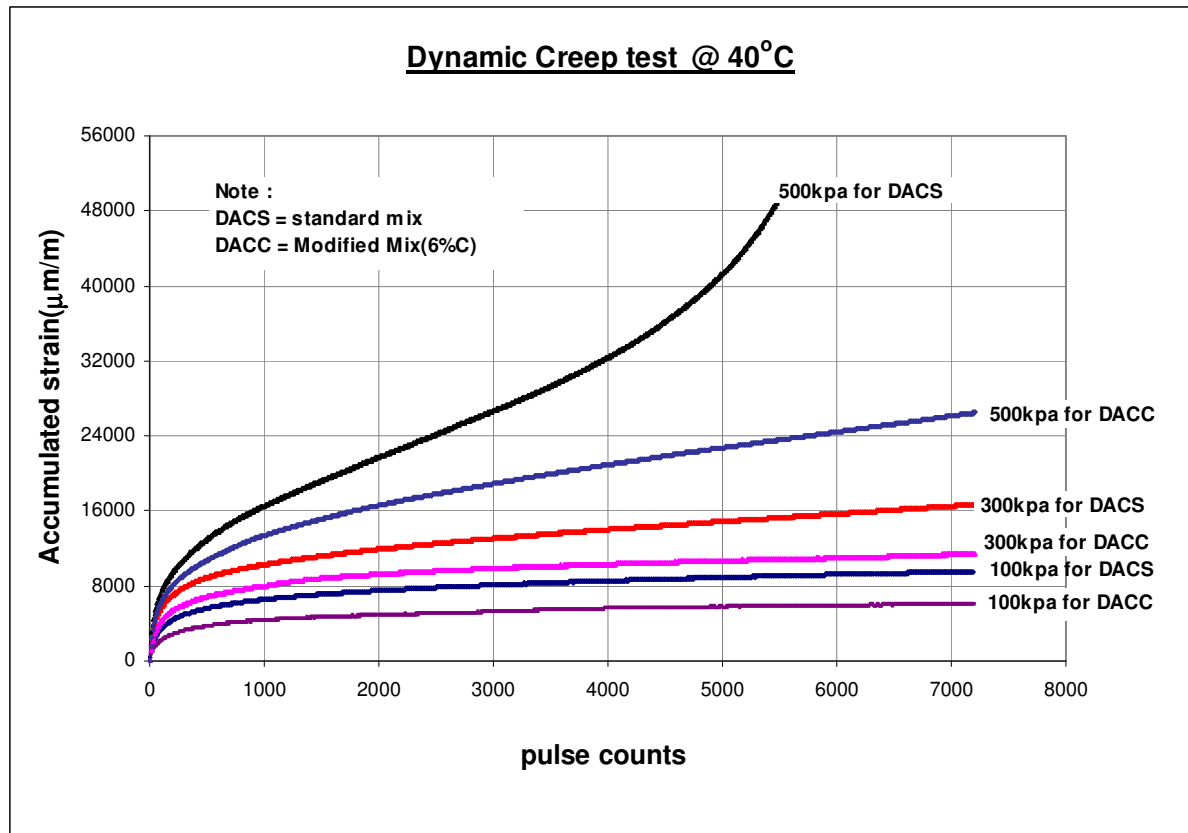


Figure 55: Dynamic creep test results at 40°C

6.3.3.2 50°C test temperature

Figure 56 shows the output results of dynamic creep test at 50°C test temperature. From the figure it can be seen that:

- after the 7200 pulses, both types of dense mixtures don't reach the tertiary stage for applied load levels of 100kpa and 200kpa;
- both types of dense mixtures reach the tertiary stage if applied load was 300kpa; the standard dense mixtures reached the tertiary stage after about 3750 pulses where as the cloisite modified dense mixtures reached the tertiary stage after about 5250 pulses;
- at an applied load of 300kpa the standard dense mixture specimens failed by excessive deformation before 5000 pulse counts were reached where as the cloisite modified dense mixture specimens did not fail completely at 7200 pulse counts;
- in most cases deformations in the primary stage of the standard dense mixture specimens are bigger than those of the cloisite modified dense mixture specimens.

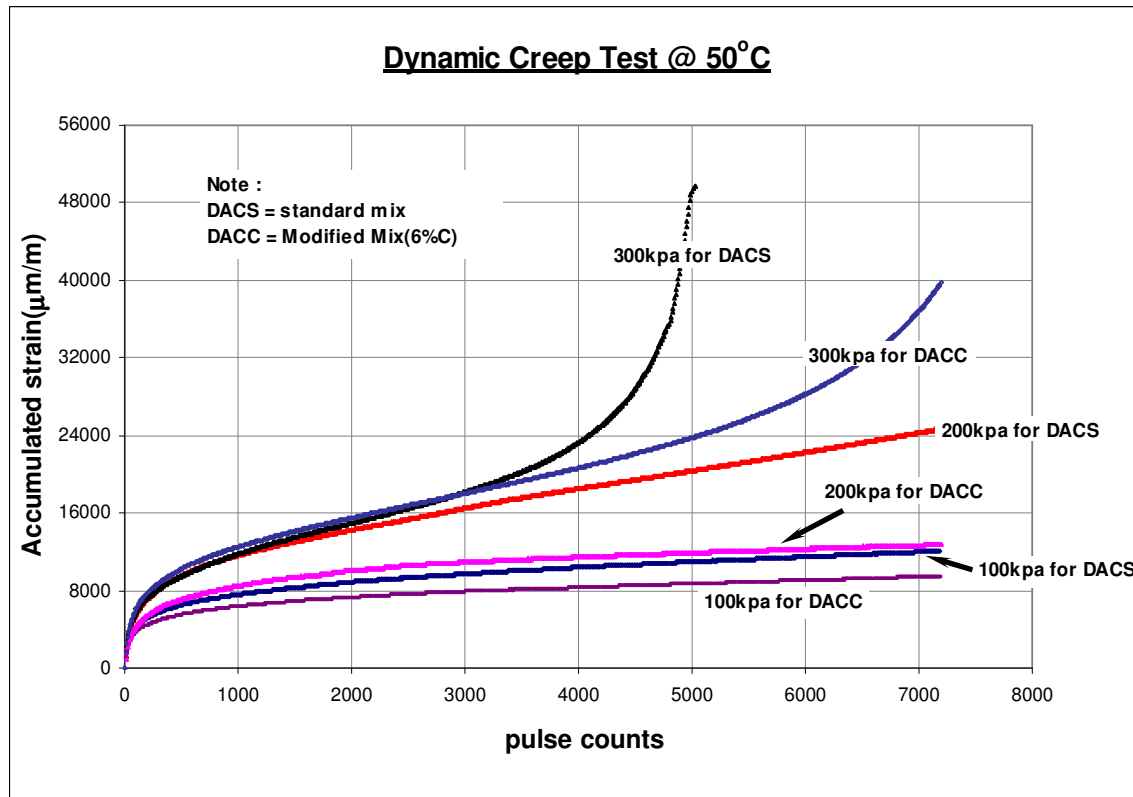


Figure 56: Dynamic creep test results at 50°C

6.3.3.3 60°C test temperature

Dynamic creep test results obtained at 60°C test temperature is given in figure 57. From the results the following can be noticed:

- the standard dense mixture specimens reach the tertiary stage for all applied load levels (100, 150 and 200kpa) whereas the 6% cloisite modified dense mixture specimens did not reach tertiary stage at the applied load of 100kpa;
- the standard dense mixture specimens reach the tertiary stage at about 5000, 3500 and 2000 pulse counts for the applied loads of 100, 150 and 200kpa respectively; the specimens of the cloisite modified dense mixture reached the tertiary stage at 5200 and 3000 for the applied loads of 150 and 200kpa respectively;
- for applied load of 200kpa, specimens of both mixtures failed before reaching the maximum pulse count of 7200 pulses;
- for the applied load of 150kpa, specimens of standard dense mixture failed before reaching the maximum pulse count of 7200 pulses whereas specimens of the cloisite modified dense mixture did not show complete failure at 7200 pulse counts;
- In all cases deformations in the primary stage of the standard dense mixture specimens are bigger than those of the cloisite modified dense mixture specimens.

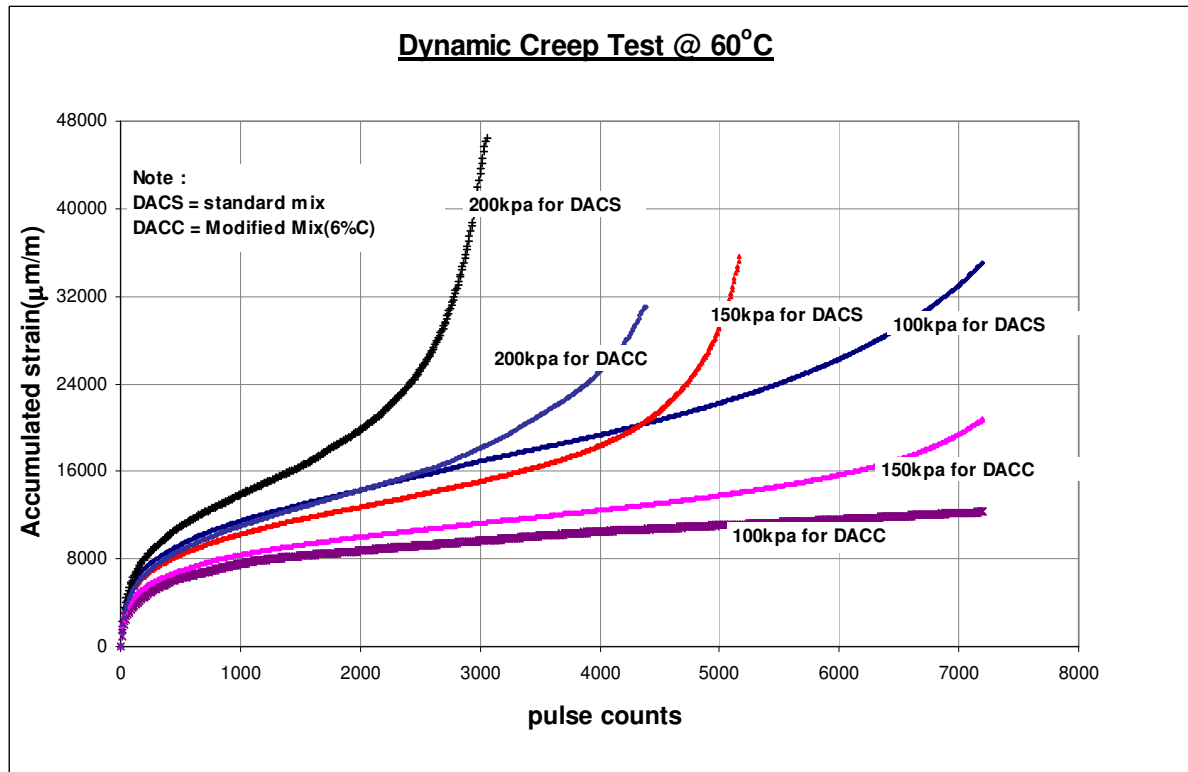


Figure 57: Dynamic creep test results at 60°C

6.3.4 Test result analysis and comparison

The relatively constant rate of permanent deformation in the secondary stage (K) and the flow number, which is the number of pulse counts where tertiary stage starts, are the two parameters which are recommended as rutting resistance indicators of asphalt mixtures [12,15]. In this study work both parameters are used to compare the rutting resistance of the two dense mixture types. If the test result did not reach the tertiary stage then the permanent strain at 7200pulses together with K values is used for comparison. The definition of K and flow number (Fn) can also be seen in figure 14. The rutting resistance indicators are given in table 54 and table 55 for the standard and cloisite modified dense mixtures respectively.

Temperature (°C)	Load (kpa)	Slope(K) ((µm/m)/pulse)	Flow number(Fn)	accumulated strain (µm/mm) @7200 pulses
40°C	100	0,34	*	9532
	300	0,92	*	16736
	500	5,1	4200	>50000
50°C	100	0,62	*	12083
	200	1,93	*	24689
	300	4,5	3750	>50000
60°C	100	2,5	5000	35108
	150	2,8	3500	>50000
	200	5,9	2000	>50000

Table 54: Rutting resistance indicators for standard dense mix

Temperature (°C)	Load (kpa)	Slope(K) (($\mu\text{m}/\text{m}$)/pulse)	Flow number(Fn)	accumulated strain @7200 pulses
40°C	100	0,2	*	6014
	300	0,42	*	11444
	500	1,75	*	26500
50°C	100	0,39	*	9414
	200	0,69	*	12757
	300	2,5	5250	39730
60°C	100	0,63	*	12320
	150	1,27	5200	20790
	200	3,3	3000	>50000

*it was not found until the end of 7200 load repetitions

Table 55: Rutting resistance indicators for 6% cloisite modified dense mix

The values of K are also given graphically in figure 58. However, for the values of Fn and permanent strain @ 7200pulses , the tabular values are used for comparison since these values are difficult to represent them in the graph.

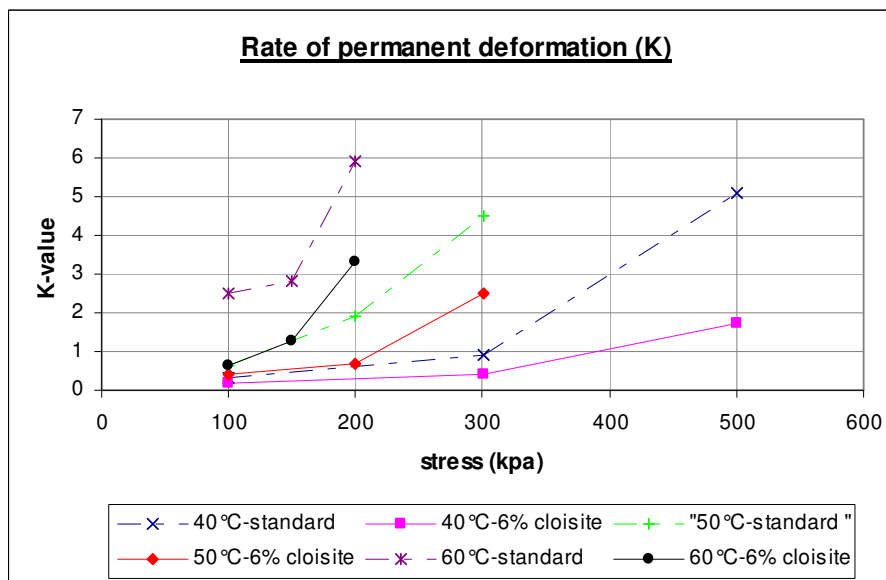


Figure 58: Rate of permanent deformation (K)

From the analysis and comparison of K values of the standard and 6% cloisite modified dense mixtures we can make the following observations.

- For all the test temperatures and loading conditions, the K values of the standard dense mixture is higher than the K values of the 6% cloisite modified dense mixture.
- At 40°C the K values of the standard dense mixture is about 1.7 to 2.9 times higher than the K values of the 6% cloisite modified dense mixture.
- At 50°C the K values of the standard dense mixture is about 1.6 to 2.8 times higher than the K values of the 6% cloisite modified dense mixture.

- At 60°C the K values of the standard dense mixture is about 1.8 to 4 times higher than the K values of the 6% cloisite modified dense mixture.

Analysis and comparison of Fn values of the standard and 6% cloisite modified dense mixtures shows the following.

- No Fn value was found at 40° C in all loading conditions for the 6% cloisite modified dense mixture. However, with the standard dense mixture an Fn value is found at about 4200 pulses for the applied load of 500kpa. Hence the Fn value for the cloisite modified dense mixture is > 1.5 times the Fn value of the standard dense mixture for the load of 500kpa
- At 50°C, Fn value was only found at the 300kpa loading condition. The Fn value of the cloisite modified dense mixture is about 1.5 times that of the standard mixture
- At 60°C, the Fn value of the cloisite modified dense mixture is about 1.5 times the Fn value of the standard dense mixture at load levels of 150kpa and 200kpa. But, at load levels of 100kpa, Fn was only found in the standard dense mixture. From the results it can be seen that the Fn value of the 6% cloisite mixture is at least 1.5 times that of the standard dense mixture.
- From the above analysis it can be summarized that the Fn value of the 6% cloisite is 1.5 times or more than the Fn value of the standard dense mixture if found.

In those tests where no tertiary stage is found, analysis and comparison of the permanent deformation at 7200 pulse counts (PD @7200) reveals the following.

- At all test temperatures and loading conditions, the PD @7200 of the standard dense mixture is higher than that of the 6% cloisite modified dense mixture.
- At 40°C the PD @7200 of the standard dense mixture is about 1.5 times higher than that of the 6 % cloisite dense mixture for the applied loads of 100 kpa and 300kpa
- At 50°C the PD @7200 of the standard dense mixture is about 1.3 and 1.9 times higher than that of the 6 % cloisite dense mixture for the applied loads of 100 kpa and 200kpa respectively.

For those test results which have tertiary stages, it is of no use to compare the PD @7200 pulse counts. After reaching this stage the rate of deformation increases rapidly and the specimen starts failing.

All the rutting resistance indicators proved that the 6% cloisite modified dense mixture showed a better performance with respect to rutting resistance as compared to the standard dense mixture. This conclusion is inline with the conclusion made about the rutting analysis of the binders.

6.4 Fatigue Resistance test

In this section fatigue resistance characterization of the 6% cloisite modified dense mixture and the standard dense mixture is discussed and presented. The discussion comprises:

- ✓ typical fatigue resistance test result;
- ✓ test result analysis and comparison of fatigue life of the modified and unmodified dense asphalt mixtures at different test temperatures and loading conditions.

6.4.1 Purpose of performing the test

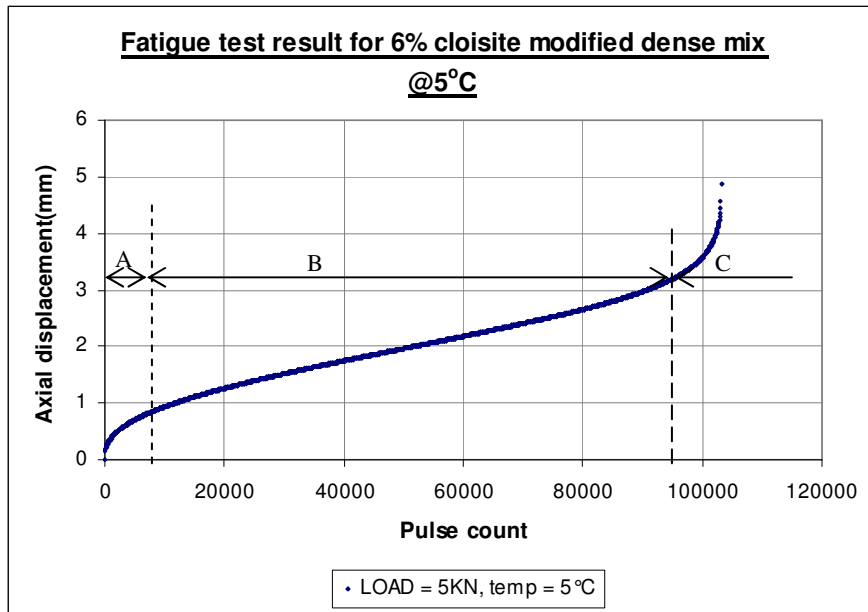
Fatigue resistance test is performed to determine the fatigue resistance of the standard and 6% cloisite modified dense mixtures at different test temperatures and loading conditions and to make a comparative analysis of their fatigue resistance.

6.4.2 Typical fatigue resistance test result

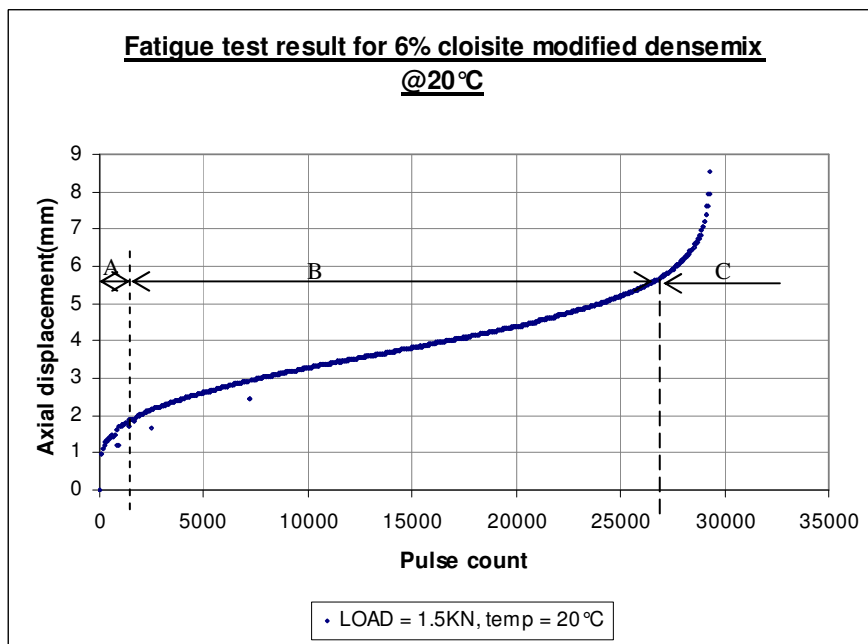
An indirect tensile test with diametral compression load was used to evaluate the fatigue resistance of the standard and modified dense mixtures. In this test, a constant repetitive load is applied and the resulting vertical deflection is measured in relation to time (pulse counts). In this study, the fatigue life of a specimen is defined as the number of load repetitions at which specimen fracture occurs. Normally the result is reported as stress or strain versus the resulting fatigue life and commonly referred as S-N curve. Here it is reported as stress versus fatigue life. A typical fatigue resistance test result at 5°C and 20°C for specific applied loads is given in figure 59.

From figure 59 the following observations can be made.

- The shape of the axial displacement versus time curves is more or less the same for both test temperatures (5 and 20°C). Section A: initial stage and a region of decreasing rate of axial displacement; section B: the second stage and a stage of constant rate of displacement and section C: a section of increasing rate of displacement.
- Section C is the region where specimen failure occurs.
- The axial displacement in the initial stage (section A) is larger for specimens tested at 20° C than those tested in 5°C (in this typical example about 2 times).
- The axial displacement in the region of constant slope (section B) is larger for specimens tested at 20° C than those tested in 5°C (in this typical example about 1.8 times).



a) fatigue resistance test result at 5°C



b) fatigue resistance test result at 20°C

Figure 59: Typical fatigue resistance test result

6.4.3 Test result analysis

The analysis of the fatigue test result comprises the following points:

- 1) find the radial stress (σ) from the amplitude of the applied compressive load using the indirect tensile formula of Eq.4;

- 2) find the fatigue life for each applied load (Number of load repetitions till the specimens fails by fracture, N_f);
- 3) find the logarithmic values of the radial stress and fatigue life;
- 4) find a linear relationship between the values computed in step3 and that gives us the classical fatigue relationship between N_f and σ .

Based on these steps a relationship between N_f and σ is obtained for the two mixture types and the two test temperatures considered.

6.4.3.1 Relationship between N_f and σ at 5°C

The test results of N_f which correspond to each radial stress at 5°C are given in table 56 and it is shown graphically in figure 60 and figure 61.

Standard dense Mix				6 %cloisite modified dense mix			
Specimen	void content	Stress(kpa)	N	Specimen	void content	Stress(kpa)	N
*DACS-II-54	2.8%	759,0	204672	*DACC-6%C-32	3.3%	765,4	203520
DACS-II-86	1.98%	890,0	113536	DACC-6%C-29	3.50%	882,5	103168
DACS-II-56	2.48%	1065,0	66240	DAC-6%C-104	3.78%	1065,0	46496
DACS-II-87	2.37%	1246,1	31664	DAC-6%C-102	3.47%	1235,5	24168
DACS-II-9	2.24%	1436,3	16248	DAC-6%C-31	3.29%	1416,0	13648
DACS-II-48	1.99%	1597,5	11584	DAC-6%C-89	3.42%	1597,5	8536
DACS-II-105	2.7%	1890,6	5296	DAC-6%C-10	4.0%	1890,6	3904
DACS-II-61	1.99%	2179,5	2720	DAC-6%C-75	3.17%	2130,1	2184

* *DACS* = standard dense mixture and **DACC* = cloisite modified dense mix

Table 56: relationship between N_f and σ for standard dense mixture at 5°C

The relationship between σ and N_f at 5°C is given in Eq.19 and is determined by means of the linear regression analysis done on the data shown in figure 61.

For standard dense mixture (5°C)

For 6% cloisite modified dense mix(5°C)

$$\text{Log } N = -4.1077 \log \sigma + 17.19$$

$$\text{Log } N = -4.3624 \log \sigma + 17.879$$

$$N = 1.549 \times 10^{17} \left(\frac{1}{\sigma} \right)^{4.1077}$$

$$N = 7.568 \times 10^{17} \left(\frac{1}{\sigma} \right)^{4.362} \quad (\text{Eq.19})$$

In Eq. 19 σ is given in kpa

The **k** values and **R-square** values @ 5°C are summarized in table 57.

Mixture type	k1	k2	R ²
standard dense mix	1,549x 10 ¹⁷	4,1077	0,9964
6% cloisite modified dense mix	7,568x 10 ¹⁷	4,362	0,9995

Table 57: k and R-square values at 5°C test temperature

Refer equation 6 in section 2.4.3 for definition of k1 and k2

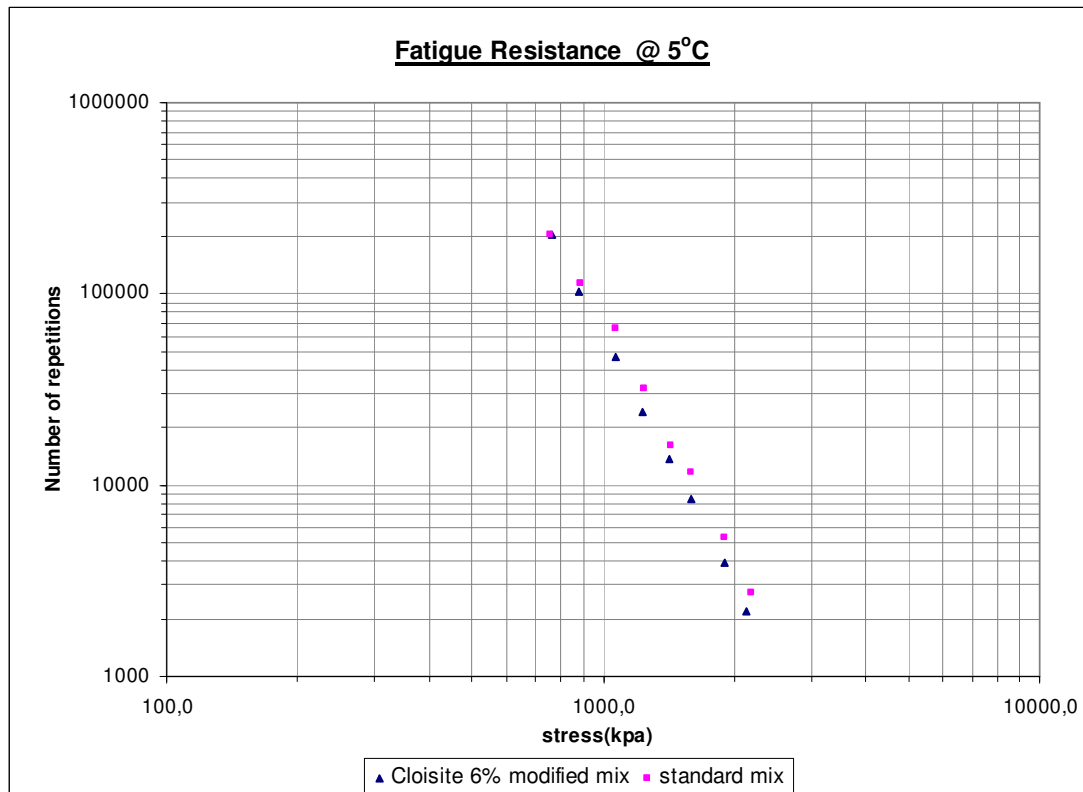


Figure 60: S-N curve at 5°C for standard and 6% cloisite modified dense mixes

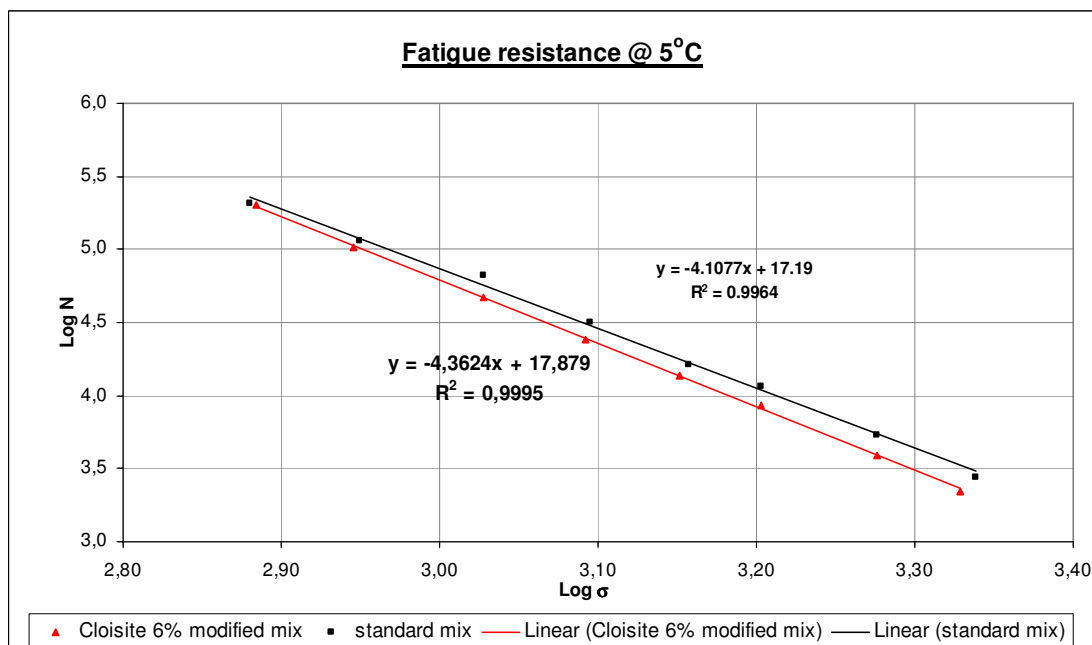


Figure 61: Relationship between logarithmic values of N_f and σ at 5°C

From the result analysis given in figure 60 and figure 61, it can be seen that a nice linear fit is obtained between σ and N_f .

6.4.3.2 Relationship between N_f and σ at 20°C

The relationship between N_f and corresponding radial stress at 20°C are given in table 58 and figure 62 and figure 63.

Standard dense Mix				6 %cloisite modified dense mix			
Specimen	Void content	Stress(kpa)	N	Specimen	Void content	Stress(kpa)	N
DACS-II-45	2.4%	162,5	149760	DAC-6%C-92	3.4%	159,3	277632
DACS-II-84	2.23%	187,4	70416	DAC-6%C-41	3.50%	186,9	135072
DACS-II-102	2.78%	224,4	36360	DAC-6%C-76	3.59%	222,5	77904
DACS-II-42	2.37%	265,5	22752	DACC-6%C-13	3.73%	269,3	29304
DACS-II-83	2.45%	309,8	13842	DAC-6%C-37	3.71%	308,9	21060
DACS-II-30	2.32%	357,0	7920	DAC-6%C-43	3.83%	354,0	10188
DACS-II-16	2.0%	424,8	4870	DAC-6%C-96	3.6%	433,4	5850
DACS-II-79	2.50%	482,7	3861	DAC-6%C-61	3.26%	489,5	4572

*DACS = standard dense mixture and *DACC = cloisite modified dense mix

Table 58: relationship between N_f and σ for standard dense mixture at 20°C

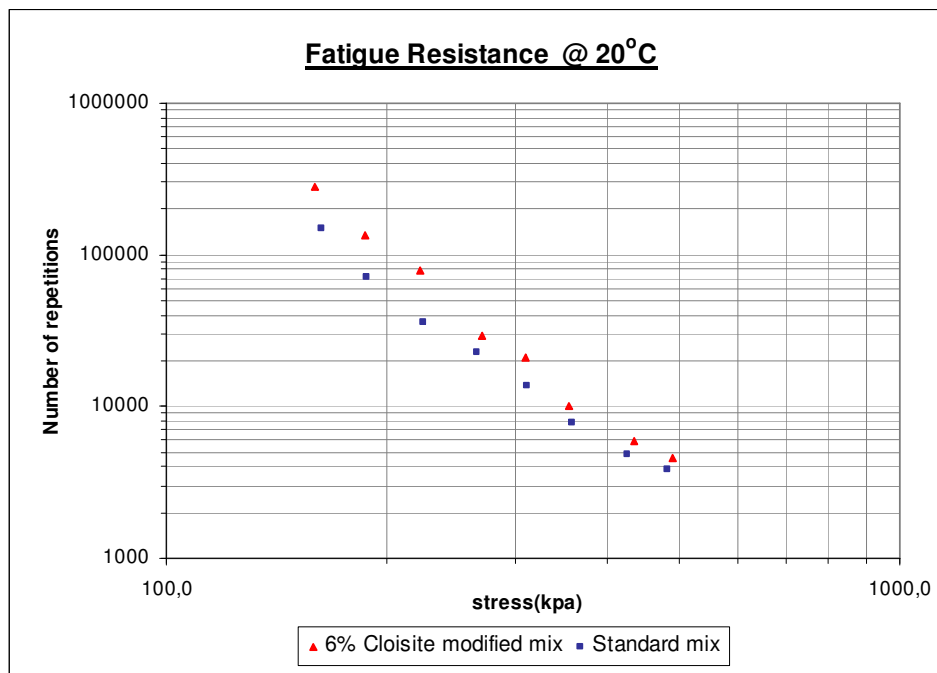


Figure 62: S-N curve at 20°C for standard and 6% cloisite modified dense mixes

As the result analysis of figure 62 and figure 63 shows a nice linear fit is also obtained between N_f and σ at 20°C. The R^2 values which are very close to 1 for both mixture types; this can be seen in figure 63.

Based on the linear regression analysis done on the logarithmic values of N_f and σ , the relationship between N_f and σ at 20°C is given in Eq.20:

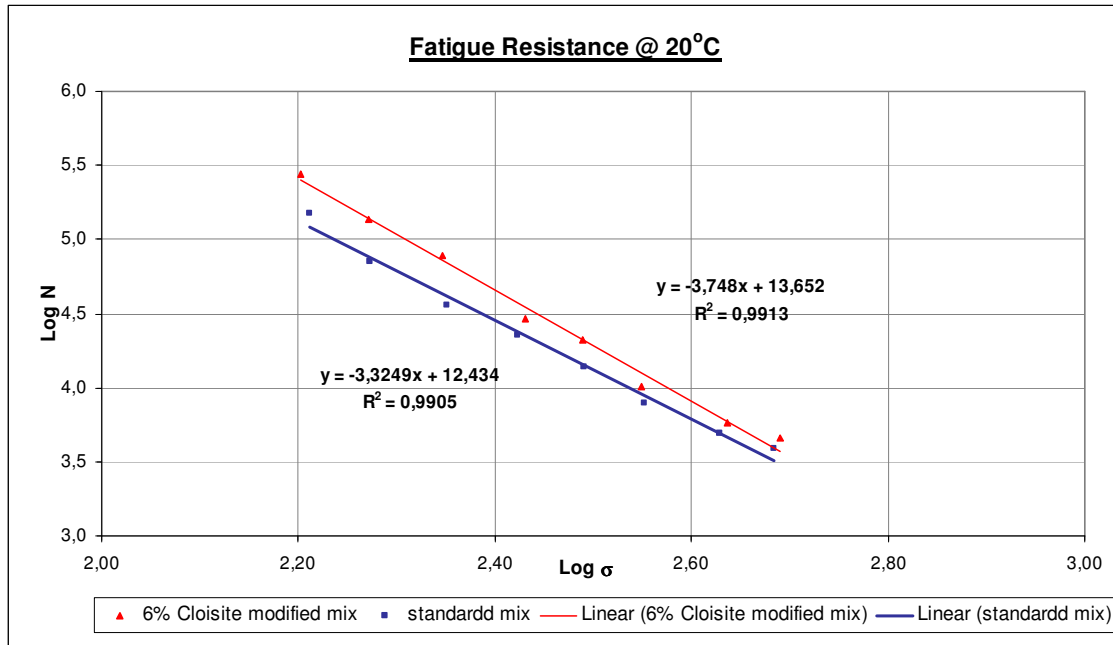


Figure 63: Relationship between logarithmic values of N_f and σ at 20°C

For standard dense mix(20°C)

For 6% cloisite modified dense mix(20°C)

$$\text{Log } N = -3.3249 \log \sigma + 12.434$$

$$\log N = 3.75 \log \sigma + 13.65$$

$$N = 2.716 \times 10^{12} \left(\frac{1}{\sigma} \right)^{3.3249}$$

$$N = 4.467 \times 10^{13} \left(\frac{1}{\sigma} \right)^{3.75}$$

(Eq.20)

In Eq. 20 σ is given in kpa

The **k** values and **R-square** values at 20°C are given in table 59.

Mixture type	k1	k2	R ²
standard dense mix	2.716×10^{12}	3.3249	0,9964
6% cloisite modified dense mix	4.467×10^{13}	3.748	0,9995

Table 59: **k** and **R-square** values at 5°C test temperature

Refer equation 6 in section 2.4.3 for definition of k1 and k2

6.4.4 Fatigue life comparison

Based on the analysis done on section 6.4.3, a comparison is made between the fatigue life of the 6% cloisite modified dense mixture and the standard dense mixture. The fatigue life comparison is performed by taking the fatigue life of the standard dense mixture as a reference and comparing the fatigue life of the 6% cloisite modified dense mixture in reference to it.

6.4.4.1 Fatigue life comparison at 5 °C

The comparison of the fatigue life at 5 °C of the two mixture types considered is given in table 60 and figure 64.

Stress(kpa)	Nc*	Ns**	Nc/NS
762	203520	204672	99%
886	103168	113536	91%
1065	46496	66240	70%
1241	24168	31664	76%
1426	13648	16248	84%
1598	8536	11584	74%
1891	3904	5296	74%
2155	2184	2720	80%
Average			81%

*Nc= fatigue life of 6% cloisite modified dense mixture , **Ns= fatigue life of standard dense mix

Table 60: Fatigue life comparison at 5 °C

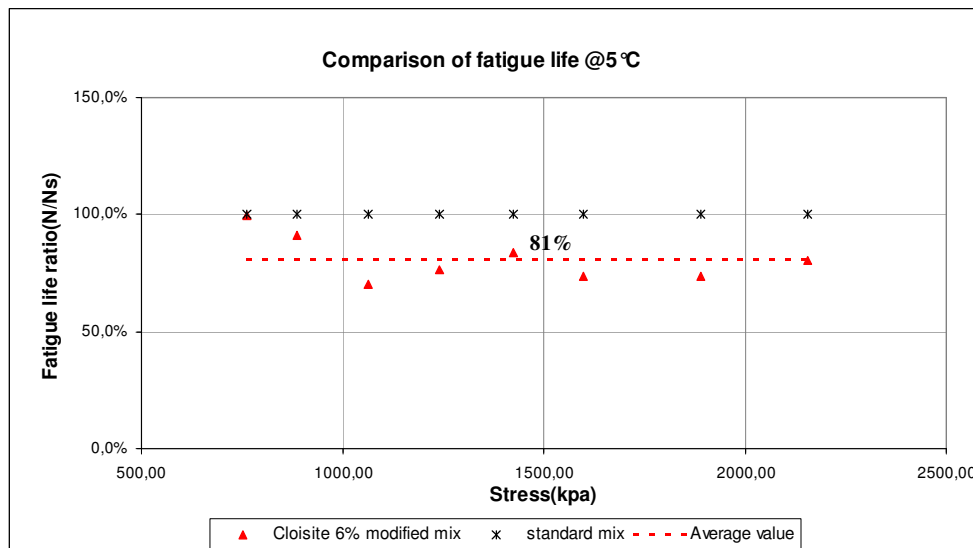


Figure 64: Fatigue life comparison at 5 °C

Based on the comparison made on the fatigue life at 5 °C of the two dense mixture types, the following observations can be made.

- The standard dense mixture performed better than the 6% cloisite modified dense mixture for all loading conditions.
- The fatigue life of the 6% cloisite modified dense mixture ranges in 70% - 100% of the fatigue life of the standard dense mix.
- At low loading stress the fatigue life of the 6% cloisite is more or less the same as the fatigue life of the standard dense mix.
- At high loading stresses the fatigue life of the 6% cloisite modified dense mixture is about 75 to 80 % of the fatigue life of the standard dense mix.

- On average the fatigue life of the 6% cloisite modified dense mixture is about 81% of the fatigue life of the standard dense mixture (considering all loading levels).

The comparison of the fatigue resistance parameter, $G^* \sin \delta$, of the standard 40/60 binder and 6% cloisite modified 40/60 binders also proves that the fatigue life of the standard binder is better than that of the 6% cloisite modified 40/60 binder. At 5°C, the $G^* \sin \delta$ of the 6% cloisite modified 40/60 binder is about 1.2 times higher than that of the standard 40/60 binder and this shows 83% efficiency based on the fatigue resistance performance analysis of the binder. This conclusion is in line with the conclusion drawn about the fatigue performance of the modified and unmodified dense mixtures.

6.4.4.2 Fatigue life comparison at 20°C

Fatigue life comparison at 20 °C for the two mixture types is given in table 61 and figure 65.

Stress(kpa)	Nc*	Ns**	Nc/NS
160,9	277632	149760	185%
187,2	135072	70416	192%
223,5	77904	36360	214%
267,4	29304	22752	129%
309,3	21060	13842	152%
355,5	10188	7920	129%
429,1	5850	4870	120%
486,1	4572	3861	118%
Average			155%

*Nc= fatigue life of 6% cloisite modified dense mixture , **Ns= fatigue life of standard dense mixture

Table 61: Fatigue life comparison at 20°C

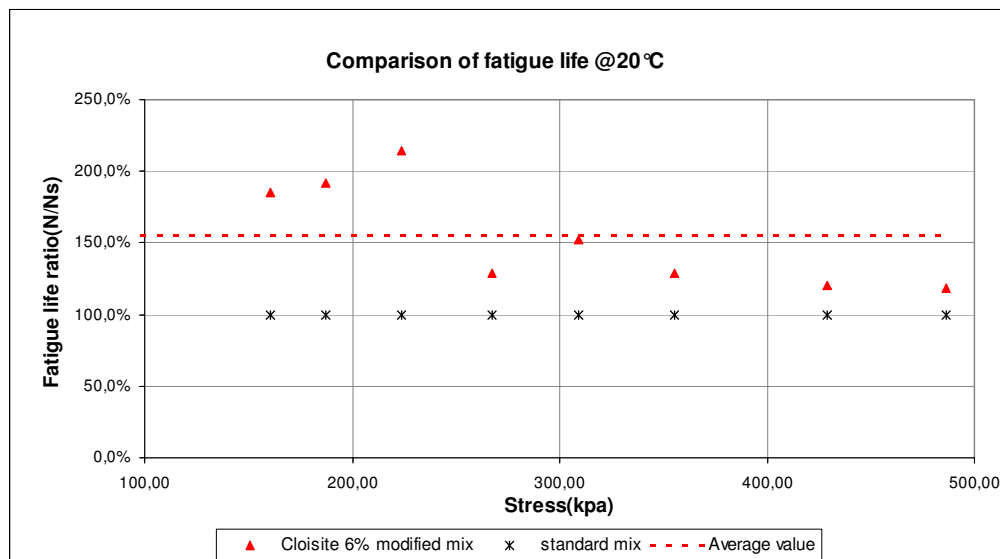


Figure 65: Fatigue life comparison at 20°C

The comparison of the fatigue life at 20°C of the two dense mixture types shows the following.

- The 6% cloisite modified dense mixture performed better than the standard dense mixture for all loading conditions.
- The fatigue life of the 6% cloisite modified dense mixture is in the range of 120% -200% of the fatigue life of the standard dense mix.
- At low stress levels, the fatigue life of the 6% cloisite is about 200% of the fatigue life of the standard dense mix.
- At high stress levels, the fatigue life of the 6% cloisite modified dense mixture is about 120 to 150 % of the fatigue life of the standard dense mix.
- On average the fatigue life of the 6% cloisite modified dense mixture is about 155% of the fatigue life of the standard dense mixture (considering all loading levels).

The comparison of the fatigue resistance parameter, $G^*\sin\delta$, of the standard 40/60 binder and 6% cloisite modified 40/60 binders at 20°C proves that the fatigue life of the standard binder is better than that of the 6% cloisite modified 40/60 binder. At 20°C, the $G^*\sin\delta$ of the 6% cloisite modified 40/60 binder is about 1.4 times that of the standard 40/60 binder and this shows a reduction in fatigue life due to the modification. This is not in line with the conclusion drawn about the fatigue performance of the modified and unmodified dense mixtures.

6.4.4.3 Fatigue life relationship at 5°C and 20°C

As discussed before, the standard dense mixture performs better in fatigue resistance than the 6% cloisite modified dense mixture at 5°C where as at 20°C the 6% cloisite modified dense mixture performs better than the standard dense mixture. This controversial analysis results might be due to two possible reasons:

1. Creep might have occurred in addition to fatigue failure at 20° C testing temperature. The 6% cloisite modified dense mixture has better performance in creep resistance than the standard dense mixture;
2. At 20°C testing temperature there is a small rest period in the load pulse; however at 5°C testing temperature the load pulse has no rest period. This rest period can possibly have some influence on the fatigue performance of the dense mixtures.

From the analysis of the fatigue life of both testing temperatures the following points can also be observed.

- The void content of the specimens of the 6% cloisite modified dense mixture is higher than those specimens of the standard dense mixture.
- The fatigue curves at both testing temperatures show nice fit with the data

- The slope of the fatigue line (k_2) at 5 °C is larger than the slope of the fatigue line at 20°C
- At both testing temperature, the ratio N_c/N_s (see table 60 and 61) is higher at low stress levels.
- At both testing temperatures, the slope of the fatigue line (k_2) of the 6% cloisite modified dense mixture is larger than the slope of the standard dense mixture.

6.4.4.4 Fatigue life using Medani's equation

In this section fatigue characteristics of asphalt mixtures is developed at 5°C and 20°C using Medani's equation at a loading time of 125ms(equal to the loading time used in fatigue tests above).

The basic principle of fatigue analysis based on Wohler relationship is usually described as:

$$N_f = k_1 \left(\frac{I}{\epsilon} \right)^{k_2} \text{ or } \log N_f = \log k_1 - k_2 \log \epsilon \quad (\text{Eq 21})$$

Where: N_f = number of strain applications to failure

e = strain at the bottom of the asphalt layer

k_1, k_2 = factors depending on the composition and properties of the asphalt mixture

It has been proved that the constant k_2 strongly depends on the slope of the master curve of the stiffness modulus. In addition the constant k_1 is related to binder characteristics and asphalt mixture properties. Studies have been done in Delft University of Technology to relate these fatigue constants with binder and asphalt characteristics. The procedures to find these constants (according to Meadni) are:

Determination of k_2

The exponent of the fatigue relationship, k_2 , can be calculated using :

$$k_2 = \frac{2}{m(0.541 + \frac{0.346}{m} - 0.0325V_a)} \quad (\text{Eq 22})$$

Where : V_a = void content (%)

$$m = \frac{d(\log S_{mix})}{d(\log t)} \quad (\text{Eq 23})$$

Where : m = slope of the master curve of mixture stiffness

S_{mix} = stiffness of the mxiture (Mpa)

t = loading time (s)

Determination of $\log k_1$

The intercept value $\log k_1$ is computed as :

$$\log k_1 = 6.589 - 3.762n + \frac{3209}{S_{mix}} + 2.332 \log V_b + 0.149 \frac{V_b}{V_a} + 0.928PI - 0.0721T_{R\&B} \quad (\text{Eq 24})$$

Where : PI = penetration index of the bitumen

V_b = volume percentage of bitumen

$T_{R\&B}$ = softening point of bitumen($^{\circ}\text{C}$)

The other variables are described above.

The penetration index is defined as :

$$PI = \frac{20(1 - 25A)}{1 + 50A} \quad (\text{Eq 25})$$

Where: A is the temperature susceptibility, which is the slope of the straight line plot between the logarithm of penetration and temperature, or

$$A = \frac{\text{Log}(\text{pen @ } T1) - \text{Log}(\text{pen @ } T2)}{T1 - T2} \quad (\text{Eq 26})$$

Where T1 and T2 = temperature values ($^{\circ}\text{C}$)

For the PI computation, one can take T1 = 25 $^{\circ}\text{C}$ and T2 = softening point value. In addition the penetration @ $T_{R\&B} \sim 800$

The relationship between binder stiffness and loading time is given in figure 66. The relationship between mixture stiffness and loading time is given in figure 67. Figure 66 is given here in order to make a comparison between the slopes of the binder stiffness and the mixture stiffness.

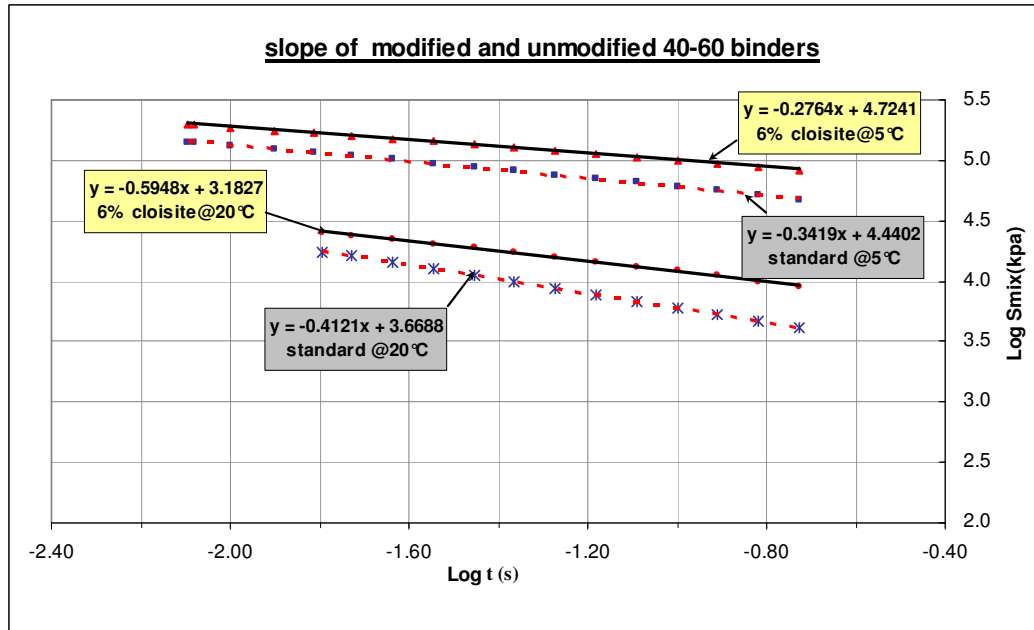


Figure 66: slope of modified and unmodified 40-60 binders

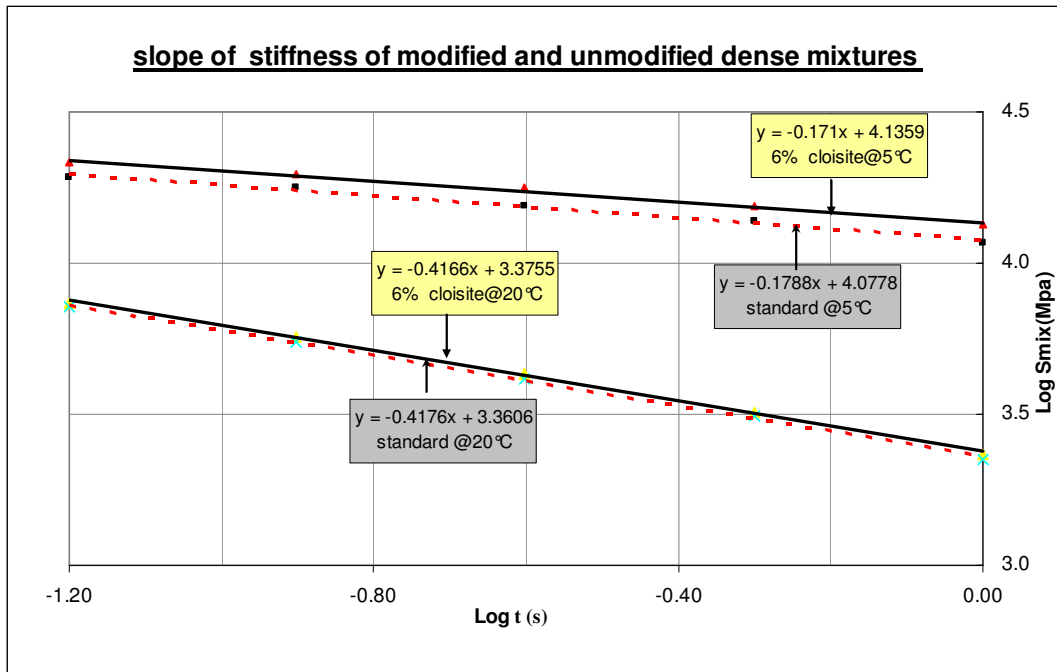


Figure 67: slope of modified and unmodified dense mixtures

From the analysis of the two figures the following observation can be made.

- The absolute value of the slope of the stiffness is bigger at 20°C than at 5°C in both cases.
- The absolute value of the slope of the stiffness of the standard binder is bigger than that of the 6% cloisite modified binder at both temperature values.
- For a given temperature value, the absolute value of the slopes of the standard and 6% cloisite modified dense mixtures are more or less the same.

Based on the above discussed equations, the computation of the two constant factors in the fatigue relationship is summarized in table 62.

Standard dense Mix	5°C							
	m	Va	Vb	PI	T _{R&B}	S _{mix}	k ₂	log K1
	0.179	2.32%	13.5%	-0.9	49.6	17758	4.658	-11.7
6% cloisite modified dense Mix	20°C							
	m	Va	Vb	PI	T _{R&B}	S _{mix}	k ₂	log K1
	0.418	2.38%	13.5%	-0.9	49.6	5451	3.705	-7.74
6% cloisite modified dense Mix	5°C							
	m	Va	Vb	PI	T _{R&B}	S _{mix}	k ₂	log K1
	0.17	3.49%	12.9%	0.17	57.6	19636	4.777	-12.07
6% cloisite modified dense Mix	20°C							
	m	Va	Vb	PI	T _{R&B}	S _{mix}	k ₂	log K1
	0.417	3.58%	12.9%	0.17	57.6	5683	3.824	-8.10

Table 62: Computation of the constant factors in fatigue relationship

The fatigue relationships for the two dense mixture types are summarized in table 63.

Standard dense mixture	
5°C	20°C
Log N = -11.7 -4.658 Logε	Log N = -7.74 -3.705 Logε
6% cloisite modified dense mixture	
5°C	20°C
Log N = -12.07 -4.777 Logε	Log N = -8.10 -3.824 Logε

Table 63: Fatigue relationship based on Medani's Equations

Based on the above developed fatigue relationships, the fatigue life computation for a selected strain values are given in table 64 and the corresponding fatigue curves are shown in figure 68.

strain (μm/m)	5°C		20°C		5°C	20°C
	standard mix	6% cloisite modified mix	standard mix	6% cloisite modified mix		
200	367833	394747	1025259	1104038	1.07	1.08
400	14567	14400	78615	77982	0.99	0.99
600	2203	2076	17502	16546	0.94	0.95
800	577	525	6028	5508	0.91	0.91
1000	204	181	2637	2347	0.89	0.89

Note : N_c = fatigue life of 6% cloisite modified dense mixture and N_s = fatigue life of standard dense mixture

Table 64: Fatigue life comparison for selected strain values

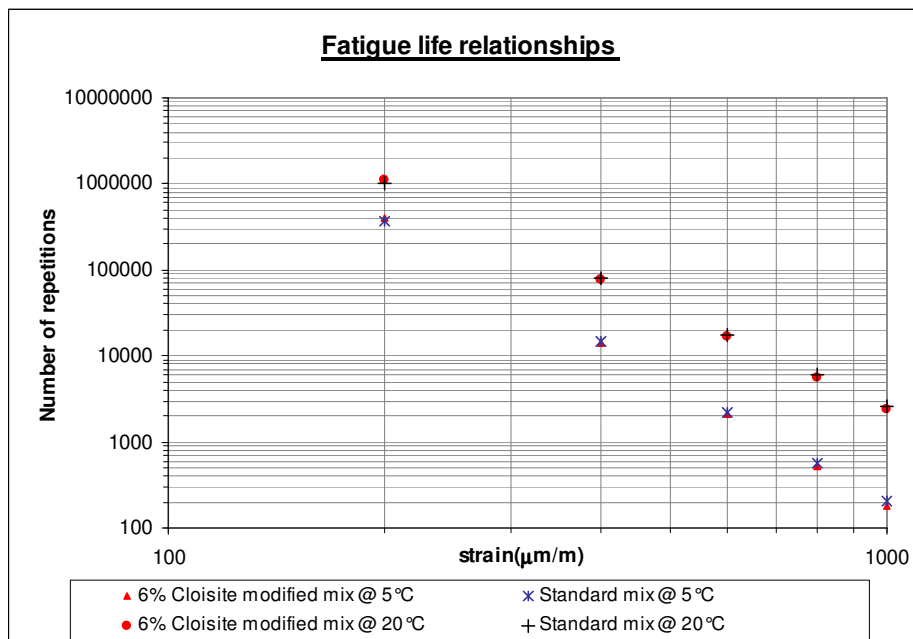


Figure 68: fatigue life comparison for selected strain values

Based on the fatigue life comparison of table 64 and figure 68 the following conclusions can be made.

- At both temperature values, the standard dense mixture performs a bit better than the 6% cloisite modified dense mixture especially at higher strain values.
- Both mixture types perform better in fatigue resistance at 20°C than at 5°C
- At smaller values of strain, the 6% cloisite modified dense mixture performs a bit better than the standard dense mixture.

7 Conclusions and Recommendations

This chapter discusses the conclusions drawn from the different tests performed, analyzed and compared. The conclusion includes specific conclusions about nanoclay characterization, rheological analysis of asphalt binders and asphalt mixtures and finally overall conclusion is given. The recommendations are given at the end of this chapter.

7.1 Conclusions on nanoclay characterization

Conclusions drawn from the nanoclay characterization are:

The microscopic analysis shows that the nanoclay materials have bigger aspect ratio; the particles are not uniform in size and arrangement. In addition, the nanofill particles look curly and smaller in size as compared to the cloisite particles.

The X – ray analyses proved presence of Si, O, Mg, Al, Fe elements which are expected in montmorillonite clay in both nanoclay materials. Presence of nitrogen is not detected in X-ray analysis. The X – ray analyses also proved that the nanoclay materials are small in size and poor in crystalline shape.

The plastic limit analysis of the two nanoclay materials proved that the nanoclay materials are family of the expansive type of clay.

7.2 Conclusions on Rheology of asphalt binders

The findings of the rheological test analyses and comparison are summarized in table 65. The influence of the clay modification on the different performance parameters is described in a scale range between -5 to 5. If the clay modification influences the performance parameter very negatively then it is assigned -5, if it has no influence at all then it is assigned 0 and if the improvement is very positive then it is assigned 5.

performance parameter	6% nanofill + 70/100	modified 40/60 binder	
		with 3% cloisite	with 6% cloisite
Empirical Rheology test			
penetration(unaged)	0	2	4
softening point (unaged)	0	2	4
short term ageing			
retained penetration	4	1	1
increment in softening point	4	1	1
long term ageing (RCAT)			
retained penetration	2	1	1
increment in softening point	2	1	2
long term ageing (PAV)			
retained penetration	3	—	—
increment in softening point	3	—	—
DSR Rheology test			
increment in stiffness (unaged)	1	2	5
decrement in phase angle(unaged)	0	2	4
short term ageing			
based on stiffness analysis	5	2	2
based on phase angle analysis	3	2	2
long term ageing (RCAT)			
based on stiffness analysis	3	2	2
based on phase angle analysis	3	1	1
long term ageing (PAV)			
based on stiffness analysis	3	—	—
based on phase angle analysis	3	—	—
rutting parameters			
$G^*/\sin\delta$ –unaged	2	4	5
$G^*/\sin\delta$ –short term aged	-1	3	4
$G^*/\sin\delta$ –long term aged	-1	2	4
fatigue resistance parameters			
$G^*\sin\delta$ –unaged	-1	-1	-1
$G^*\sin\delta$ –short term aged	0	0	-1
$G^*\sin\delta$ –long term aged	0	-1	-2

Table 65: Summary of rheological comparison results

7.3 Conclusions on performances tests of asphalt mixtures

The summary of the comparison results of the different performance related tests on the modified and the unmodified dense asphalt mixture is summarized in table 66. Similar to the rheological results comparison approach, the influence of the nanoclay modification on the dense asphalt mixture performance is given in scale range between -5 to 5. - 5 is assigned if the impact of the nanoclay modification is very negative and 5 is assigned if there is very positive impact due to the modification.

performance parameter	Dense asphalt mixtures	
	standard	6% cloistie modified
Indirect tensile strength		
ITS result	0	3
fracture energy until failure	0	4
total fracture energy		3
resilient modulus test		
resilient modulus value	0	3
master curve fitting		
WLF	5	5
Arrhenuis	5	5
dynamic creep test		
deformation in primary stage	0	3
flow number	0	4
rate of permanent deformation (K)	0	5
permanent deformation@7200	0	4
failure due to excessive deformation	0	5
Fatigue resistance test		
ITT fatigue results		
5°C		
fatigue life (Nf)	0	-1
20°C		
fatigue life (Nf)	0	2
4 bending point(Medani's Equation)		
5°C		
fatigue life (Nf)	0	-1
20°C		
fatigue life (Nf)	0	-1

Table 66: Summary of comparison results of performance tests on dense mixtures

7.4 General Conclusions

Tests performed on binders and dense asphalt mixtures proved that the cloisite nanoclay modifications helped to increase the stiffness, to improve the rutting resistance of the standard 40/60 binder. This is especially true if the 6% cloisite modification is used. In addition, the indirect tensile strength and fracture energy values are increased due to 6% cloisite modification. The nanofill (6%) modification helps to improve the ageing resistance of the 70/100 binder in the short term and long term too. However, when it comes to fatigue resistance performance, the standard binders/mixtures were performing better than the nanoclay modified binders /mixtures especially at low test temperatures. From overall result analyses and comparisons, the overall modifications observed due to the nanoclays are not at the stage to justify application at large scale.

7.5 Recommendations

It is strongly believed that the improvement is related to the chemical additive that opens up the clay structure and which is responsible for the binding of the clay mineral with the bitumen. Hence, further studies on the chemistry of the nanoclay and bitumen and further development of the nanoclay technology is recommended to utilize the full potential of the nanoclay modification.

References

- [1] Prf. dr.ir.A.A.A. Molenaar, 2003, Road Materials (part III), Delft ,the Netherlands
- [2] Prf.dr.ir.A.A.A. Molenaar, 2003, structural design of pavements (part III), Delft ,the Netherlands
- [3] Prf.dr.ir.A.A.A. Molenaar, 2003, structural evaluation and strengthening of flexible pavements using deflection measurements and visual condition surveys, Delft, the Netherlands
- [4] T.J.Pinnavaia and G.W.Beall, 2000, polymer–clay nanocomposites, John Wiley and Sons Ltd, England
- [5] Krishnamoorti, Ramanan and Vaia Richard.A, 2002, Polymer nanocomposites, Washington
- [6] Leif A. Carlsson, 1991, Thermoplastic composite materials, Elsevier science publishers B.V., Amsterdam
- [7] Y.C.Ke and P.stroeve, 2005, polymer–layered silicate and silica nanocomposites, Elsevier science publishers B.V., Amsterdam
- [8] Al-malaika, A.Golovoy, C.A. Wilkie ,2001, specialty polymer additives principles and applications, Blackwell science Ltd, London
- [9] Daniel Petrus Nicolaas Vlasseveld ,2005, fiber reinforced polymer nanocomposites, Delft, the Netherlands
- [10] Dr. John Read and Mr. David Whiteoak, 2003, The Shell Bitumen Hand book, UK
- [11] NCHRP report 459, 2001, characterization of modified asphalt binders in superpave mix design, Washington D.C.
- [12] NCHRP report 465, 2002, simple performance test for superpave mix design, Washington D.C.
- [13] TRB report number 1454, 1994, Asphalt concrete mixture design and performance, Washington D.C.
- [14] TRB report number 1590, 1997, Asphalt mixture quality characteristics and performance, Washington D.C.
- [15] TRB report number 1789, 2002, bituminous paving mixtures materials and construction, Washington D.C.
- [16] TRB report number 1832, 2003, bituminous paving mixtures, Washington D.C.
- [17] TRB report number 1891, 2004, bituminous paving mixtures, Washington D.C.
- [18] TRB report number 1488, 1995, unmodified and modified asphalt binders, Washington D.C
- [19] T.O.Medani ,2006, Design principles of surfacings on orthotropic steel bridge decks, Phd thesis ; Delft university of Technology, the Netherlands

- [20] J.Groenendijk,1998, accelerated testing and surface cracking of asphalt concrete pavements, Phd thesis ;Delft university of Technology , the Netherlands
- [21] Dr. Robert N. Hunter, 2000, asphalt in road construction, Thomas Telfort ltd, London
- [22] Erkens, mw. S.M.J.G., 2002,Asphalt concrete response(ACRe), Phd thesis ;Delft university of Technology , the Netherlands
- [23] Molenaar, ir. J.M.M.,2004, Performance related characterization of the mechanical behavior of asphalt mixtures , Phd thesis ;Delft university of Technology , the Netherlands
- [24] Yang H. Haung ,2004, pavement design and analysis, Prentice-Hall, New jersey
- [25] TA instruments-waters LLC , 2004 , Rheology Advantage Data Analysis Manual
- [26]<http://www.iprime.umn.edu/pdfs/NanoWorkshop/Hunter1.I'MPnano050310.pdf>,
Nanocomposite Organoclays
- [27] D.B Ghile, A.A.A. Molenaar, M.F.C. van de ven, J. Besamusca, CROW conference WW2006, Nanotechnology applied to bitumen to improve asphalt mixture behavior , Doorwerth, The Netherlands
- [28] Prf.dr.A.A.A. Molenaar, D.B Ghile, Ir.M.F.C. van de ven ,December 2005, report number 7-04-110-25, CROW report, Effect of nano-clay modification on rheology of bitumen ,The Netherlands
- [29]EN-NEN 12697-23, 2004, Determination of the indirect tensile strength of bituminous specimens, European standard
- [30]EN-NEN 12697-24, 2004, resistance to fatigue of bituminous mixtures, European standard
- [31]EN-NEN 12697-25, 2004, bituminous mixtures – test methods for hot mix asphalt –part 25 – cyclic compression test, European standard
- [32]EN-NEN 12697-26, 2004, bituminous mixtures – test methods for hot mix asphalt –part 26 – stiffness, European standard
- [33]EN-NEN 15323, 2005, accelerated long-term ageing conditioning by rotating cylinder method (RCAT), European standard
- [34]EN-NEN 14769, 2005, accelerated long-term ageing conditioning by pressure ageing vessel (PAV), European standard

Appendix A

This appendix comprises some tests which are not shown in the main part of the thesis report; the pictorial representations of the tested specimens of the modified and unmodified dense asphalt mixes.

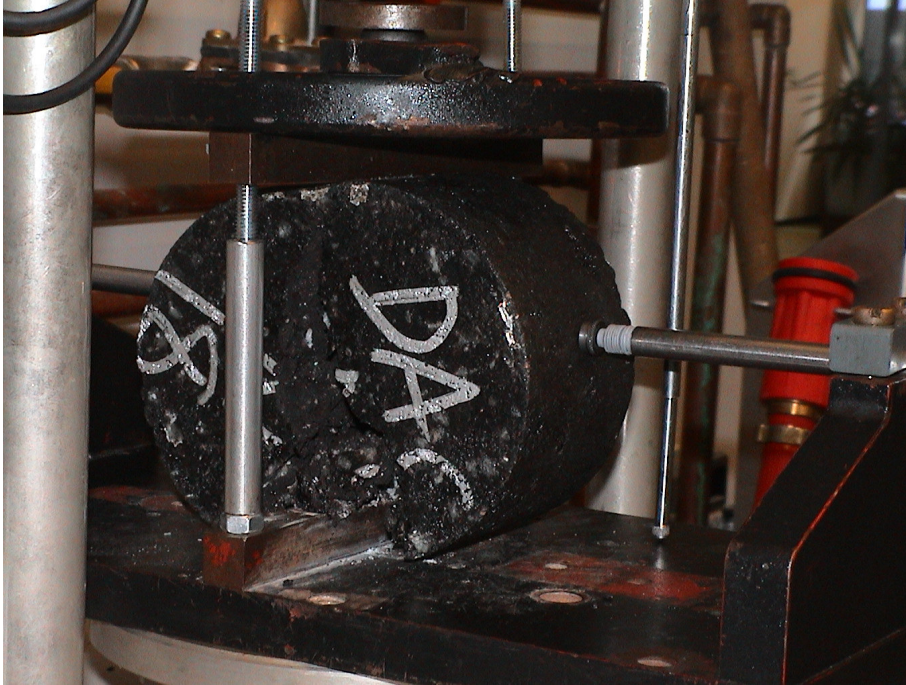


Figure1 : Indirect tensile strength test set-up



Figure 2 : Indirect tensile strength tested specimens

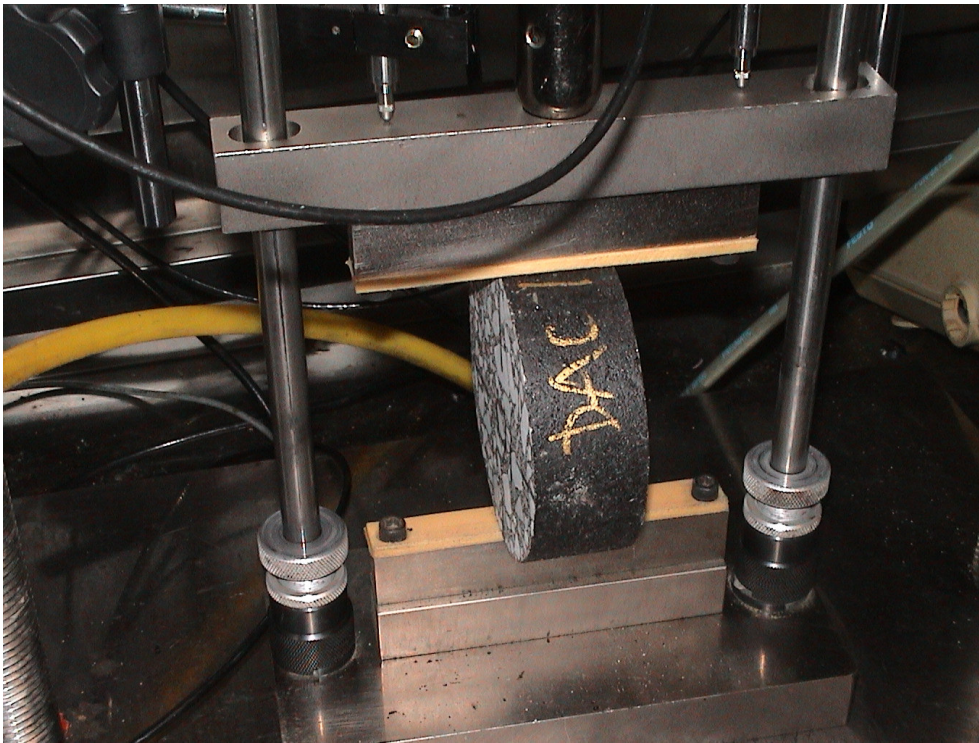


Figure 3 : Fatigue resistance test set-up



Figure 4 : Fatigue resistance tested specimens @ 5°C



Figure 5 : Dynamic creep tested specimens @ 40, 50 and 60°C



Figure 6 : Dynamic creep tested specimens @ 50°C and 200kpa (6% cloisite modified)

Appendix B

This appendix comprises typical examples of actual density computation, void content and actual density results of standard and 6% cloisite modified dense mixes.

Permanent Deformation							
Specimen nr.	Dry weight [g]	Weight under water [g]	Towel-dried weight [g]	T _{water} [°C]	ρ _{water} [kg/m ³]	Calculated volume [mm ³]	D _{specimen} [kg/m ³]
DAC-II-S4	1088,6	645,8	1088,7	20,8	1000	443,7	2453,5
DAC-II-S6	1093,3	648,5	1093,4	20,8	1000	445,7	2453,0
DAC-II-S8	1084,6	642,5	1084,8	20,8	1000	443,1	2447,8
DAC-II-S13	1085,9	643,9	1086,0	20,8	1000	442,9	2451,8
DAC-II-S14	1079,8	638,1	1080,0	20,8	1000	442,7	2439,1
DAC-II-S19	1079,7	637,7	1079,9	20,8	1000	443,0	2437,3
DAC-II-S20	1086,4	643,9	1086,5	20,8	1000	443,4	2450,2
DAC-II-S22	1085,0	642,4	1085,1	20,8	1000	443,5	2446,5
DAC-II-S23	1083,1	641,2	1083,2	20,8	1000	442,8	2446,0
DAC-II-S25	1084,8	642,7	1084,9	20,8	1000	443,0	2448,8
DAC-II-S26	1080,0	639,6	1080,2	20	1000	441,4	2446,8
DAC-II-S31	1066,6	630,3	1066,7	20	1000	437,2	2439,7
DAC-II-S32	1082,0	639,5	1082,1	20	1000	443,4	2440,2
DAC-II-S33	1082,1	639,9	1082,3	20	1000	443,2	2441,6
DAC-II-S34	1086,3	642,4	1086,4	20	1000	444,8	2442,2
DAC-II-S36	1087,4	644,4	1087,6	20	1000	444,0	2449,1
DAC-II-S40	1088,6	645,6	1088,9	20	1000	444,1	2451,3
DAC-II-S41	1083,6	641,8	1083,7	20	1000	442,7	2447,7
DAC-II-S44	1090,8	645,9	1090,9	20	1000	445,8	2446,8
DAC-II-S47	1080,7	637,0	1080,8	20	1000	444,6	2430,7
DAC-II-S62	1085,9	642,4	1086,0	20	1000	444,4	2443,5
DAC-II-S65	1088,7	645,2	1088,8	20	1000	444,4	2449,8
DAC-II-S73	1079,4	637,5	1079,5	20,4	1000	442,8	2437,7
DAC-II-S78	1077,2	635,6	1077,3	20,4	1000	442,5	2434,4
DAC-II-S80	1078,3	636,3	1078,5	20,4	1000	443,0	2434,1
DAC-II-S82	1082,9	639,7	1083,1	20,4	1000	444,2	2437,9
DAC-II-S85	1085,8	643,9	1086,0	20,4	1000	442,9	2451,6
DAC-II-S89	1066,2	631,7	1066,4	20,4	1000	435,5	2448,3
DAC-II-S90	1084,1	641,4	1084,2	20,4	1000	443,6	2443,9
DAC-II-S93	1087,3	645,3	1087,7	20,4	1000	443,2	2453,3
DAC-II-S95	1087,6	643,7	1087,7	20,4	1000	444,8	2445,1
DAC-II-S103	1086,0	642,5	1086,1	20,4	1000	444,4	2443,7

Table 1 : Typical example of actual density computation

Permanent Deformation					
6% cloiste dense mix			Standard dense mix		
Specimen nr.	D _{specimen} [kg/m ³]	Void Content (VC) [%]	Specimen nr.	D _{specimen} [kg/m ³]	Void Content (VC) [%]
DAC-6%C-2	2443,3	2,78%	DAC-II-S4	2453,5	1,9%
DAC-6%C-3	2442,7	2,80%	DAC-II-S6	2453,0	1,9%
DAC-6%C-4	2446,9	2,64%	DAC-II-S8	2447,8	2,1%
DAC-6%C-5	2440,4	2,89%	DAC-II-S13	2451,8	2,0%
DAC-6%C-7	2437,2	3,02%	DAC-II-S14	2439,1	2,5%
DAC-6%C-11	2427,7	3,40%	DAC-II-S19	2437,3	2,5%
DAC-6%C-22	2416,1	3,86%	DAC-II-S20	2450,2	2%
DAC-6%C-23	2425,1	3,50%	DAC-II-S22	2446,5	2,2%
DAC-6%C-30	2429,6	3,32%	DAC-II-S23	2446,0	2,2%
DAC-6%C-39	2429,3	3,33%	DAC-II-S25	2448,8	2,1%
DAC-6%C-40	2410,5	4,08%	DAC-II-S26	2446,8	2,2%
DAC-6%C-46	2427,8	3,39%	DAC-II-S31	2439,7	2,4%
DAC-6%C-48	2414,4	3,93%	DAC-II-S32	2440,2	2,4%
DAC-6%C-55	2435,9	3,07%	DAC-II-S33	2441,6	2,4%
DAC-6%C-56	2416,2	3,86%	DAC-II-S34	2442,2	2,3%
DAC-6%C-60	2422,9	3,59%	DAC-II-S36	2449,1	2,1%
DAC-6%C-62	2440,3	2,90%	DAC-II-S40	2451,3	2,0%
DAC-6%C-63	2426,4	3,45%	DAC-II-S41	2447,7	2,1%
DAC-6%C-64	2433,1	3,19%	DAC-II-S44	2446,8	2,2%
DAC-6%C-66	2428,4	3,37%	DAC-II-S47	2430,7	2,8%
DAC-6%C-67	2413,4	3,97%	DAC-II-S62	2443,5	2,3%
DAC-6%C-68	2415,1	3,90%	DAC-II-S65	2449,8	2,0%
DAC-6%C-74	2425,2	3,50%	DAC-II-S73	2437,7	2,5%
DAC-6%C-77	2430,9	3,27%	DAC-II-S78	2434,4	2,7%
DAC-6%C-82	2434,2	3,14%	DAC-II-S80	2434,1	2,7%
DAC-6%C-84	2422,6	3,60%	DAC-II-S82	2437,9	2,5%
DAC-6%C-85	2427,3	3,42%	DAC-II-S85	2451,6	2,0%
DAC-6%C-86	2428,4	3,37%	DAC-II-S89	2448,3	2,1%
DAC-6%C-87	2426,4	3,45%	DAC-II-S90	2443,9	2,3%
DAC-6%C-88	2425,8	3,48%	DAC-II-S93	2453,3	1,9%
DAC-6%C-91	2436,9	3,03%	DAC-II-S95	2445,1	2,2%
DAC-6%C-95	2425,4	3,49%	DAC-II-S103	2443,7	2,3%
DAC-6%C-99	2421,8	3,63%			
DAC-6%C-100	2423,3	3,57%			
DAC-6%C-103	2432,0	3,23%			
DAC-6%C-108	2440,1	2,90%			

Table 2 : actual density and void content of specimens tested for dynamic creep test

Dynamic Stiffness					
6% cloiste dense mix			Standard dense mix		
Specimen nr.	D _{specimen} [kg/m ³]	Void Content (VC) [%]	Specimen nr.	D _{specimen} [kg/m ³]	Void Content (VC) [%]
DAC-6%C-8	2420,9	3,67%	DAC-II-S3	2447,9	2,1%
DAC-6%C-9	2416,5	3,84%	DAC-II-S5	2445,8	2,2%
DAC-6%C-12	2421,5	3,65%	DAC-II-S15	2440,1	2,4%
DAC-6%C-18	2431,0	3,27%	DAC-II-S17	2441,1	2,4%
DAC-6%C-21	2422,8	3,59%	DAC-II-S24	2439,6	2,4%
DAC-6%C-24	2415,7	3,88%	DAC-II-S28	2446,0	2,2%
DAC-6%C-28	2427,2	3,42%	DAC-II-S35	2441,0	2,4%
DAC-6%C-31	2430,5	3,29%	DAC-II-S37	2440,5	2,4%
DAC-6%C-35	2418,5	3,76%	DAC-II-S38	2445,1	2,2%
DAC-6%C-38	2418,3	3,77%	DAC-II-S43	2442,8	2,3%
DAC-6%C-45	2426,9	3,43%	DAC-II-S49	2435,1	2,6%
DAC-6%C-57	2407,4	4,20%	DAC-II-S52	2424,3	3,1%
DAC-6%C-58	2412,3	4,01%	DAC-II-S54	2431,5	2,8%
DAC-6%C-59	2409,9	4,11%	DAC-II-S57	2447,0	2,1%
DAC-6%C-72	2413,7	3,96%	DAC-II-S69	2434,2	2,7%
DAC-6%C-78	2414,2	3,94%	DAC-II-S74	2426,2	3,0%
DAC-6%C-79	2422,7	3,60%	DAC-II-S88	2443,4	2,3%
DAC-6%C-97	2425,0	3,50%	DAC-II-S92	2441,3	2,4%
DAC-6%C-98	2433,4	3,17%	DAC-II-S96	2448,8	2,1%
DAC-6%C-102	2425,8	3,47%	DAC-II-S101	2435,9	2,6%
			DAC-II-S105	2432,4	2,7%
			DAC-II-S110	2424,5	3,0%

Table 3 : actual density and void content of specimens tested for resilient modulus

Indirect Tensile Strength					
6% cloiste dense mix			Standard dense mix		
Specimen nr.	D _{specimen} [kg/m ³]	Void Content (VC) [%]	Specimen nr.	D _{specimen} [kg/m ³]	Void Content (VC) [%]
DAC-6%C-1	2426,9	3,43%	DAC-II-S1	2442,7	2,32%
DAC-6%C-10	2413,4	3,97%	DAC-II-S10	2446,1	2,18%
DAC-6%C-19	2432,8	3,20%	DAC-II-S21	2438,4	2,49%
DAC-6%C-26	2426,2	3,46%	DAC-II-S29	2447,7	2,12%
DAC-6%C-37	2419,8	3,71%	DAC-II-S46	2430,6	2,80%
DAC-6%C-53	2408,9	4,15%	DAC-II-S48	2451,0	1,99%
DAC-6%C-80	2421,1	3,66%	DAC-II-S51	2425,7	3,00%
DAC-6%C-81	2424,2	3,54%	DAC-II-S91	2446,0	2,19%
DAC-6%C-101	2419,7	3,72%	DAC-II-S94	2440,2	2,42%
DAC-6%C-107	2427,3	3,41%			

Table 4 : actual density and void content of specimens tested for ITS

Fatigue test					
6% cloiste dense mix			Standard dense mix		
Specimen nr.	D _{specimen} [kg/m ³]	Void Content (VC) [%]	Specimen nr.	D _{specimen} [kg/m ³]	Void Content (VC) [%]
DAC-6%C-13	2419,5	3,73%	DAC-II-S9	2444,6	2,24%
DAC-6%C-14	2425,9	3,47%	DAC-II-S12	2437,1	2,54%
DAC-6%C-17	2424,8	3,51%	DAC-II-S16	2450,8	2,00%
DAC-6%C-25	2401,7	4,44%	DAC-II-S27	2442,0	2,35%
DAC-6%C-29	2425,1	3,50%	DAC-II-S30	2442,7	2,32%
DAC-6%C-32	2431,3	3,26%	DAC-II-S42	2441,5	2,37%
DAC-6%C-41	2425,1	3,50%	DAC-II-S45	2440,2	2,42%
DAC-6%C-42	2403,2	4,37%	DAC-II-S55	2439,7	2,44%
DAC-6%C-43	2416,8	3,83%	DAC-II-S56	2438,6	2,48%
DAC-6%C-44	2413,2	3,98%	DAC-II-S61	2450,9	1,99%
DAC-6%C-47	2404,8	4,31%	DAC-II-S64	2450,6	2,00%
DAC-6%C-61	2431,3	3,26%	DAC-II-S66	2421,6	3,16%
DAC-6%C-70	2406,5	4,24%	DAC-II-S79	2438,3	2,50%
DAC-6%C-73	2416,3	3,85%	DAC-II-S83	2439,6	2,45%
DAC-6%C-75	2433,4	3,17%	DAC-II-S84	2445,1	2,23%
DAC-6%C-76	2422,8	3,59%	DAC-II-S86	2451,2	1,98%
DAC-6%C-89	2427,1	3,42%	DAC-II-S87	2441,4	2,37%
DAC-6%C-92	2427,8	3,40%	DAC-II-S102	2431,2	2,78%
DAC-6%C-93	2421,0	3,67%	DAC-II-S108	2421,0	3,19%
DAC-6%C-96	2423,7	3,56%			
DAC-6%C-104	2418,0	3,78%			
DAC-6%C-105	2402,3	4,41%			

Table 5 : actual density and void content of specimens tested for fatigue resistance test

Appendix C

This appendix comprises typical examples of frequency sweep analysis of nanofill modified 70/100 DSR results. In addition typical examples of shift factor graphs in relation to temperatures and master curves of stiffness and phase angle of PAV aged modified and unmodified 70/100 binder are presented.

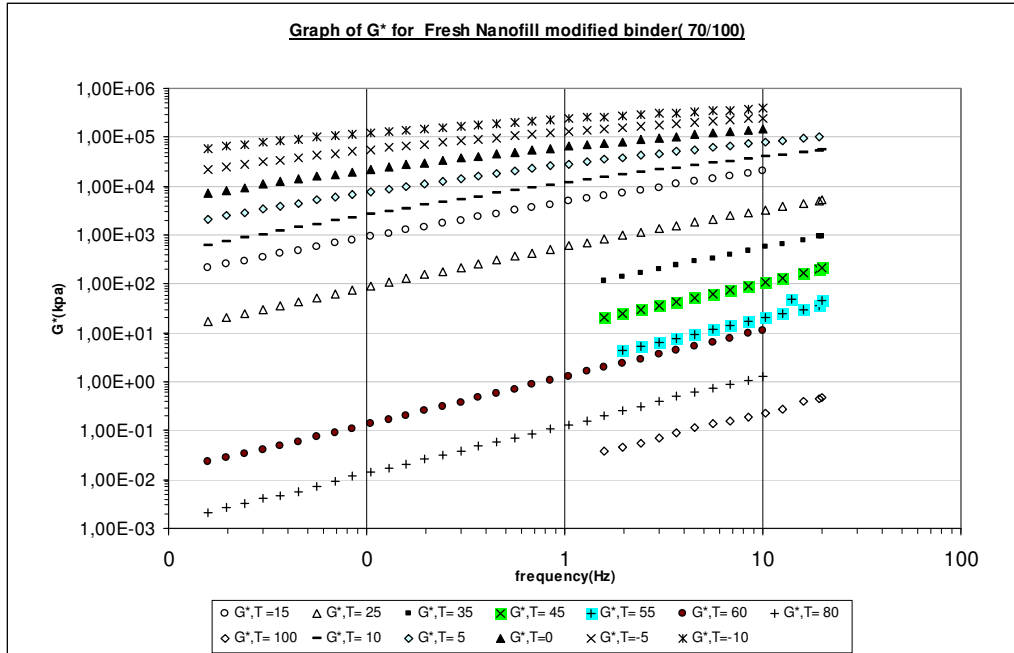


Figure 7 : Frequency sweep analysis of stiffness of nanofill modified 70/100

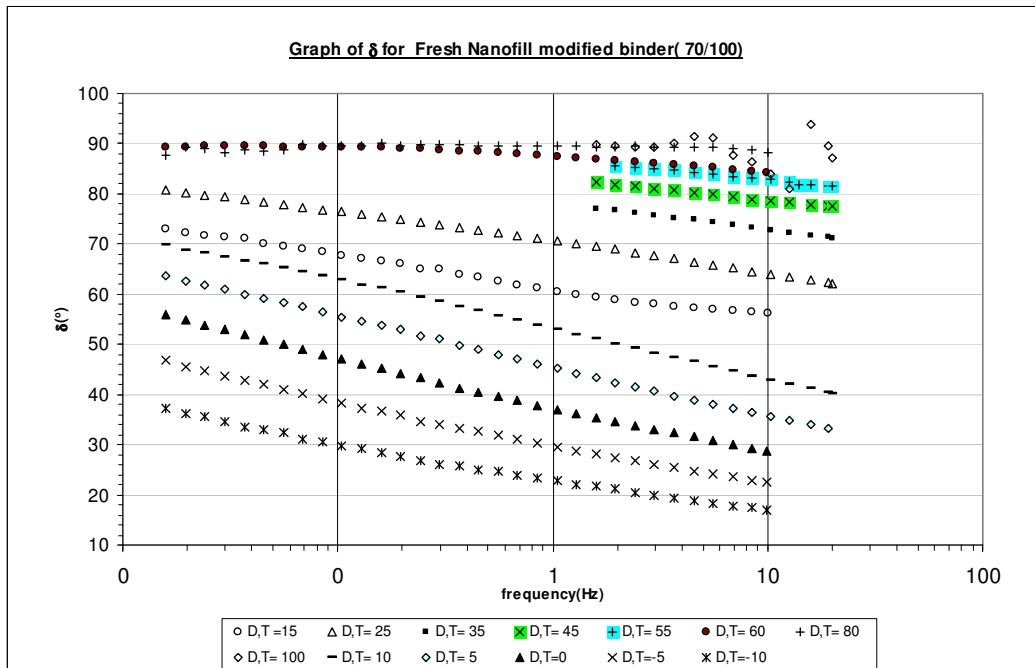


Figure 8 : Frequency sweep analysis of phase angle of nanofill modified 70/100

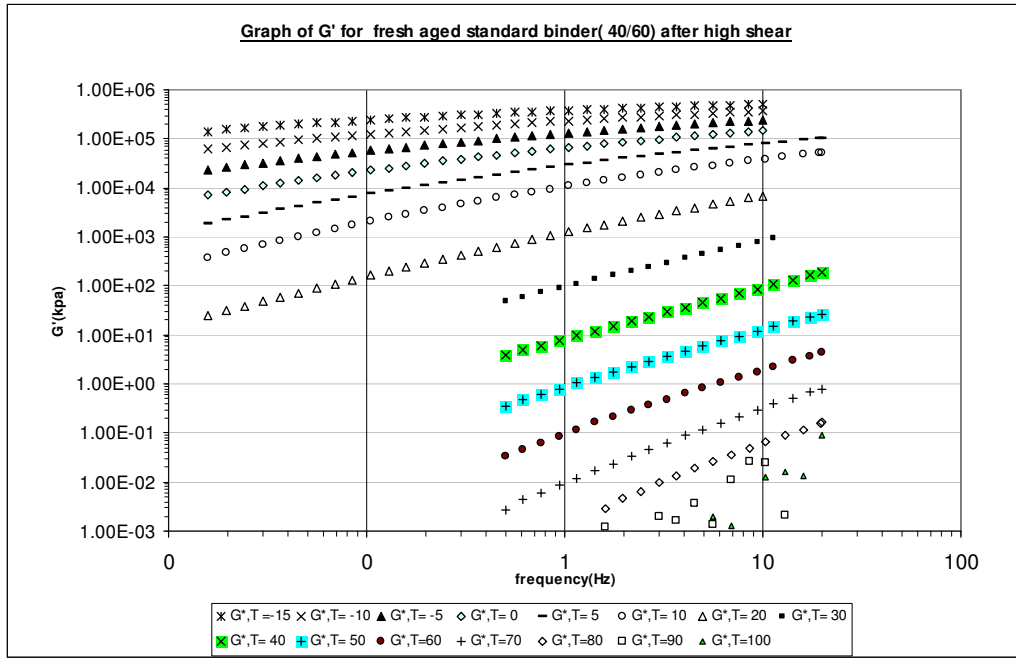


Figure 9 : Frequency sweep analysis of G' of standard 40/60

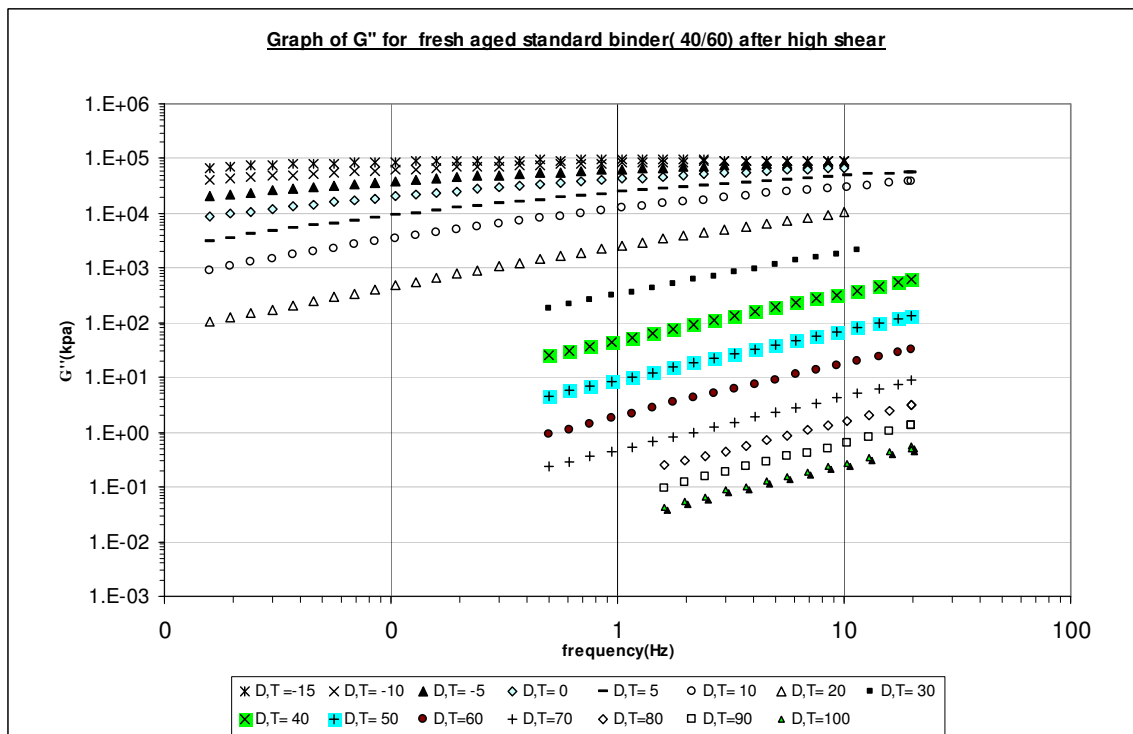


Figure 10 : Frequency sweep analysis of G'' of standard 40/60

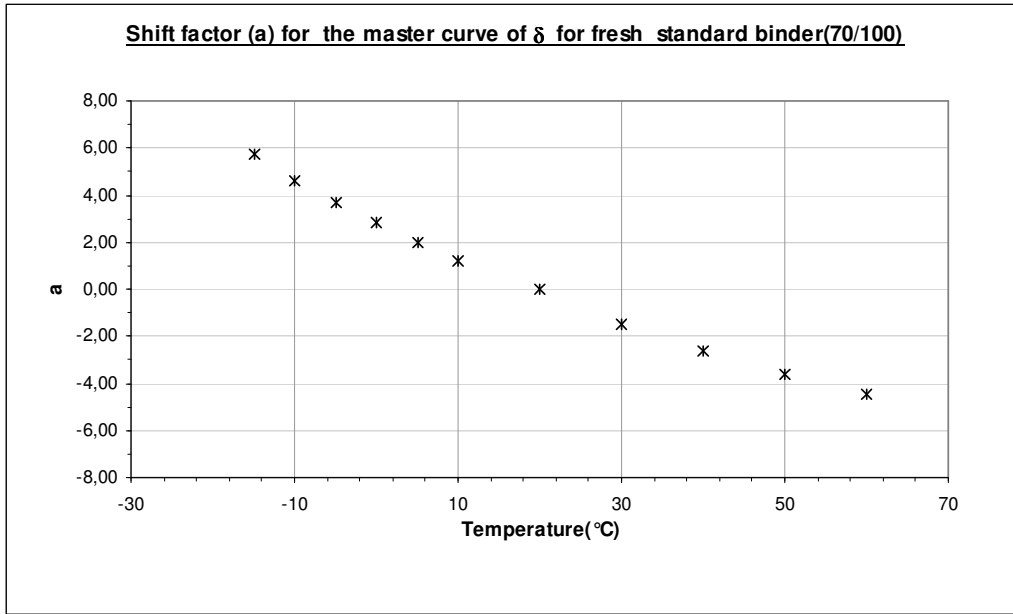


Figure 11 : shift factor values at different temperatures in master curve construction of phase angle

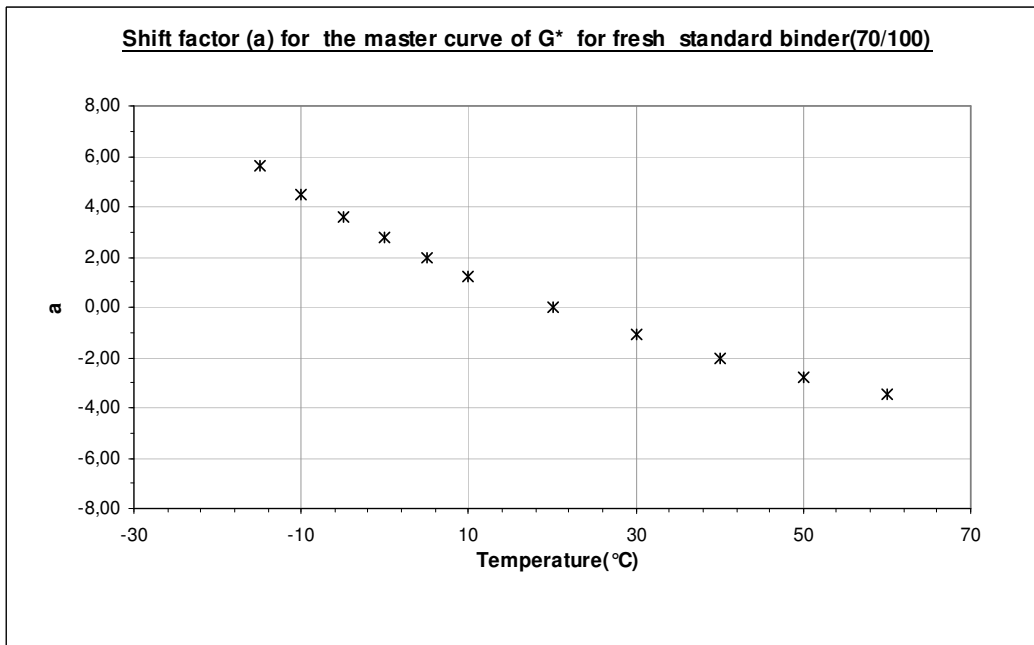


Figure 12: shift factor values at different temperatures in master curve construction of stiffness

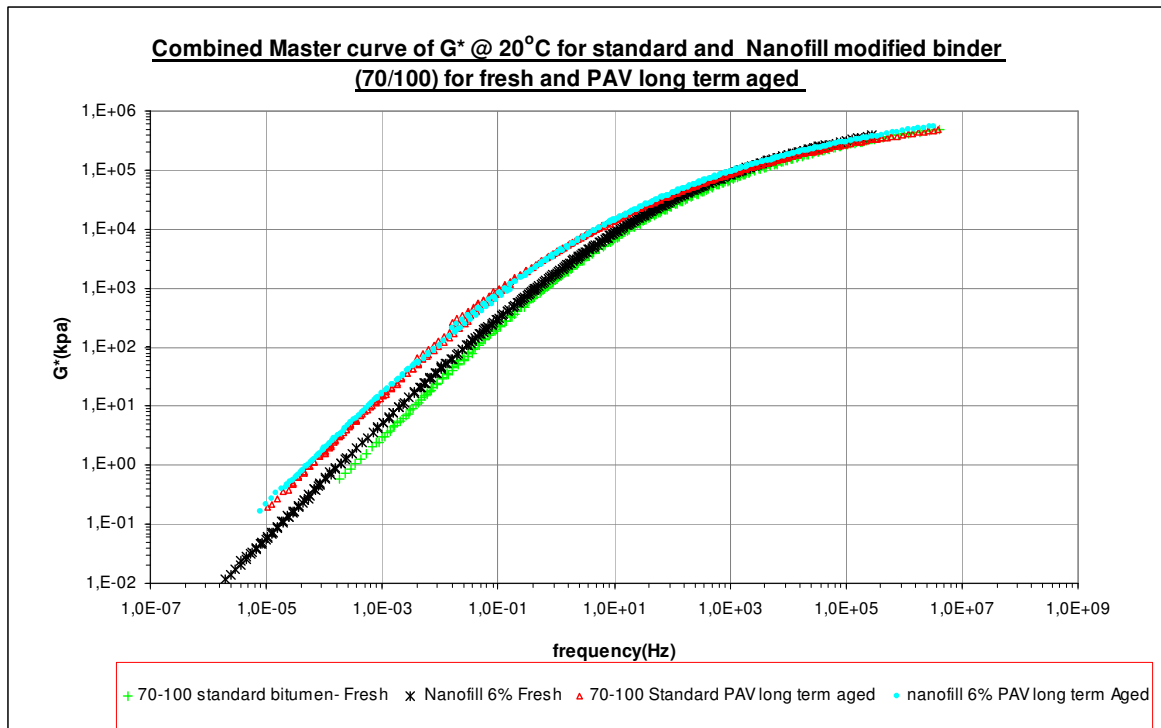


Figure 13: Master curve of stiffness of PAV long term aged standard and nanofill (6%) modified 70/100 binders

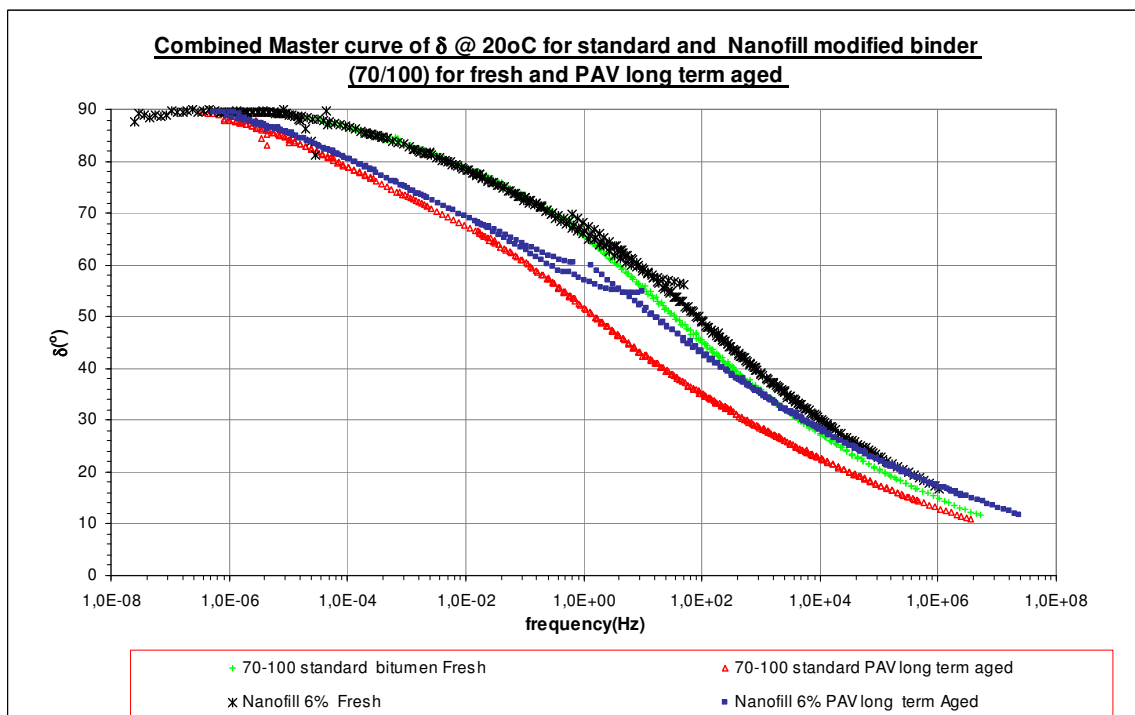


Figure 14: Master curve of phase angle of PAV long term aged standard and nanofill (6%) modified 70/100 binders

Appendix D

This appendix comprises ways of selection of specimens for different tests , graphical examples of resilient modulus computation for a selected temperature, graphical representation of shift factors in master curve construction of asphalt mixes, typical example of dynamic creep test with constant load but with variation in temperature. In addition a typical example of fatigue curve comprising results of 5 and 20 °C is presented.

NO.	Class	number of observations	Mid Values	Relative Frequency	Cumulative Frequency
1	2,10-2,20	17	2,15	18,5%	18,5%
2	2,20-2,30	13	2,25	14,1%	32,6%
3	2,30-2,40	20	2,35	21,7%	54,3%
4	2,40-2,50	6	2,45	6,5%	60,9%
5	2,50-2,60	6	2,55	6,5%	67,4%
6	2,60-2,70	11	2,65	12,0%	79,3%
7	2,70-2,80	10	2,75	10,9%	90,2%
8	2,80-2,90	9	2,85	9,8%	100,0%
Total		92		100,0%	

Table 5 : Void content distribution of the standard dense mix

Selection of number of Specimens in each void content Class								
Class	number of observations	Test types						sum
		Permanent deformation	Fatigue test	Dynamic Stiffness test	Indirect Tensile strength	Kerosine effect test	Hot air blowing test	
2,10-2,20	17	6	4	4	2	1	1	17
2,20-2,30	13	5	3	3	1	1	1	13
2,30-2,40	20	7	4	5	2	1	1	20
2,40-2,50	6	2	1	1	1	0	0	6
2,50-2,60	6	2	1	1	1	0	0	6
2,60-2,70	11	4	2	3	1	1	1	11
2,70-2,80	10	3	2	2	1	1	1	10
2,80-2,90	9	3	2	2	1	0	0	9
Total	92	32	19	22	9	5	5	92

Table 6 : selection of number of specimens in each void content class

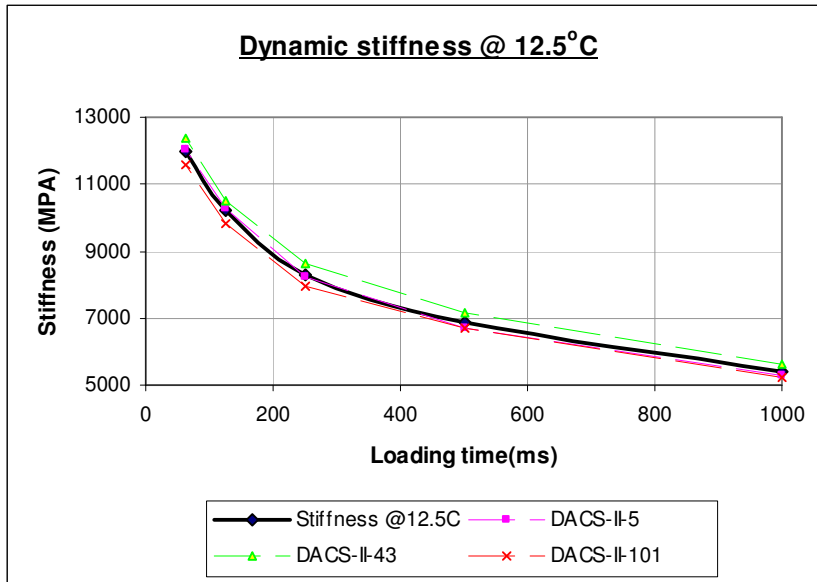


Figure 15: Typical graphical analysis of resilient modulus at 12.5°C

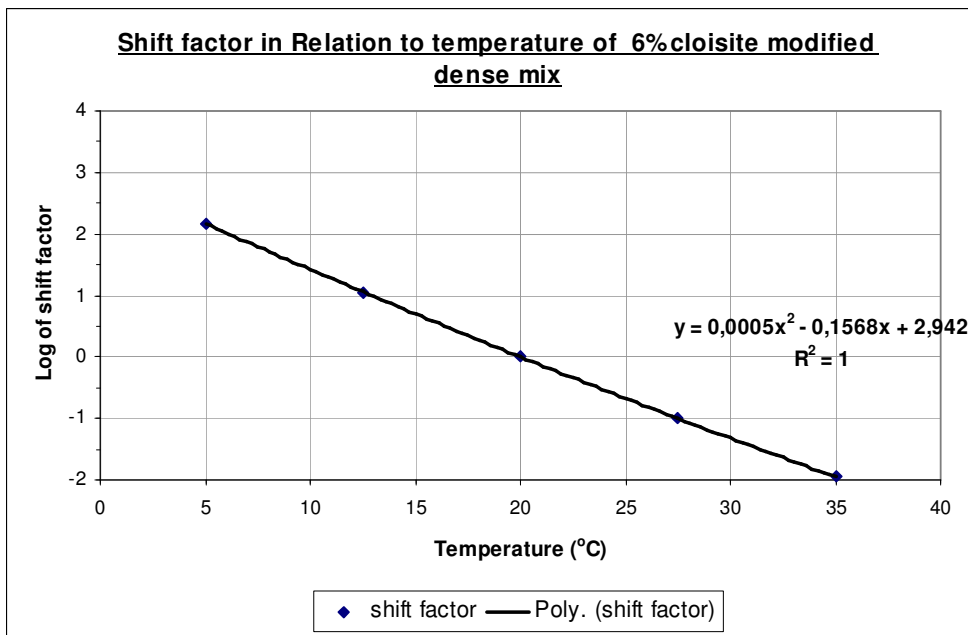


Figure 16: Typical example of shift factor in relation to temperature

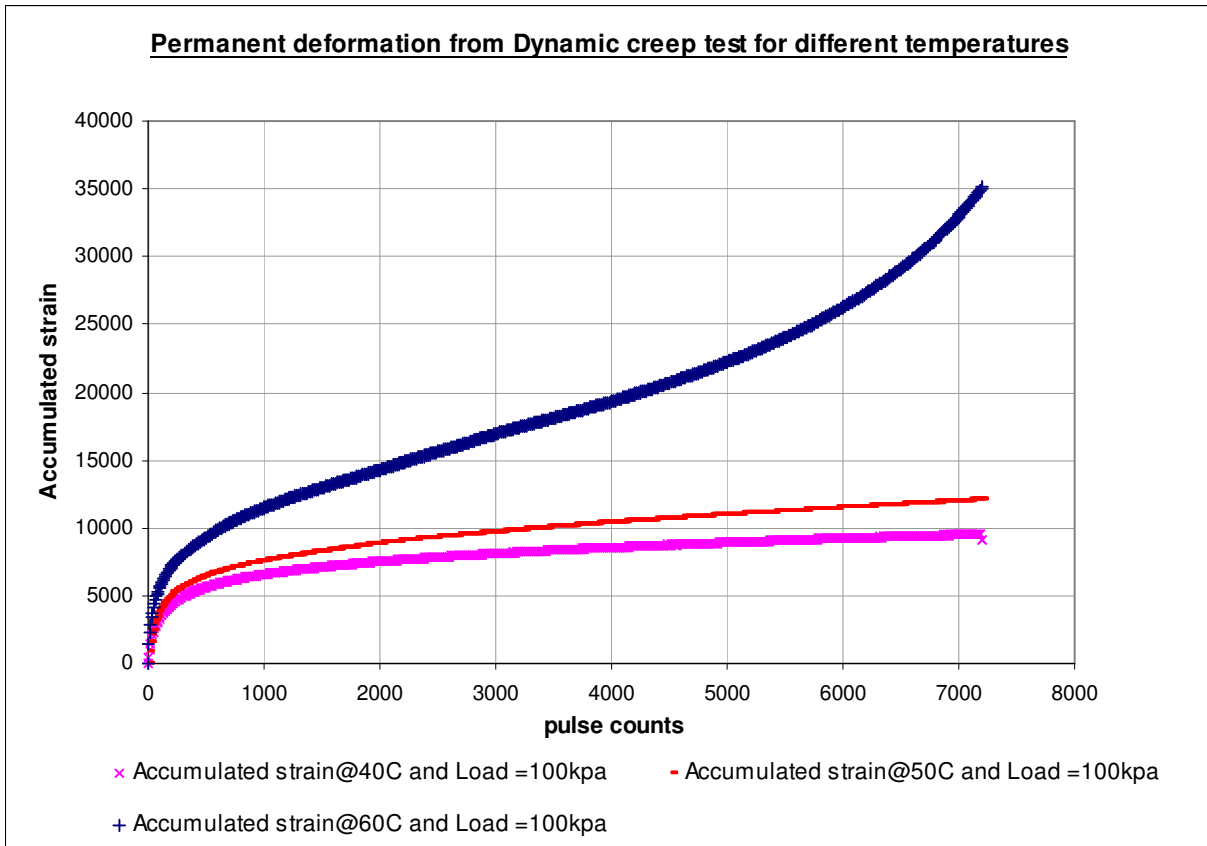


Figure 17: Example of effect of temperature on dynamic creep test

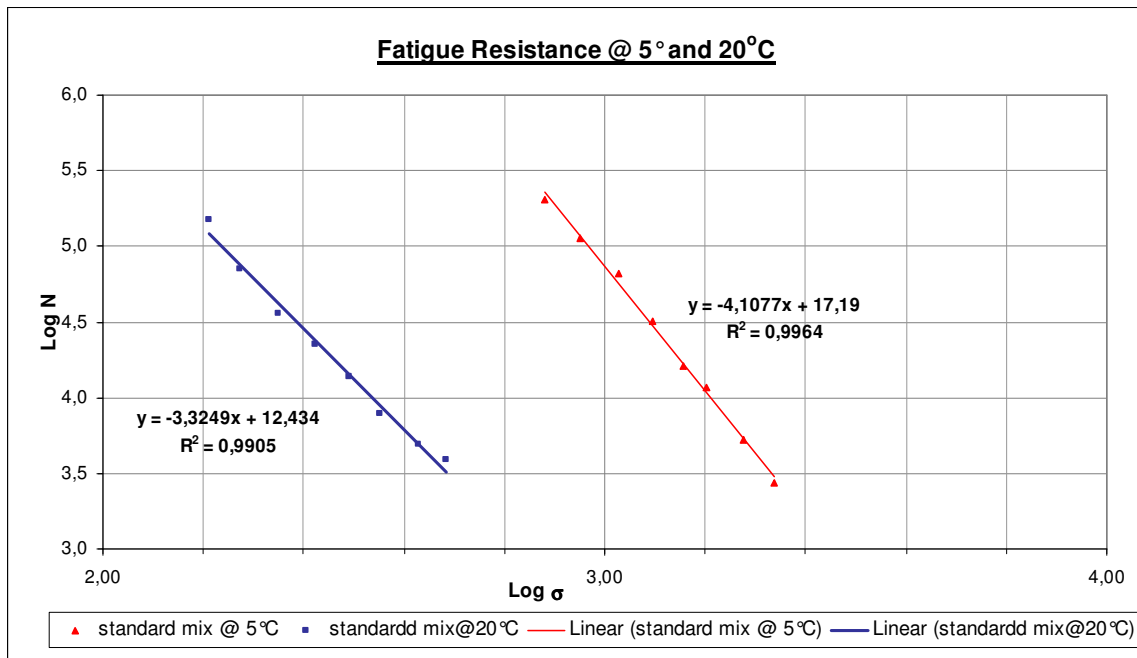


Figure 18: Example of effect of temperature on fatigue resistance test

Appendix E

Procedures in DSR test

The procedures in DSR test are as follows

1. Switch on all the appliances: two appliances related to the test equipment and the computer
2. Open the air pressure valve. Very important
3. Open Rheology test software
4. Click AR-Rheology
5. Create connection between the different appliances in the computer by:
 - Instrument -----Rotational mapping -----Perform mapping
6. Opening the Geometry Icon and selecting the correct diameter and gap size required for the different plates. For 8mm: a gap of 2mm is required and for 25mm and 40 mm a gap of 1mm is required.
7. Placing the different plates, and lowering the upper plate and setting a zero point by clicking on the zero point setting Icon and this setting is ended by saying yes
8. The position of the upper plate can be fixed either by clicking in the up and down arrows or by typing in the *required values* column the space (gap) of the upper plate above the zero point
9. Placing the specimen on the bottom plate and making sure that it is enough for the required gap. If not other specimens can be added on top of it.
10. Once the specimen is placed in place, the upper plate is lowered till it almost touches the specimen.
11. Fixing the temperature inside the test equipment to around 50°C and close the equipment till the required temperature is reached.
12. Open the door and by steps of 200-250um lower the upper plate and trim the bitumen on the edges and continue this step till a final step of : required gap + 50um is reached.
13. Lower the upper plate to the final gap and close the door
14. Open the frequency sweep dialogue box and fix all the required inputs about frequency, temperature and strain values
15. Click the file name and directory icon and change the names and directory as required
16. Run the test and check if the test is running oke.